

ESTIMATION OF VESSEL WALL COMPLIANCE USING ACOUSTIC REFLECTOMETRY

By
Héctor M. Figueroa Roldán

A Thesis submitted in partial fulfillment of the requirements for the degree of

MASTER OF SCIENCES
IN
ELECTRICAL ENGINEERING

UNIVERSITY OF PUERTO RICO
MAYAGÜEZ CAMPUS
2006

Approved by:

Miguel Vélez Reyes, Ph.D.
Member, Graduate Committee

Date

Shawn Hunt, Ph.D.
Member, Graduate Committee

Date

Eduardo J. Juan, Ph.D.
President, Graduate Committee

Date

Ricky Valentín, Ph.D.
Representative of Graduate Studies

Date

Isidoro Couvertier, Ph.D.
Chairperson of the Department

Date

Abstract

This thesis focuses on the estimation of rubber tube wall compliance using a pulse echo-acoustic reflectometry technique. Five rubber latex tubes of different thicknesses were studied using a transient acoustic pulse, instead of continuous sinusoidal waves. An acoustic Hanning pulse was designed with a wide bandwidth to study the resonance frequency of the tubes, and the tube wall compliance was estimated from reflection analysis. This method was applied using a reflectometer inside the tubes. Planar propagation was considered and given that the pulses travel into the system, the mechanical properties could be measured faraway, in contrast with other methods employed. An acoustic transmission line model was used to compute the natural frequency f_r , the input characteristic acoustic impedance and to predict from them, the values of the transversal frequencies f_{res} and f_2 . The natural frequency of the system occurs when the medium and wall tube vibrate at the same frequency, while the transversal frequencies occur when the characteristic impedance reaches minimum and maximum values, respectively. The wall compliance of rubber latex tubes was estimated via computer simulations, and acoustical and mechanical measurements. Two mathematical expressions were used to estimate the wall compliance C_w^* and C_w^{**} , which were compared to the mechanical measurement and model predictions of compliance. The wall compliance estimated acoustically, mechanically and simulated exhibited the same trend, with error averages for C_w^* of 77.7% and of 20.5% for C_w^{**} with respect to the values of compliance obtained from the transmission line model. Additionally, the error average between the values obtained mechanically and via simulation was 66.6%, with respect to the mechanical values. The results obtained from this research could serve as the groundwork for the development of a non-invasive device that can be used clinically to determine the pathological condition of compliant biological conduits such as veins, arteries and airways.

Resumen

En esta tesis se investiga como la ductilidad de un tubo puede ser estimada usando la técnica de “Pulse-Echo Acoustic Reflectometry”. Cinco tubos de látex con diferentes diámetros fueron interrogados usando un pulso acústico transiente en vez de señales senosoidales continuas en el tiempo. Un pulso acústico Hanning fue diseñado con un ancho de banda amplio para poder estudiar las frecuencias de resonancia de los tubos y de las señales obtenidas estimar las propiedades visco-elásticas de la pared del tubo. Este método fue aplicado usando un reflectómetro dentro del tubo. Se considero propagación acústica planar, y dado a que los pulsos viajan dentro del sistema las propiedades mecánicas pueden ser medidas a una posición distante, a diferencia de otros métodos empleados. Un modelo acústico de línea de transmisión fue usado para computar la frecuencia natural f_r , la impedancia característica de entrada y predecir de esta los valores de las frecuencias transversales f_{res} y f_2 . La frecuencia natural del sistema ocurre cuando el medio y los tubos resuenan, mientras que las frecuencias transversales ocurren cuando la impedancia característica alcanza un valor mínimo y máximo, respectivamente. Dos expresiones matemáticas fueron usadas para estimar la ductilidad de los tubos acústicamente C_w^* y C_w^{**} , en conjunto con el estimado mecánicamente y el computado por simulación C_w . De los valores obtenidos se observo, que la ductilidad disminuyo a medida que el ancho de la pared aumento. El promedio del error para C_w^* fue 77.7% mientras que para C_w^{**} fue 20.5% con respecto al simulado. Adicionalmente, se observaron diferencias con un promedio de un 66.3% entre los valores mecánicos y los simulados, con respecto a los valores mecánicos. Los resultados obtenidos de esta investigación pueden servir como base para el desarrollar dispositivos que puedan ser usados en aplicaciones clínicas para determinar condiciones patológicas de una forma no invasiva dentro de conductos biológicos tales como venas arteria y vías respiratorias.

To my parents Héctor M. Figueroa and Iritza Roldán, my brothers Elix X. Figueroa and Julio Figueroa, my nephews Elix G. Figueroa, Julian Figueroa and Elix X. Figueroa, my grandmothers Carmen and Manuela, my aunt Ivette Figueroa, my friend Maria Fernanda Naranjo. Thanks for your unconditional love and support.

Acknowledgement

This research was primarily supported by the National Institute of Health NIH, MBRS-SCORE program.

I wish to be grateful to Dr. Eduardo J. Juan for your guidance, tolerance, support, friendship and help. Thanks for trusting in me and allowing me to have the honor to work as a part of your team. You gave me the opportunity to grow as a better engineer and person. I will never forget your nobility and always be grateful for all of what you did.

I want to thank the Department of Electrical and Computer Engineering of the University of Puerto Rico for giving me the opportunity to grow intellectually and thanks to UPRM and PRIDCO for the economic support throughout these years.

I also want to thanks to my colleagues and friends, María Fernanda Naranjo Bueno, Miguel Angel Goenaga, Maria Elena Torres, Luis Guillermo Giraldo, Fabián Benitez, Luis Quintero, Diego Aponte and Carlos Niño for their unconditional friendship and support.

Table of Contents

1	Introduction.....	1
1.1	Clinical Problems.....	1
1.1.1	Respiratory diseases.....	1
1.1.2	Cardiovascular disease.....	3
1.2	Measurement of compliance.....	3
1.2.1	Arterial Compliance.....	3
1.2.1.1	IVUS elastography.....	5
1.2.1.2	IVUS Palpography.....	5
1.2.2	Airways Compliance.....	6
1.2.2.1	Spirometry.....	7
1.3	Tube wall compliance estimation by acoustic reflectometry.....	7
1.4	Objectives.....	8
1.5	Organization.....	9
2	Background.....	10
2.1	Time domain acoustic reflectometry.....	10
2.1.1	Principles.....	10
2.1.2	Basic Theory.....	11
2.1.3	Sound propagation in tube.....	13
2.2	Transmission Line Model.....	14
2.3	Compliance Estimation.....	21
2.3.1	Wall compliance estimation by transversal frequencies.....	21
2.3.2	Wall compliance estimation by natural and resonant frequencies.....	21
2.4	Summary.....	22
3	Sensitivity Analysis.....	23
3.1	Method.....	23
3.2	Results and Discussion.....	26
3.2.1	Wall properties effects.....	26
3.2.1.1	Inner wall diameter effects.....	27
3.2.1.2	Wall thickness effects.....	31
3.2.1.3	Wall density effects.....	34

3.2.1.4	Young's modulus effects	38
3.2.1.5	Wall viscosity effects.....	41
3.2.1.6	Young's modulus and wall thickness effects.....	45
3.2.2	Pulse echo acoustic reflectometry assessment.....	48
3.2.2.1	Analysis of a signal whose quality factor $Q = 149.5$	49
3.2.2.2	Analysis of a signal with a known quality factor $Q = 88$	54
4	Wall Compliance Estimation Using Pulse-Echo Acoustic Reflectometry	58
4.1	Methodology.....	58
4.1.1	Compliance estimation via volumetric tests	58
4.1.2	Acoustic reflectometer	59
4.1.2.1	Loudspeaker/source tube coupling	60
4.1.2.2	Source tube/test object coupling	61
4.1.2.3	Analog Band pass Filter.....	61
4.1.3	Acoustic Pulse Generation.....	62
4.1.3.1	Inverse filter technique	62
4.1.3.2	Cross-correlation.....	64
4.1.4	Wall compliance and characteristic acoustic impedance estimation	65
4.2	Complex Modulus of rubber like material.....	66
4.2.1	Dynamic Young's modulus	66
4.2.2	Stress-strain test	67
4.3	Noise Removal.....	68
4.4	Results and Discussion	69
4.4.1	Volumetric Test	69
4.4.2	Acoustic Hanning pulse created using inverse filtering technique.....	72
4.4.3	Acoustic characteristic impedance results	76
4.4.3.1	Tubes experimentation without foreign material.....	76
4.4.3.2	Tubes experimentation with foreign material	82
4.4.3.3	With vs. without foreign material discussion	88
4.5	Transmission Line Model vs. Echo-Acoustic Reflectometry	91
4.5.1	Tube of 0.119 cm of thickness with inner wall of 0.647 cm	92
4.5.2	Tube of 0.159 cm of thickness with inner wall of 0.647 cm	94
4.5.3	Tube of 0.198 cm of thickness with inner wall of 0.647 cm	96
4.5.4	Tube of 0.238 cm of thickness with inner wall of 0.647 cm.....	98
4.5.5	Tube of 0.317 cm of thickness with inner wall of 0.647 cm	100
4.6	Noise Removal.....	102
4.7	Tubes wall compliance results.....	108

4.7.1	Wall compliance estimation by acoustic input impedance	109
4.7.2	Wall compliance estimation by reflection coefficient and natural response	111
5	Conclusion and Recommendations.....	114
5.1	Recommendations.....	116

List of Tables

Table I Physical properties for air filled pipes used on experiments.....	16
Table II Transmission line model parameters.....	25
Table III Rubber pipe physical properties values used for simulation.	28
Table IV Quality factor, damping ratio and resonant frequencies obtained from simulations.....	29
Table V Rubber pipe physical properties values used for simulation used to determine wall thickness effects.....	32
Table VI Quality factor, damping ratio and resonant frequencies obtained from simulation.....	32
Table VII Rubber pipe physical properties values used for simulation.....	35
Table VIII Quality factor, damping ratio and resonant frequencies obtained from simulation.....	36
Table IX Rubber pipe physical properties values used for simulation.	39
Table X Quality factor, damping ratio and resonant frequencies obtained from simulations.....	39
Table XI Rubber pipe physical properties values used for simulation.	42
Table XII Quality factor, damping ratio and resonant frequencies obtained from simulations.....	43
Table XIII Rubber pipe physical properties values used for simulation.	46
Table XIV Quality factor, damping ratio and resonant frequencies obtained from simulation.....	46
Table XV Rubber pipe physical properties values used for simulation.....	49
Table XVI Transversal frequencies and wall compliance for various values of N	53
Table XVII Transversal frequencies and wall compliance for various values of N	53
Table XVIII Rubber pipe physical properties values used for simulation.....	54
Table XIX Transversal frequencies and wall compliance for various values of N	56

Table XX	Transversal frequencies and wall compliance for various values of N	57
Table XXI	Approximate Young's modulus of rubber.....	68
Table XXII	Wall compliance measurements for different rubber pipes using volumetric tests	71
Table XXIII	Experimental transversal frequencies obtained from the characteristic impedance.....	81
Table XXIV	Experimental transversal frequencies obtained from the characteristic impedance.....	87
Table XXV	Experimental transversal frequencies obtained from the characteristic impedance.....	91
Table XXVI	Transmission line model parameters used in simulation for a tube with wall thickness of 0.119 cm.	93
Table XXVII	Transmission line model parameters used in simulation for a tube with wall thickness of 0.159 cm.	95
Table XXVIII	Transmission line model parameters used in simulation for a tube with wall thickness of 0.198 cm.	97
Table XXIX	Transmission line model parameters used in simulation for a tube with wall thickness of 0.238 cm.	99
Table XXX	Transmission line model parameters used in simulation for a tube with wall thickness of 0.317 cm.	101
Table XXXI	Transmission line model parameters used in Simulation	108
Table XXXII	Wall compliance.....	108

List of Figures

Fig. 1.1 (a) Airways in people without asthma. (b and c) Airways in people with asthma [8].	2
Fig. 1.2 Change of arterial wall compliance caused by fatty material deposit [11].	3
Fig. 1.3 Echogram (left) and elastogram (right) of a vessel mimicking phantom containing an isoechoic soft lesion between 7 and 11 o'clock. The lesion is invisible in the echogram, while it is clearly depicted in the elastogram [28].	6
Fig. 1.4 Examples of strain palpograms corresponding to an elastically homogeneous vessel phantom. Showing the strain palpograms produced using pressure differences of 2 and 7 mmHg [28].	6
Fig. 2.1 Overview of time domain acoustic reflectometry	11
Fig. 2.2 Behavior of a propagating acoustic pulse on different media.	12
Fig. 2.3 Lumped model for acoustic-electrical models in one dimensional wave propagation on a short segment of pipe.	15
Fig. 3.1 Characteristic acoustic impedance $Z_I(f)$ for different inner diameters.	29
Fig. 3.2 Reflection coefficient $R(f)$ for different inner diameters.	30
Fig. 3.3 Wall compliance (C_w) values for different tests.	30
Fig. 3.4 Characteristic acoustic impedance $Z_I(f)$ for different thicknesses in cm.	33
Fig. 3.5 Reflection coefficient $R(f)$ for different thicknesses in cm.	33
Fig. 3.6 Wall compliance (C_w) values for different thicknesses.	34
Fig. 3.7 Characteristic acoustic impedance $Z_I(f)$ for different wall densities in g/cm^3 .	36
Fig. 3.8 Reflection coefficient $R(f)$ for different wall densities in g/cm^3 .	37
Fig. 3.9 Wall compliance (C_w) values for different wall densities in g/cm^3 .	37
Fig. 3.10 Characteristic acoustic impedance $Z_I(f)$ for different Young's modulus in dyne/cm^2 .	40
Fig. 3.11 Reflection coefficient $R(f)$ for different Young's modulus in dyne/cm^2 .	40
Fig. 3.12 Wall compliance (C_w) values for different Young's modulus in dyne/cm^2 .	41

Fig. 3.13 Characteristic acoustic impedance $Z_I(f)$ for different wall viscosity values in $\text{dyne}\cdot\text{s}/\text{cm}^2$	43
Fig. 3.14 Reflection coefficient $R(f)$ for different wall viscosity values in $\text{dyne}\cdot\text{s}/\text{cm}^2$	44
Fig. 3.15 Wall compliance (C_w) for different wall viscosity values. Test 1 $\eta = 300$ $\text{dyne}\cdot\text{s}/\text{cm}^2$, Test 2 $\eta = 250$ $\text{dyne}\cdot\text{s}/\text{cm}^2$, Test 3 $\eta = 200$ $\text{dyne}\cdot\text{s}/\text{cm}^2$, Test 4 $\eta = 150$ $\text{dyne}\cdot\text{s}/\text{cm}^2$, Test 5 $\eta = 100$ $\text{dyne}\cdot\text{s}/\text{cm}^2$	44
Fig. 3.16 Characteristic acoustic impedance $Z_I(f)$ for different Young's modulus and thickness values. Test 1, $E = 1.8\text{E}7$ dyne/cm^2 , $h = 0.317$ cm; Test 2, $E = 1.9\text{E}7$ dyne/cm^2 , $h = 0.238$ cm; Test 3, $E = 2.1\text{E}7$ dyne/cm^2 , $h = 0.198$ cm; Test 4, $E = 2.3\text{E}7$ dyne/cm^2 , $h = 0.159$ cm; Test 5, $E = 2.6\text{E}7$ dyne/cm^2 , $h = 0.159$ cm.	47
Fig. 3.17 Reflection coefficient $R(f)$ for different Young's modulus and thickness values. Test 1, $E = 1.8\text{E}7$ dyne/cm^2 , $h = 0.317$ cm; Test 2, $E = 1.9\text{E}7$ dyne/cm^2 , $h = 0.238$ cm; Test 3, $E = 2.1\text{E}7$ dyne/cm^2 , $h = 0.198$ cm; Test 4, $E = 2.3\text{E}7$ dyne/cm^2 , $h = 0.159$ cm; Test 5, $E = 2.6\text{E}7$ dyne/cm^2 , $h = 0.159$ cm.	47
Fig. 3.18 Wall compliance for different Young's modulus and thickness values. Test 1, $E = 1.8\text{E}7$ dyne/cm^2 , $h = 0.317$ cm; Test 2, $E = 1.9\text{E}7$ dyne/cm^2 , $h = 0.238$ cm; Test 3, $E = 2.1\text{E}7$ dyne/cm^2 , $h = 0.198$ cm; Test 4, $E = 2.3\text{E}7$ dyne/cm^2 , $h = 0.159$ cm; Test 5, $E = 2.6\text{E}7$ dyne/cm^2 , $h = 0.159$ cm.	48
Fig. 3.19 Example of the incident pulse used to interrogate the systems (a) Example of the Hanning pulse at a cutoff frequency of 6 kHz in time domain. (b) <i>FFT</i> of the Hanning pulse.	49
Fig. 3.20 (a) Example of the obtained sequence $y[n]$ when a Hanning pulse interrogates the system. (b) Reflected acoustic pulse in time domain.	50
Fig. 3.21 Reflection coefficient $R^*(f)$ when length N in the reflection signal was varied. .	51
Fig. 3.22 Characteristic acoustic impedance $Z_1^*(f)$ when length N in the reflection signal was varied.	52
Fig. 3.23 Reflected acoustic pulse in time domain.	54
Fig. 3.24 Reflection coefficient $R^*(\omega)$ when length N in the reflection signal was varied.	55
Fig. 3.25 Characteristic acoustic impedance $Z_1^*(\omega)$ when length N in the reflection signal was varied.	55
Fig. 4.1 Mechanical estimations setup.....	58
Fig. 4.2 Experimental setup utilized to perform the acoustic measurements.	59

Fig. 4.3 Pulse-echo acoustic reflectometry system.....	60
Fig. 4.4 Loudspeaker/source tube coupler.....	60
Fig. 4.5 Coupling between the source tube and object under investigation.....	61
Fig. 4.6 Example of block diagram used in the design of the custom made analogous filter.	61
Fig. 4.7 Inverse procedure to obtain $H(j\omega)$	63
Fig. 4.8 Electrical pulse $E(t)$ that generates an acoustic pulse $p(t)$	64
Fig. 4.9 Engineering stress-strain curve [42].....	67
Fig. 4.10 Volume vs. pressure. Curves include linear fitting with its mathematical expressions for latex tubes. a) $h = 0.159$ cm, b) $h = 0.159$ cm, c) $h = 0.198$ cm, d) $h =$ 0.238 cm, e) $h = 0.317$ cm.	71
Fig. 4.11 Local wall compliance for latex tubes. Test 1 $h = 0.159$ cm, Test 2 $h = 0.159$ cm, Test 3 $h = 0.198$ cm, Test 4 $h = 0.238$ cm, Test 5 $h = 0.317$ cm.....	72
Fig. 4.12 Reflectometer and extension tube used to generate an acoustic pulse to interrogate the latex tubes.....	73
Fig. 4.13 Input and output pulses used to determine the frequency response $H(\omega)$ of the system (referring to the DENON amplifier, preamplifier and reflectometer). a) Electric pulse $x[n]$ of $50 \mu\text{s}$ designed in order to interrogate the system. b) Output signal $y[n]$ resulting from the perturbation $x(t)$	74
Fig. 4.14 Signal obtained after deconvolution. It contains three acoustic pulses: the incident, first reflection and second reflection. The incident pulse is a positive Hanning and the reflected, a negative Hanning pulse.	75
Fig. 4.15 Fourier transform of the incident pulse, reflected pulse and noise. The incident pulse is represented by the color blue. The reflected pulse is represented by the color green. The noise is represented by the color red.....	75
Fig. 4.16 Signal recorded at a sampling rate of 300 kS/s for a tube with an inner diameter of 0.647 cm and wall thickness of 0.119 cm.....	77
Fig. 4.17 a) Incident signal of $50 \mu\text{s}$ of duration, recorded at a sampling rate of 300 kS/s. b) Reflected signal recorded at a sampling rate of 300 kS/s.....	78
Fig. 4.18 Fast Fourier Transforms of the incident, reflected and noise signals experimentally measured for latex tubes with different wall thicknesses. a) $h = 0.159$ cm, b) $h = 0.159$ cm, c) $h = 0.198$ cm, d) $h = 0.238$ cm, e) $h = 0.317$ cm.	80

Fig. 4.19 Characteristic acoustic impedance for latex tubes with different wall thicknesses. Test 1 $h = 0.159$ cm, Test 2 $h = 0.159$ cm, Test 3 $h = 0.198$ cm, Test 4 $h = 0.238$ cm, Test 5 $h = 0.317$ cm.	82
Fig. 4.20 Signal recorded at a sampling rate of 300 kS/s for a tube with a inner diameter of 0.647 cm and wall thickness of 0.119 cm.	83
Fig. 4.21 a) Incident signal of 50 μ s of duration, recorded at a sampling rate of 300 kS/s. b) Reflected signal recorded at a sampling rate of 300 kS/s.	84
Fig. 4.22 Fast Fourier Transforms of the incident, reflected and noise signals experimentally measured for latex tubes with different wall thickness values. a) $h = 0.159$ cm, b) $h = 0.159$ cm, c) $h = 0.198$ cm, d) $h = 0.238$ cm, e) $h = 0.317$ cm.	86
Fig. 4.23 Characteristic acoustic impedance for latex tubes with different wall thicknesses. Test 1 $h = 0.159$ cm, Test 2 $h = 0.159$ cm, Test 3 $h = 0.198$ cm, Test 4 $h = 0.238$ cm, Test 5 $h = 0.317$ cm.	88
Fig. 4.24 Characteristic acoustic impedance for latex tubes with different wall thickness, with foreign materials and without foreign materials. a) $h = 0.159$ cm, b) $h = 0.159$ cm, c) $h = 0.198$ cm, d) $h = 0.238$ cm, e) $h = 0.317$ cm.	91
Fig. 4.25 Comparison of simulated reflected signal (blue) with acoustically obtained (green) for a latex tube with wall thickness of 0.119 cm.	93
Fig. 4.26 Comparison of characteristic acoustic impedances obtained by simulation (blue) with the acoustically measured (red) for a latex tube with wall thickness of 0.119 cm. The reflectometer impedance is plotted in green.	94
Fig. 4.27 Comparison of simulated reflected signal (blue) with acoustically obtained (green) for a latex tube with wall thickness of 0.159 cm.	95
Fig. 4.28 Comparison of characteristic acoustic impedances obtained by simulation (blue) with acoustically measured (red) for a latex tube with wall thickness of 0.159 cm. The reflectometer impedance is plotted in green.	96
Fig. 4.29 Comparison of simulated reflected signal (blue) with acoustically obtained (green) for a latex tube with wall thickness of 0.198 cm.	97
Fig. 4.30 Comparison of characteristic acoustic impedances obtained by simulation (blue) with acoustically measured (red) for a latex tube with wall thickness of 0.198 cm. The reflectometer impedance is plotted in green.	98
Fig. 4.31 Comparison of simulated reflected signal (blue) with acoustically obtained (green) for a latex tube with wall thickness of 0.238 cm.	99

Fig. 4.32 Comparison of characteristic acoustic impedances obtained by simulation (blue) with acoustically measured (red) for a latex tube with wall thickness of 0.238 cm. The reflectometer impedance is plotted in green.	100
Fig. 4.33 Comparison of simulated reflected signal (blue) with acoustically obtained (green) for a latex tube with wall thickness of 0.317 cm.	101
Fig. 4.34 Comparison of characteristic acoustic impedances obtained by simulation (blue) with acoustically measured (red) for a latex tube with wall thickness of 0.317 cm. The reflectometer impedance is plotted in green.	102
Fig. 4.35 Signal obtained in TLM simulation (blue) and measured acoustically (green). Dash line represents the forced response and dot-dash the natural response. The ellipse outlines the missed information.	103
Fig. 4.36 Characteristic acoustic impedance of a tube with wall thickness of 0.119 cm when the length of the reflected signal was varied.	104
Fig. 4.37 Parameters behavior in iteration twenty of Gauss-Newton Algorithm.	104
Fig. 4.38 Comparison among the estimated signal (green) and the natural response of the system (blue). The error between them is plotted in red.	105
Fig. 4.39 Acoustic signal obtained after applying Gauss-Newton algorithm.	105
Fig. 4.40 Comparison of characteristic acoustic impedances obtained by system identification (green) with the acoustically measured (blue) for latex tubes with wall thickness: a) $h = 0.159$ cm, b) $h = 0.159$ cm, c) $h = 0.198$ cm, d) $h = 0.238$ cm, e) $h = 0.317$ cm.	107
Fig. 4.41 Wall compliance obtained mechanically (Mc), acoustical (Ac), mathematically (Eq) and by system identification (SI) at 1000 samples. Tube 1: $E = 2.6E7$ dyne/cm ² , $h = 0.119$ cm; Tube 2: $E = 2.3E7$ dyne/cm ² , $h = 0.159$ cm; Tube 3: $E = 2.1E7$ dyne/cm ² , $h = 0.198$ cm; Tube 4: $E = 1.9E7$ dyne/cm ² , $h = 0.238$ cm; Tube 5: $E = 1.8E7$ dyne/cm ² , $h = 0.317$ cm.	110
Fig. 4.42 Transversal frequencies: a) acoustical ($fres$), mathematical ($fresc$) and system identification ($fresSI$), b) acoustical ($f2$), mathematical ($f2c$) and system identification ($f2SI$). Tube 1: $h = 0.119$ cm, Tube 2: $h = 0.159$ cm, Tube 3: $h = 0.198$ cm, Tube 4: $h = 0.238$ cm, Tube 5: $h = 0.317$ cm.	110
Fig. 4.43 Wall compliance obtained mechanically (Mc), acoustical (Ac), mathematically (Eq) and by system identification (SI) at 600 samples. Tube 1: $E = 2.6E7$ dyne/cm ² , $h = 0.119$ cm; Tube 2: $E = 2.3E7$ dyne/cm ² , $h = 0.159$ cm; Tube 3: $E = 2.1E7$ dyne/cm ² , $h = 0.198$ cm; Tube 4: $E = 1.9E7$ dyne/cm ² , $h = 0.238$ cm; Tube 5: $E = 1.8E7$ dyne/cm ² , $h = 0.317$ cm.	112

Fig. 4.44 Transversal frequencies: a) acoustical (f_{res}), mathematical (f_{resc}) and system identification (f_{resSI}); b) acoustical (f_2), mathematical (f_2c) and system identification (f_2SI). Tube 1: $h = 0.119$ cm, Tube 2: $h = 0.159$ cm, Tube 3: $h = 0.198$ cm, Tube 4: $h = 0.238$ cm, Tube 5: $h = 0.317$ 112

1 Introduction

1.1 Clinical Problems

Historically, hollow conduits in the human body such as arteries, veins, and the esophagus, were considered passive structures that did not have the ability to voluntarily relax and contract [1]. Today, these conduits are viewed as complex and active structures that possess the ability to contract as needed. The ability of these conduits to expand and relax is known as compliance, and over the past decade, researchers have begun to link how the respiratory and cardiovascular diseases affect the compliance of biological conduits[2-5].

Cardiovascular and respiratory diseases are the number one and three [6, 7] causes of death in the world, respectively. Some techniques used to diagnose these diseases are based on the measurement of the total or localized compliance of blood vessels or the respiratory tract.

The main goal of this research was to evaluate the feasibility of employing pulse-echo acoustic reflectometry to estimate the local wall compliance of non-rigid tubes. This acoustic method was experimentally tested and validated using latex tubes of various wall thicknesses, filled with air. The acoustic method is based on transmission line model and might result in an inexpensive technique to diagnose diseases in respiratory airways and blood vessels.

1.1.1 Respiratory diseases

According to the USA Lung Organization [6] more than 35 million of Americans have chronic lung diseases and every year over 349,000 die, making lung diseases responsible for one in every seven deaths. Asthma and chronic obstructive pulmonary disease (COPD) are the most common obstructive lung diseases. They are associated with substantial health impairment, work disability, and change in wall compliance.

Asthma is an inflammatory condition of the bronchial airways. It makes the airways increase the production of mucus. That mucus is added into the inner walls producing an

obstruction. Normally, asthma causes chest tightness, coughing and wheezing. If severe, it can cause shortness of breath and low blood oxygen levels. Fig. 1.1 shows the normal (a), swelled (b) and muscle (c) tightening in human airways caused by asthma.

COPD is a term that refers to chronic bronchitis diseases and emphysema of the lungs. COPD is characterized by obstruction to airflow that interferes with normal breathing. It does not include other obstructive diseases such as asthma. Chronic bronchitis is the inflammation and eventual scarring of the bronchial tubes lining. When the bronchi are inflamed and/or infected, less air is able to flow from the lungs caused by an obstruction of a heavy mucus or phlegm. Once the bronchial tubes have been irritated over a long period of time, excessive mucus is constantly produced, the bronchial tubes lining becomes thickened, an irritating cough develops, air flow may be hampered and the lungs become scarred. The bronchial tubes then become an ideal breeding place for bacterial infections within the airways, which eventually impedes airflow. [6]

From Fig. 1.1 (a) depicts a normal airways, the mucus around the tube are relaxes, allowing the airways to stay open. Figure (b) it can be seen that the accumulation of mucus in the airways changes the cross-sectional area and therefore changes the wall compliance and Figure (c) depict the conduits in people with asthma, the muscles around the airways can spasm, swollen and filled with mucus. These changes can be measured as a change in the system compliance, which provides information about the airway's conditions and allows diagnosing abdominal conditions. This method does not provide information about the tissues properties. Different techniques used to asses the total compliance on human airways will be explained in the compliance measurement section.

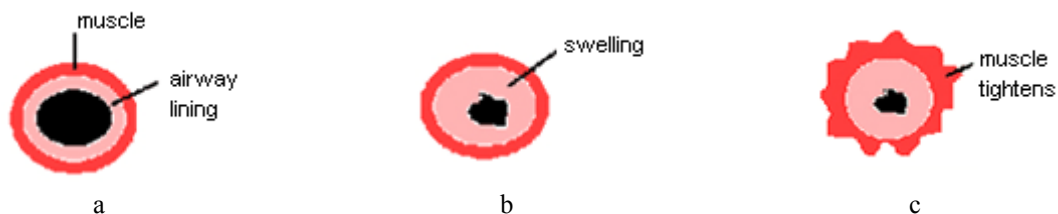


Fig. 1.1 (a) Airways in people without asthma. (b and c) Airways in people with asthma [8].

1.1.2 Cardiovascular disease

The World Health Organization (WHO) estimates that 16.6 million people around the globe die of cardiovascular diseases each year [9]. The American Heart Association (AHA) estimates that 1.2 million Americans will have a first or recurrent coronary attack and 479,000 of these people will die [10]. Statistically, one person dies every 30 seconds from heart disease, making it the leading cause of deaths in the world.

A heart attack occurs when the blood supply to part of the heart muscle (the myocardium) is severely reduced or stopped because one or more of the heart's arteries is blocked. The process usually begins with atherosclerosis, which is the buildup of fatty deposits (plaque) inside artery walls [10]. The plaque can rupture, causing a blood clot to form and blocking the artery as shown in Fig. 1.2. If the blood supply is cut off for more than a few minutes, the heart muscle cells suffer permanent injury or die. This can kill or disable someone, depending on how much heart muscle is damaged.

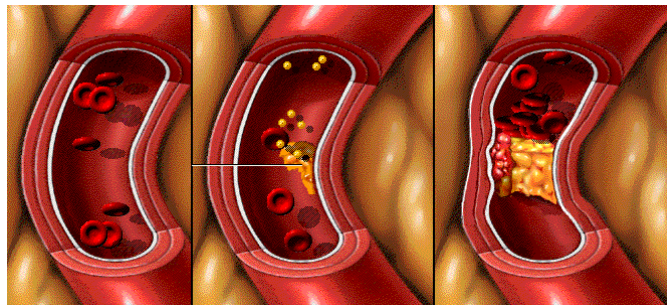


Fig. 1.2 Change of arterial wall compliance caused by fatty material deposit [11].

1.2 Measurement of compliance

1.2.1 Arterial Compliance

Measurements of arterial stiffness are used to estimate the artery's ability to expand and contract with each cardiac pulsation and relaxation. This is called total compliance and is defined as the change of volume divided by the change in pressure. Screening and advanced diagnostic tests are implemented today in which invasive and non-invasive sophisticated techniques are used to provide detail about the blood vessel structure and function.

Classical methods have investigated how to assess the vessel wall compliance properties, analyzing the aortic pressure decay in diastole [12] and calculating the systolic aortic input impedance [13, 14]. Impedance plethysmography [15] has been used as an indirect noninvasive method to estimate total arterial compliance. The distension curve of peripheral arteries can be assessed by Doppler signal processing of ultrasound radio-frequency signals [16]. The mechanical behavior of the aorta has also been studied using angiography [17], echocardiography [18], sonometry [19], magnetic resonance imaging [20], echo-tracking system [21], pulse pressure method, decay time method [17], volume-to-aortic pulse pressure ratio (SV/PP) [22], Pulse Pressure Method [23], Helmholtz resonators [18] and others. In experimental settings, central aortic compliance has been calculated from pressure-diameter relationships using sono-micrometers [21, 22, 24-26]. This method is considered the gold standard but cannot be applied in humans.

Estimation of the total arterial compliance has long interested clinicians and researchers of the cardiovascular physiology. Different techniques that provide excellent visualization of the arterial stiffness are used to diagnose the total compliance of arteries in clinical investigation [1] such as pulse pressure (PP), pulse wave velocity ultrasound with doppler techniques, augmentation index (AI) and pulse contour analysis (PCA). The most widely and accepted method is the Diastolic Decay Time Method (DTM), which is based on the two-element Windkessel model. But a recent study showed that pulse pressure method (PPM) is the most accurate method [27] used to estimate total arterial compliance. PPM is an iterative technique to estimate arterial compliance from simultaneous pressure and flow measurement, PPM does not necessitate knowledge of the whole pressure pulse and it does not require zero flow in diastole.

Stress tests, nuclear stress tests, and angiograms are methods currently used today by physicians for the diagnostic of total compliance. These are external techniques which assess the condition of the cardiovascular system, but they do not provide information about the local compliance and the internal wall conditions.

Recently, the internal wall compositions of the vessels or arteries are being studied using intravascular ultrasound image (IVUS). This is the only commercially available technique, which provides real-time high-resolution images allowing precise tomographic assessment of lumen area, plaque size, and composition of a coronary segment, and

therefore provides new insights into the diagnosis of coronary disease, regardless the presence or absence of stenosis. The arteries wall local compliance has been the most frequent target by the IVUS, specifically elastography and palpography analysis. These techniques open the horizon for studies of arterial stiffness in clinical practice.

1.2.1.1 IVUS elastography

IVUS elastography is a method for measuring the local elastic properties using intravascular ultrasound. This method is able to obtain the mechanical characterization of the vessel through ultrasound images at two levels of intravascular pressure and then estimates the difference between two images using cross-correlation algorithms with interpolation around the peak, in order to obtain the strain properties of the vessel tissues. Knowledge of these elastic properties is useful for guiding interventional procedures and detection of vulnerable plaques.

1.2.1.2 IVUS Palpography

Palpography is an inexpensive real time intravascular ultrasound technique, used to measure the elasticity properties in human conduits such as arterials systems. In general this method measures the radial strain by cross-correlating the signals at different intraluminal pressures. In Fig. 1.4 the compound images represent the known strain palpograms which are created by color coding, and which are superimposed over the resultant IVUS image. This method is similar to elastography, but the palpography algorithm produces better clinic image and is more robust.

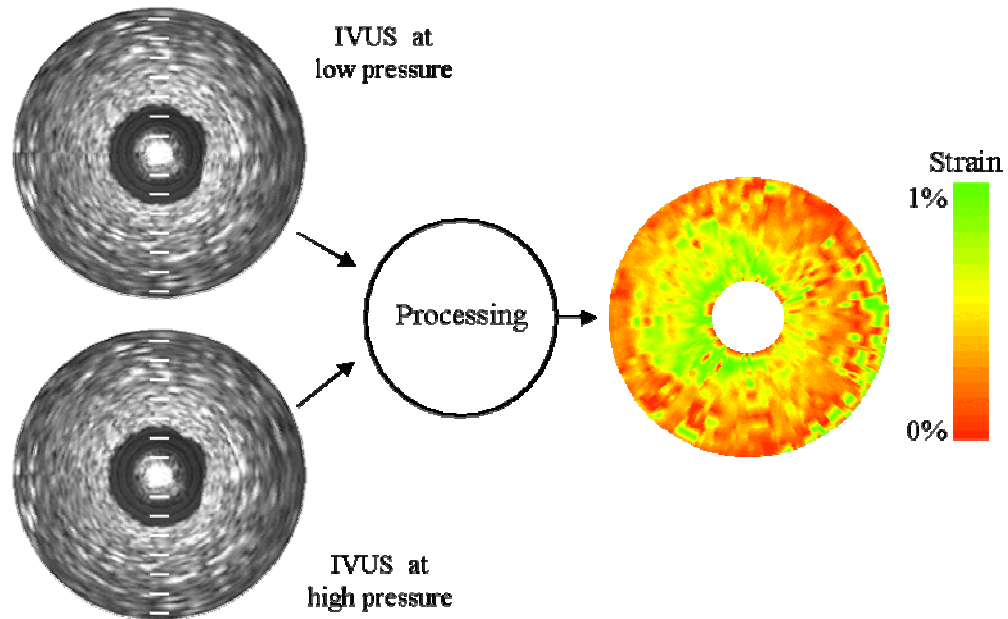


Fig. 1.3 Echogram (left) and elastogram (right) of a vessel mimicking phantom containing an isoechoic soft lesion between 7 and 11 o'clock. The lesion is invisible in the echogram, while it is clearly depicted in the elastogram [28]

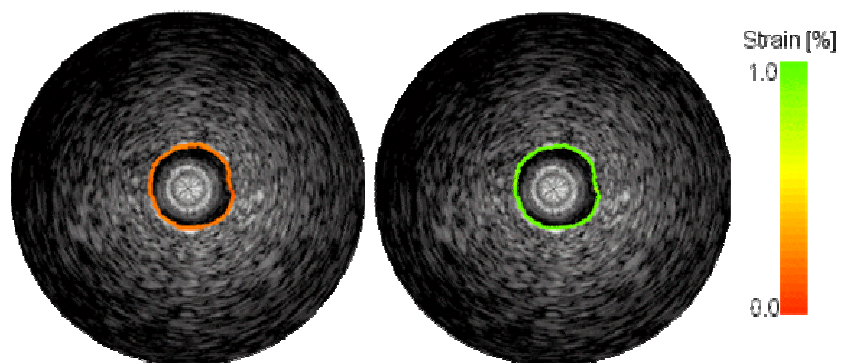


Fig. 1.4 Examples of strain palpograms corresponding to an elastically homogeneous vessel phantom. Showing the strain palpograms produced using pressure differences of 2 and 7 mmHg [28].

1.2.2 Airways Compliance

The most important methods currently employed to detect the airways stiffness are lung function tests such as spirometry. These techniques provide information of the total system making possible the evaluation of the respiratory system.

Recently, an acoustic transmission line model (TLM) has been used to obtain information of the cross sectional area profile and wall discontinuity [29]. Wayne L.

Capper, Guelke, and Bunn [29, 30] used TLM and time domain acoustic reflectometry in order to obtain quantitative information of the attenuation plot and indirectly compute the local wall compliance in order to measure the input impedance of the mouth and diagnose certain pathological conditions where the airways walls become excessively compliant.

1.2.2.1 Spirometry

Spirometry test consists of analyzing the breathing with an instrument called a spirometer. The spirometer records the amount and the rate of air that is breathed in and out over a specified time, allowing physicians to obtain information about the respiratory system, making the analysis of the total system compliance possible.

1.3 Tube wall compliance estimation by acoustic reflectometry

We propose pulse-echo acoustic reflectometry as a noninvasive technique to detect pathological anomalies of the airways and blood vessels. The goal is to estimate the wall compliance through the measurement of transversal frequencies, since these frequencies are dependant only upon the tube wall properties; they are obtained from the computed characteristic acoustic impedance. This technique was implemented using an acoustic pulse to interrogate the system and to obtain its time domain response, and from this response compute the reflection coefficient and characteristic acoustic impedance. The importance of the transient pulse is that, it can be designed with a specific bandwidth to interrogate the system between the resonant frequencies without having to make a frequency sweep as with sinusoid interrogation. This technique provides an innovative tool to measure the wall local compliance, without the necessity of touching the tube wall, inflating the tubes, or being near or underneath the affected area to estimate the tube wall properties.

Transmission line theory was used in order to study the acoustic behavior of different tubes in different media such as water and air. This analysis allowed us to observe the behavior of the characteristic acoustic impedance and conclude what type of material should be used in the experiments. Air-filled latex tubes exhibit its resonance frequencies in the audible ranges and can be measured with standard microphones. The selected

tubes had different thickness in order to observe the changes in the characteristic impedance shape and the change in wall compliance. The obtained results were compared with the results obtained from a volumetric technique and with those predicted by the transmission line model.

1.4 Objectives

The main objective of this research was to determine the feasibility of employing time-domain acoustic reflectometry to estimate and detect changes in the mechanical wall compliance of air-filled latex tubes of various thicknesses. Of particular interest was to investigate how changes in tube wall thickness affect the shape of the characteristic acoustic impedance $Z_o(j\omega)$ curve, and therefore, how the tube wall compliance changes. Knowledge of the relationship between tube wall compliance and the transversal frequency obtained from the characteristic acoustic impedance magnitude curve can be used to determine tube wall compliance from measurements of its acoustic impedance.

An acoustic transmission line model was implemented on computer simulations in order to generate simulated data when the different parameters varied and compare the results of the characteristic acoustic impedance shape with the acoustically measured. The latex tubes were tested in the laboratory using acoustic reflectometry, stress-strain and volumetric test, and these experimental results were compared with the simulations. These comparisons helped us to understand the quality of the transmission line model to predict the compliance of non-rigid conduits.

The methods developed and results obtained from this research could serve as groundwork for the development of a device that can be used clinically to determine the vulnerability of atherosclerotic plaque and estimate the arterial mechanical compliance, using pulse-echo acoustic reflectometry. This technique uses a transient acoustic pulse designed with a specific bandwidth to interrogate the system. This is an innovative tool to estimate the local wall compliance in a cost-effective manner without touching the tube wall, inflating the tubes, or to be near or underneath the affected area, to estimate the tube wall property.

1.5 Organization

This thesis document is divided into five chapters. The first chapter introduces the clinical problem related to the wall compliance changes in biological conduits, methods employed to measure compliance and the research objectives. The second chapter contains the background theory of acoustic reflectometry, a model of sound propagation in non-rigid tubes using transmission line analogies. The associated equations to compute the wall compliance were derived from the solution of the transversal and natural frequencies. The third chapter details the implementation of the sensitivity analysis where the properties of the tube such as Young's modulus, inner diameter, wall thickness, wall density and wall viscosity were varied by simulation, using a lumped transmission line model for a section of compliant tubes to observe their effects on the characteristic acoustic impedance. Chapter four provide a complete description of the measurement system of pulse echo acoustic reflectometry, and an experiment results. Finally the last chapter contains the conclusions from the in vitro and computer simulation studies and provides the recommendation for the feature work.

2 Background

In this section we present the background in which this research project was based. Initially, we present a brief history of time domain acoustic reflectometry followed by its principles and basic theory. The next section explains the acoustical electric analogies and transmission line model (TLM) that were used to predict the characteristic acoustic impedance of different compliant tubes. Finally, we explain how the wall compliance was estimated using mechanical methods.

2.1 Time domain acoustic reflectometry

Acoustic pulse reflectometry was originally developed as a seismological technique for the observation of stratifications in the Earth's crust. Since then it has been used to characterize and determine systems' properties. This technique has been employed in different areas such as sonar and radar to locate moving targets, in electric transmission line faults, measurement of area-distance profiles of musical instruments [31], survey the composition of layers in seismography, and in medical diagnostic.

In the early seventies, a medical research team led by Sondhi noted the potential of acoustic pulse reflectometry as a method for measuring airway dimensions. In 1977, Jackson [31] published an investigation of area profiles developed in dogs in which the tracheas and lungs were measured using a pulse reflectometer. It was not until 1980 that the first measurements on human patients were carried out by Fredberg [31], and from this moment the noninvasive acoustic pulse reflectometry has been a method used to diagnose human health conditions. Recently, the acoustic reflectometry is used as a noninvasive technique to measure the cross sectional area profile of vocal tract, and airways conduits.

2.1.1 Principles

Time domain acoustic reflectometry is a concept used to study the properties of systems using acoustic pulses. In this research, compliant tubes were interrogated using planar waves that propagated into the source tube. Fig. 2.1 shows in more detail all the

parts that constitute a reflectometer such as speaker, microphone, source tube and object under investigation.

The principle of acoustic reflectometry consists in an acoustic pulse that is generated by a speaker, travels into the source tube and then into the object under investigation. The acoustic pulse undergoes partial reflection at each change of acoustic impedance caused by change in area profile or by changes in wall material properties. The incident and reflected acoustic signals are recorded by a microphone located in the source tube, and analyzed to obtain the reflection coefficient and the input characteristic acoustic impedance $Z_0(j\omega)$ of the compliant tubes.

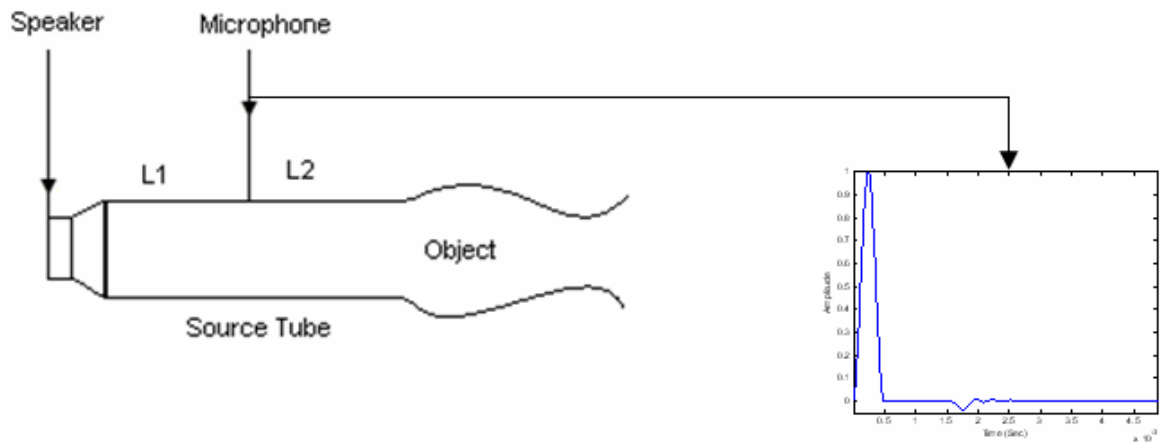


Fig. 2.1 Overview of time domain acoustic reflectometry

2.1.2 Basic Theory

According to acoustic reflectometry principles, when a sound wave travels inside a pipe and encounters an impedance change caused by a cross sectional area change, or changes in wall properties, or thickness, a portion of the wave is transmitted, and another part is reflected as shown in Fig. 2.2 [32-34]. The characteristic acoustic impedance $Z(j\omega)$ of each medium is defined as the ratio of the pressure and volume velocity and is mathematically expressed as

$$Z(j\omega) = \frac{P(j\omega)}{U(j\omega)} \quad \frac{\text{dyne} \cdot \text{s}}{\text{cm}^5}, \quad (2.1-1)$$

where $P(j\omega)$ is the sound pressure in dyne/cm^2 and $U(j\omega)$ is the volume velocity in cm^3/s . Note that the unit of force is the dyne which is equal to $1 \text{ g}\cdot\text{cm}/\text{sec}^2$. For planar wave propagation in a lossless tube the characteristic impedance $Z(j\omega)$ is determined by:

$$Z_0 = \frac{\rho_0 c}{S} \quad \frac{\text{dyne}\cdot\text{s}}{\text{cm}^5} \quad (2.1-2)$$

where ρ_0 is the density of the gas in g/cm^3 , c is the sound speed in cm/s and S is the cross sectional area in cm^2 . Note that for lossless tube the characteristic impedance is constant.

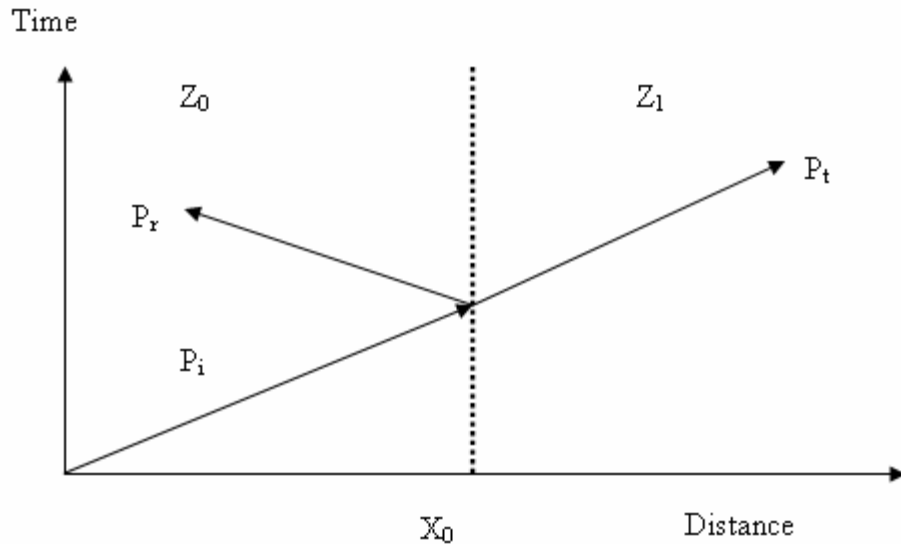


Fig. 2.2 Behavior of a propagating acoustic pulse on different media.

In the case of a lossy tube, the characteristic acoustic impedance is frequency dependent. Different models are used to describe its behavior such as acoustic-electric analogies, mechanical models between others. In our case the characteristic acoustic impedance will be described using the transmission line model described in section 2.

To describe wave propagation into the tube, we consider a planar wave $P_i(x,t)$ that travel inside the cylindrical pipe. A portion of the sound $P_t(x,t)$ is transmitted to the second boundary and other portion of sound $P_r(x,t)$ is reflected through the first boundary

at a distance $x = x_0$ as shown in Fig. 2.2. The mathematical expression in function of pressure and volume velocity is described as:

$$P_i(x_0, t) + P_r(x_0, t) = P_t(x_0, t) \quad (2.1-3)$$

and

$$U_i(x_0, t) - U_r(x_0, t) = U_t(x_0, t) \quad (2.1-4)$$

A dimensionless reflection coefficient $R(x_0)$ at a particular boundary $x = x_0$ is defined as the ratio of the reflected pressure $P_r(x_0, t)$ and the incident pressure $P_i(x_0, t)$ and replacing equation (2.1-1, 2.1-4, 2.1-5) we get

$$R(x_0) = \frac{P_r(x_0, t)}{P_i(x_0, t)} = \frac{Z_1 - Z_0}{Z_1 + Z_0} \quad (2.1-5)$$

The estimation of the characteristic acoustic impedance of the second boundary is obtained from equation (2.1-5)

$$Z_1(j\omega) = \frac{1 + R(j\omega)}{1 - R(j\omega)} Z_0(j\omega) \quad (2.1-6)$$

2.1.3 Sound propagation in tube

The behavior of sound propagation in tubes is analogous to the behavior of electrical transmission lines and are easily describe by drawing upon electrical circuits theory and some well known results for one-dimensional wave on transmission lines [35].

To ensure an acoustic plane pulse inside the tube, it is necessary to select an excitation frequency less than the cutoff frequency f_c of the lower non-planar propagation mode which is

$$f_c = \frac{c}{1.707d} \quad (2.1-7)$$

where d is the largest diameter tube and c is the sound speed.

The minimum distance d_s required to which one can distinguish between two closely spaced reflection boundaries is given by

$$d_s = \frac{\lambda_s}{2} = \frac{c}{2f_c}, \quad (2.1-8)$$

where d_s is the minimum separation distance and λ_s is the shortest wavelength (c/f_c), will result in a composite reflection consisting of temporally overlapping reflections, thus reducing the ability to accurately measure not only the time difference between the reflections, but their respective reflection coefficients as well [36].

2.2 Transmission Line Model

It was proposed in previous studies that the behavior of sound propagation in pipes is analogous to the behavior of an electrical transmission line [36]. This analogy is convenient to use because a complex system can be described using circuit drawings and symbols like resistors, inductors, and capacitors. Each of these elements represents a physical variable of acoustic system. This approach gives an opportunity to study the behavior of sound propagation in pipes using electrical analysis concepts.

The acoustic resistance represents different mechanics losses and occurs by two phenomenon; fluid resistance or radiation resistance. Acoustical energy is changed into heat by the passage of the acoustic wave through an acoustical resistance. The resistance is due to viscosity [37]. Energy is lost by the system when the volume displacement of a fluid or gas is driven through an acoustical resistance by a pressure P .

The inductor represents the inertance. In the acoustic system the inertance is represented as the fluid contains in a tube in which all the particles move with the same phase when actuated by force due to pressure [37]. It decreases when the volume decrease, and remains constant when the volume of inertance remains constant.

The compliance is a mechanical potential energy associated with the compression of a fluid or gas. Acoustical energy increases when the fluid or gas is compressed. It increases as the gas or fluid is compressed and decreases as the gas or fluid decompressed. Acoustical compliance is the acoustic element which opposes a change in the pressure [37].

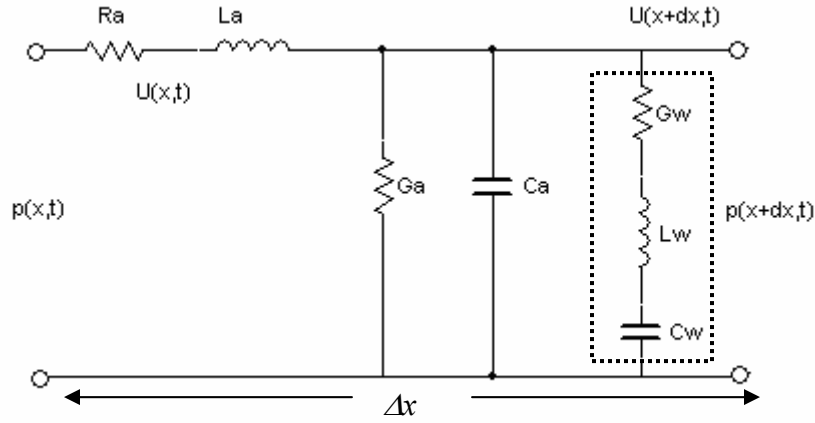


Fig. 2.3 Lumped model for acoustic-electrical models in one dimensional wave propagation on a short segment of pipe.

Now consider the length dx in the complete electrical systems depicted in Fig. 2.3 which are composed by a section of a basic TLM and an extended resonant circuit. This model was proposed by Flanagan et al. [35] in order to study the wave propagation into the pipes. The basic TLM account the losses caused by the medium whereas the extended resonant circuit account the loss caused by the pipe wall.

In this model, the voltage E is analogous with the pressure P and volume velocity U analogous to the current I . Each element in the circuit represents: fluid resistance, inertance and compliance of the lumen and tube wall. R_a , L_a , G_a and C_a represents the medium properties inside the tube, whereas wall property is represented by R_w , L_w , C_w .

The acoustic inertance L_a per unit length is

$$L_a = \frac{\rho_0}{S} \quad \frac{\text{dyne} \cdot \text{s}^2}{\text{cm}^6} \quad [36], \quad (2.2-1)$$

where ρ_0 is the density of the medium in g/cm^3 . The viscosity friction R_a at the tube wall per unit length is

$$R_a = \frac{2}{\pi r^3} \sqrt{\frac{w \rho_0 \eta}{2}} \quad \frac{\text{dyne} \cdot \text{s}}{\text{cm}^6}, \quad (2.2-2)$$

where η is the shear of the viscosity effect of the medium in $\text{dyne} \cdot \text{s/cm}^2$. Note that this viscous resistance is proportional to frequency and grows rapidly with decreasing tube

radius, as is evident by its inverse relationship to r^3 . The acoustic compliance C_a per unit length is

$$C_a = \frac{S}{\rho_0 c^2} \quad \frac{cm^4}{dyne} \quad (2.2-3)$$

The heat conductance G_a at the tube wall per unit length is

$$G_a = \frac{2\pi r(\nu-1)}{\rho_0 c^2} \sqrt{\frac{kW}{2c_p \rho_0}} \quad \frac{cm^4}{dyne \cdot s} \quad (2.2-4)$$

where ν is the ratio of specific heats at constant pressure (c_p/c_v), k is the heat conduction coefficient in $cal/cm-s-^\circ C$ and c_p is the specific heat at constant pressure in $cal/g-^\circ C$. The combined effects of viscous friction and heat conduction account for the increased, frequency dependent attenuation encountered in narrow lumen tubes. Table I lists physical properties for air.

TABLE I PHYSICAL PROPERTIES FOR AIR FILLED PIPES USED ON EXPERIMENTS

PROPERTY	SYMBOL/UNITS	Air
Density	$\rho_0 (g/cm^3)$	$1.14E-3 @ 37^\circ C$ [36]
Wall internal viscosity	$\eta (dyne \cdot s/cm^2)$	$1.86E-4 @ 20^\circ C, 1atm$ [36]
Sound speed	$C(cm)$	$35400 @ 37^\circ C$ [36]
Specific heat ratio	$\nu = C_p/C_v$	1.4 [36]
Specific heat at constant pressure	C_p	$0.24 @ 0^\circ C, 1atm$ [36]
Specific heat at constant volume	C_v	0.171 [36]
Heat conduction	K	$0.064E-3 @ 37^\circ C$ [36]

The effect of yielding wall on the acoustic behavior of non-rigid tubes is considered by incorporating the wall properties in term of their inherent resistance, inertance and compliance [30]. The series combination of these elements acts as wall conductance that can be added to the circuit model. The acoustical inertance is defined as $mass/A^2$ where A is the area perpendicular to the motion. Since the motion of the wall is in the radial direction, A is the internal surface area of the tube wall which is simply the tube circumference times the tube length l , or $2\pi rl$. The mass of the wall of this radially

sliced tube of length l is $\rho_w h A$. From definition, the volumetric inertance of the wall is given by

$$L_w = \frac{\rho_w h}{2\pi r} \quad \frac{\text{dyne} \cdot \text{s}}{\text{cm}^4}, \quad (2.2-5)$$

where ρ_w is the wall density in g/cm^3 . Small pressure variation inside the non-rigid tube caused the internal radius change making it a compliant system. The wall compliance per unit length is

$$C_w = \frac{2\pi r^3 l}{Eh} \quad \frac{\text{cm}^4}{\text{dyne}}, \quad (2.2-6)$$

where E is the young's modulus of the wall tubes in dyne/cm^2 . The wall resistance per unit length is given by

$$R_w = \frac{\eta_w h}{2\pi r^3 l} \quad \frac{\text{dyne} \cdot \text{s}}{\text{cm}^6}. \quad (2.2-7)$$

Sound pressure and volume velocity for the plane wave propagation in a uniform tube satisfy the same wave equation as do voltage and current on a uniform transmission line [36]. Applying the Kirchhoff's Laws in terms of pressure and volume velocity to the transmission line of Fig. 2.3, we have

$$p(x,t) - (R_a + j\omega L_a)\Delta x U(x,t) - p(x + \Delta x, t) = 0, \quad (2.2-8)$$

$$U(x,t) - ((G_a + j\omega C_a) + Z_w)p(x,t) - U(x + \Delta x, t) = 0, \quad (2.2-9)$$

And dividing all terms by Δx and rearranging terms and taken the limit when $\Delta x \longrightarrow 0$ we obtain

$$\frac{-dp(x)}{dx} = (R_a + J\omega L_a)U(x) \quad (2.2-10)$$

$$\frac{-dU(x)}{dx} = ((G_a + J\omega C_a) + Z_w)p(x) \quad (2.2-11)$$

From the first order coupled equations (10, 11) can be combined to give two second order uncoupled wave equation (11, 12).

$$\frac{d^2 p(x)}{dx^2} - \gamma^2 p(x) = 0 \quad (2.2-12)$$

and

$$\frac{d^2 U(x)}{dx^2} - \gamma^2 U(x) = 0, \quad (2.2-13)$$

where

$$\gamma = \sqrt{(Ra + j\omega Ca)(Ga + j\omega Ca) + Zw} = \alpha(\omega) + \beta(\omega). \quad (2.2-14)$$

The above expression gives the attenuation $\alpha(j\omega)$ and the phase coefficient $\beta(j\omega)$.

Therefore the second order differential equation of second order solution:

$$p(x) = p_0^+ e^{-\gamma x} + p_0^- e^{\gamma x} \quad (2.2-15)$$

$$U(x) = U_0^+ e^{-\gamma x} + U_0^- e^{\gamma x} \quad (2.2-16)$$

Comparison each term with the corresponding term in the expression given in the above equation leads to the conclusion that

$$\frac{p_0^+}{U_0^+} = Z_1 = \frac{-p_0^-}{U_0^-}. \quad (2.2-17)$$

Therefore the characteristic impedance is

$$Z_1(\omega) = \frac{R_a + j\omega L_a}{(G_a + j\omega C_a) + \left(\frac{1}{R_w + j\omega L_w + \frac{1}{j\omega C_a}} \right)} = \sqrt{\frac{R_a + j\omega L_a}{(G_a + j\omega C_a) + Y_w}}. \quad (2.2-18)$$

The characteristic acoustic impedance shape exhibits two points where the absolute value is maximum and minimum. These values can be indirectly calculated, because the wall property is accounted from RLC serial circuits. It is known that the RLC system resonates at a specific frequency when the capacitive and inductive reactance is the same. If we manipulate the resultant expression, the wall resonance frequency (f_{res}) can be obtained using

$$f_{res} = \frac{1}{2\pi} \sqrt{\frac{1}{L_w C_w}} = \frac{1}{2\pi r} \sqrt{\frac{E}{\rho_w}}, \quad (2.2-19)$$

where E is the dynamic young module, ρ_w is the wall density and r is the tube radius.

Note that f_{res} is inversely proportional to the lumen radius and proportional to the square root of the Young's modulus over the wall density. The walls resonance is not dependent on tube length or wall thickness [36]. At this frequency the tube exhibits an elastic behavior and alters cross sectional area in response to the pressure change. This is caused because near this frequency the impedance exhibits its minimum absolute value.

In addition, a portion of the energy involved in the radial motion of the tube wall is dissipated as a consequence of the heat conduction and wall viscosity. There is an extended frequency limit f_2 where the characteristic impedance reaches a maximum [19]. An expression for f_2 is

$$f_2 = \frac{1}{2\pi} \sqrt{\frac{C_a + C_w}{L_w C_w C_a}} = \frac{1}{2\pi} \sqrt{\frac{E}{\rho_w r^2} + \frac{2\pi r \rho_0 c^2}{h \rho_w S}}. \quad (2.2-20)$$

Therefore, the attenuation per unit length of a sound pressure wave propagating down non-rigid tubes is low at frequencies significantly below f_{res} and above f_2 , and high at frequencies between f_{res} and f_2 . An additional characteristic of f_2 also defines the frequency at which the phase velocity reaches maximum.

The frequency or frequencies at which an object tends to vibrate with when hit, struck, plucked, strummed or somehow disturbed is known as its own natural frequency. This occur because the medium and the wall tube are forced to vibrate with the source that is moved through the medium, therefore analyzing the transmission line model when

the acoustic and wall inertance are canceled with the acoustic and wall compliance, which the natural frequency is

$$f_r = \frac{1}{2\pi} \sqrt{\frac{C_a + C_w}{C_w C_a (L_a + L_w)}} = \frac{1}{2\pi} \sqrt{\frac{EhS + 2\pi r^3 \rho_0 c^2}{r^2 (h\rho_w S + 2\pi r \rho_0)}}. \quad (2.2-21)$$

A quality factor Q_w , describing the sharpness of the wall volume velocity response curve obtained from $U_w(\omega) = P_w(\omega)/Z_w(\omega)$, is determined by the maximum and minimum amount of energy that can be stored in the wall, compared with the energies that is lost during one complete period of the response. For a series *RLC* circuit, the quality factor is given as

$$Q_w = \frac{\omega_r}{BW} = \frac{\omega_r}{R_w(\omega)/L_w} = \frac{1}{R_w(\omega)} \sqrt{\frac{L_w}{C_w(\omega)}}, \quad (2.2-22)$$

where BW is the half-power bandwidth of the resonant peak located at $\omega_r = 2\pi f_r$. Substituting into the Equations 2.2-22 the definition of each parameter is obtained

$$Q_w = \frac{r \sqrt{\rho_w E_{dyn}(\omega_r)}}{\eta_w(\omega_r)}. \quad (2.2-23)$$

This expression becomes very useful in understanding how the tube radius and wall tissue properties affect Q . A wall damping factor ζ_w , that describes the degree of damping in the wall is defined as

$$\zeta_w = \frac{1}{2Q_w}. \quad (2.2-24)$$

Notice that when the wall damping factor is unity, the system is considered to be critically damped, and when the wall damping is less than and greater than unity, the system is considered to be underdamped and overdamped, respectively.

2.3 Compliance Estimation

2.3.1 Wall compliance estimation by transversal frequencies

Wayne L. Capper and et al. [29] proposed to estimate the wall compliance through the transversal frequencies observed from the characteristic acoustic impedance. These frequencies are only dependent on the tube wall parameters. As it was demonstrated in [29], the transversal resonant frequencies are

$$f_{res} = \frac{1}{2\pi} \sqrt{\frac{1}{L_w C_w (1+k^2)}} \quad (2.3-1)$$

$$f_r = \frac{1}{2\pi} \sqrt{\frac{C_a + C_w (1+k^2)}{C_w C_a (L_a + L_w) (1+k^2)}} \quad (2.3-2)$$

where k is the wall loss factor. Combining equations 2.1-1 and 2.3-2, considering a loss factor lower than 0.1, results in the following expression:

$$C_w = \left(\left(\frac{f_2}{f_{res}} \right)^2 - 1 \right) C_a \quad (2.3-3)$$

2.3.2 Wall compliance estimation by natural and resonant frequencies

Since the transverse resonance and natural frequencies are only dependent on the medium and wall properties, the wall compliance could be inferred if both frequencies are obtained. The natural frequency occurs when the imaginary parts of the transmission line model solution are canceled; it can be mathematically expressed as equation 2.2-21. This frequency can be obtained from the Fourier transform of the natural response. Additionally, the transversal resonant frequency only depends on the wall properties. Therefore, analyzing the *RLC* circuit, when $\omega_{res}^2 > \alpha^2$, the response of the system is underdamped, where ω_{res} is the transversal resonant frequency and α is the neper frequency. For this case, the damped frequency is $\omega_d^2 = \omega_{res}^2 - \alpha^2$. The transversal

resonant frequency is given by equation 2.2-19. Combining equations 2.2-19 and 2.2-21 results in an expression in which the wall compliance can be expressed as

$$C_w = \frac{\left(1 - \left(\frac{f_r}{f_{res}}\right)^2\right)}{C_a L_a (2\pi f_r)^2 - 1} C_a \quad (2.3-4)$$

where f_r is the natural frequency and f_{res} is the transversal resonant frequency. The resonant frequency is computed using the damped frequency obtained from the characteristic acoustic impedance. The neper frequency ($\alpha = R_w / (2L_w)$) is obtained examining the exponential decay of the natural response since the reflection response is given by

$$R(t) = Ae^{-\alpha t} (\cos \omega_d t + j \sin \omega_d t) \quad (2.3-5)$$

2.4 Summary

In this chapter, some important and fundamentals concepts regarding the techniques of acoustic reflectometry and transmission line model were introduced. The first section begun with the mathematic development of acoustic reflectometry in two dimensions, when an acoustic planar wave travel into hollow conduits and encounter a boundary condition caused by two different characteristic acoustic impedances. Also, the characteristic acoustic impedance of the second boundary was related to the reflection coefficient. The second section introduced a lumped transmission line model, which describes the acoustic propagation into tubes. The elements of the transmission line were related with the parameters associated with the medium and tube wall. Since the used tubes were uniform and the wave length of the incident pulse is greater than a section of the transmission line model, the analysis of a section was made using basic principles of circuit's analysis. Two expressions that describe the transversal and natural frequencies were deduced and used to obtain two expressions to estimate the wall compliance.

3 Sensitivity Analysis

This section presents the simulations that were performed using the transmission line model to represent the acoustic propagation in uniform compliant tubes. The procedures used to compute the acoustic responses in both, the frequency and time domains are presented in the first section. The second section presents the results and discussion for different tests conducted, in order to analyze how the input characteristic acoustic impedance and wall compliance are affected by different parameters such as wall density, inner diameter, Young's modulus, wall viscosity and wall thickness. The last section presents the analysis of the time domain echo-acoustic reflectometry to assess the characteristic acoustic impedance and wall compliance.

3.1 Method

Computer simulations based on the acoustic transmission line model were performed in MATLAB to analyze the characteristic acoustic impedance of compliant pipes and to determine if the local wall compliance could be estimated using acoustic reflectometry. A section Δx of a transmission line model depicted in the Fig. 2.3 was used represent a short section of compliant tube of length l . The transmission line lumped elements were computed using the equations depicted on the Table II. The input characteristic acoustic impedance and the reflection coefficient in function of frequency were computed using the equations 2.2-18 and 2.1-5 respectively. Both expressions become

$$Z_1(\omega) = \sqrt{\frac{Z_a(\omega)}{Y_a(\omega) + Y_w(\omega)}} \quad (3.1-1)$$

and

$$R(\omega) = \frac{Z_1(\omega) - Z_0}{Z_1(\omega) + Z_0}. \quad (3.1-2)$$

$Z_1(\omega)$ and $R(\omega)$ were computed as finite –length sequences in the frequency domain and are of length N . These sequences can be called the *discrete input characteristic impedance* and the *discrete reflection coefficient* respectively.

The acoustic response in time domain was computed by performing the convolution between the input acoustic pulse and the inverse fast Fourier of the reflection coefficient obtained from the equation 3.1-2 where

$$y(t) = x(t) \otimes \mathfrak{F}^{-1}\{R(\omega)\}. \quad (3.1-3)$$

Notice that $x(t)$ is the arbitrary incident pulse that will be used to interrogate the system and $\mathfrak{F}^{-1}\{R(\omega)\}$ is the inverse Fourier transforms of the reflection coefficient. The sequence $y(t)$ represents the same data that will be obtained in the second reflection experimental measurement after the incident signals. Therefore this result was used to evaluate if the wall compliance could be estimated from time domain echo-acoustic reflectometry technique.

In this research, pulse-echo acoustic reflectometry is proposed in which the acoustic reflection coefficient $R^*_{sim}(\omega)$ was computed from the relation of the output signal (reflection signal) over the input signal (incident signal) multiplied by the time shifting.

$$R^*_{sim}(\omega) = \frac{P_r(\omega) \cdot e^{j\omega T_d}}{P_i(\omega)}, \quad (3.1-4)$$

where $P_i(\omega)$ and $P_r(\omega)$ are the Fourier transforms of the incident and reflected pulse respectively, and e^{jkT_d} represents the time delay between the incident and reflected signals. The time T_d is considered because the reflection and incident pulse don't occur at the same time. The reflection coefficient of the equation 3.1-4 is based on echo-acoustic time domain reflectometry analysis, notice that it is represented by $R^*(\omega)$.

The input characteristic acoustic impedance $Z^*_{1sim}(\omega)$ was obtained considering the analysis of the acoustic reflectometry in which we have

$$Z^*_{1sim}(\omega) = \frac{1 + R^*(\omega)}{1 - R^*(\omega)} Z_0(\omega), \quad (3.1-5)$$

where $Z_0(\omega)$ is the characteristic acoustic impedance of the first medium (the reflectometer), which is expressed as

$$Z_0(\omega) = \frac{\rho_0 c}{S}. \quad (3.1-6)$$

TABLE II TRANSMISSION LINE MODEL PARAMETERS

Symbol	Description	Expression
R_a	Viscous Friction	$R_a = \frac{2}{\pi r^3} \sqrt{\frac{w \rho_0 \eta}{2}}$
C_a	Compliance	$C_a = \frac{S}{\rho_0 c^2}$
L_a	Inertance	$L_a = \frac{\rho_0}{S}$
G_a	Heat Conductance	$G_a = \frac{2\pi r(v-1)}{\rho_0 c^2} \sqrt{\frac{kw}{2c_p \rho_0}}$
R_w	Wall Resistance	$R_w = \frac{\eta_w h}{2\pi r^3}$
C_w	Mechanical Wall Compliance	$C_w = \frac{2\pi r^3}{Eh}$
L_w	Wall Inertance	$L_w = \frac{\rho_w h}{2\pi r}$

Once the input characteristic impedance was computed, the transversal resonant frequencies f_{res} and f_2 were obtained from the two peaks of the characteristic acoustic impedance shape. These two peaks will be used to compute the local wall compliance where

$$C_w^*_{Sim} = \left(\left(\frac{f_2^*}{f_{res}^*} \right)^2 - 1 \right) * C_a. \quad (3.1-7)$$

Additionally the transversal resonant frequencies f_{res} and the natural frequency f_r were obtained from the max peak of the reflection coefficient and from the Fourier transform of the natural response, respectively. Then, these two frequencies will be used to compute the local wall compliance where

$$C_w^{**sim} = \frac{\left(1 - \left(\frac{f_r^*}{f_{res}^*}\right)^2\right)}{C_a L_a (2\pi f_r^*)^2 - 1} C_a. \quad (3.1-8)$$

The transversal and natural frequencies were computed by:

$$f_{res} = \frac{1}{2\pi r} \sqrt{\frac{E}{\rho_w}} \quad (Hz), \quad (3.1-9)$$

$$f_2 = \frac{1}{2\pi} \sqrt{\frac{E}{\rho_w r^2} + \frac{2\pi r \rho_0 c^2}{h \rho_w S}} \quad (Hz), \quad (3.1-10)$$

and

$$f_r = \frac{1}{2\pi} \sqrt{\frac{EhS + 2\pi r^3 \rho_0 c^2}{r^2 (h \rho_w S + 2\pi r \rho_0)}} \quad (Hz). \quad (3.1-11)$$

3.2 Results and Discussion

The purpose of this section is to present and discuss the results obtained for wall compliance and characteristic acoustic impedance when properties such as wall thickness, wall density, inner diameter, Young's modulus and wall viscosity were varied. This section is divided in two parts that present a sensitivity analysis, where each property and dimension of the compliant pipes were varied while the others remained constant. The last part assesses the estimation of the local wall compliance using pulse-echo acoustic reflectometry.

3.2.1 Wall properties effects

A sensitivity analysis was performed in order to observe the effects of a particular property on the transversal resonant frequencies obtained from the characteristic acoustic impedance and observe the behavior of the wall compliance. The wall properties were varied considering the observed behavior of rubber-like materials found in related papers [38-40]. Table I lists the property used when the medium is air.

The reflection coefficient $R(\omega)$ and characteristic acoustic impedance $Z_1(\omega)$ were computed from 0 Hz to 20 kHz at a 10 Hz increment. These frequencies responses were computed considering the parameters of Table II.

3.2.1.1 Inner wall diameter effects

The inner wall tube diameter was varied in order to observe its effects on wall compliance, characteristic acoustic impedance and reflection coefficient. Uniform latex tubes with length $l=1\text{cm}$ and the parameters lists on Table III were considered for the diameter analysis.

Fig. 3.1 depicts the characteristic acoustic impedances as a function of frequency in Hertz. From this plot, it can be observed that the curves exhibit similar behavior, however, when the inner wall diameter decreases, the amplitude at $f=0\text{ Hz}$ and $f=\infty\text{ Hz}$ increases, the transverse frequency increases, the difference between the maximum and minimum peak decreases and the ratio f_2/f_{res} decreases.

Fig. 3.2 depicts the reflection coefficient as a function of frequency in Hz. From this plot it can be observed that the curves exhibit a similar behavior, however, when the inner wall diameter decreases, the initial and final amplitude decrease. It is important to notice that at frequencies over 14 kHz, the amplitude tends to become constant. Additionally, for the particular case when the compliant pipe inner diameter is equal to the inner diameter ($d=0.5\text{ cm}$) of the source tube, the reflection coefficient tends to zero. This can be explained because over these frequencies the pipes behave as a rigid tube and the incident pulse will propagate through the pipe.

The wall compliance values for different diameters shown in Fig. 3.3 were computed using the equation of the Table II. By observing the equation and Fig. 3.3 it can be noted that the larger the diameter, the larger the compliance value.

Analyzing specifically the characteristic acoustic impedance equation and the elements of the transmission line model when the inner wall diameters increase, it can be noted that the wall resistance, viscous friction, medium inertance and wall inertance decreases, while mechanical wall compliance, medium compliance and heat conductance increases.

When $\omega \rightarrow 0$, the characteristic acoustic impedance is equal to the square root of the viscous friction by wall resistance over the heat conductance by wall resistance plus one. When the viscous friction decreases and the heat conductance increases due to an increase in the inner wall diameter, the characteristic acoustic impedance amplitude decreases.

$$Z_0(\omega)|_{\omega=0} = \sqrt{\frac{R_w R_a}{R_w G_a + 1}} \quad (3.2-1)$$

At $\omega \rightarrow \infty$, the characteristic acoustic impedance is equal to the square root of the medium inertance divided by the medium compliance. When the medium inertance decreases and the medium compliance increases due to an increase in the inner wall diameter, the characteristic acoustic impedance amplitude decreases.

$$Z_0(\omega)|_{\omega=\infty} = \sqrt{\frac{L_a}{C_a}} \quad (3.2-2)$$

Between $1000 < \omega < 5000$, the characteristic acoustic impedance exhibits two peaks, the maximum and minimum attenuation that are located in two frequencies that are known as transversal frequencies f_{res} and f_2 . When the inner wall diameter increases, f_r and f_2 decreases. Additionally, it can be seen that the magnitude decreases when the diameter increases.

TABLE III RUBBER PIPE PHYSICAL PROPERTIES VALUES USED FOR SIMULATION.

PROPERTY	SYMBOL/UNITS	RUBBER
Density	$\rho_w (g / cm^3)$	0.92
Wall Internal Viscosity	$\eta (dyne \cdot s / cm^2)$	100
Young's Modulus of Elasticity	$E (dyne / cm^2)$	$2.3 \cdot 10^7$
Wall Thickness	$h (cm)$	0.159
Wall Radius (<i>Test 1-5</i>)	$r (cm)$	0.5, 0.55, 0.6, 0.65, 0.7

The transversal frequencies were computed from the transmission line model particular solution, and were compared with the observed values f_{res}^* and f_2^* of the characteristic acoustic impedance. Table IV lists the obtained values, it can be seen that

the transversal frequencies do not exhibit any differences between the visually obtained and calculated.

TABLE IV QUALITY FACTOR, DAMPING RATIO AND RESONANT FREQUENCIES OBTAINED FROM SIMULATIONS.

Test	Q	ζ	f_{res} (Hz)	f_2 (Hz)	f_{res}^* (Hz)	f_2^* (Hz)
d = 0.5	122	0.0041	3384	3655	3384	3655
d = 0.55	134	0.0037	3076	3347	3076	3347
d = 0.60	146	0.0034	2820	3089	2820	3089
d = 0.65	158	0.0031	2603	2871	2603	2871
d = 0.70	171	0.0029	2417	2617	2417	2617

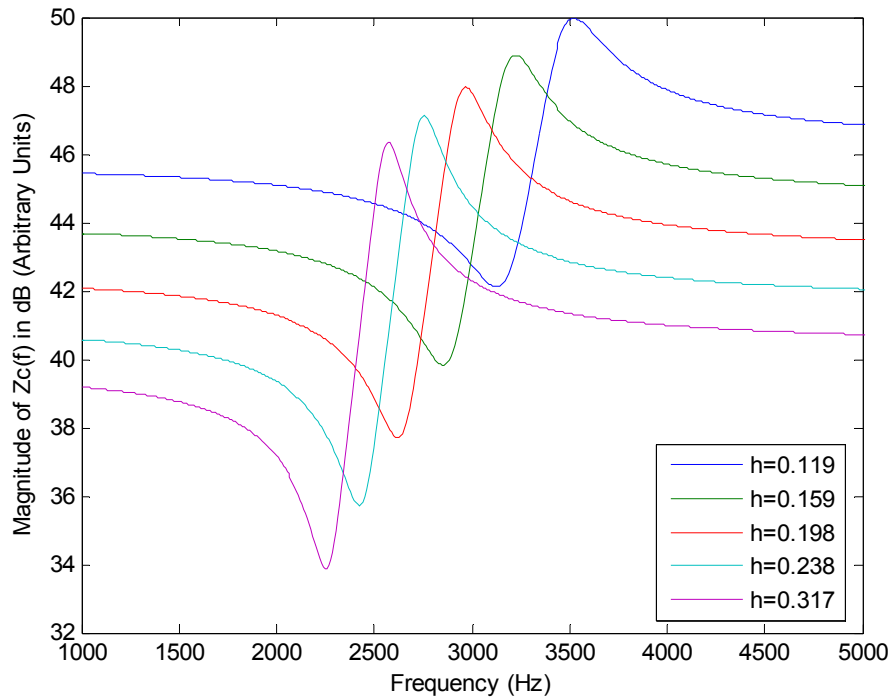


Fig. 3.1 Characteristic acoustic impedance $Z_c(f)$ for different inner diameters.

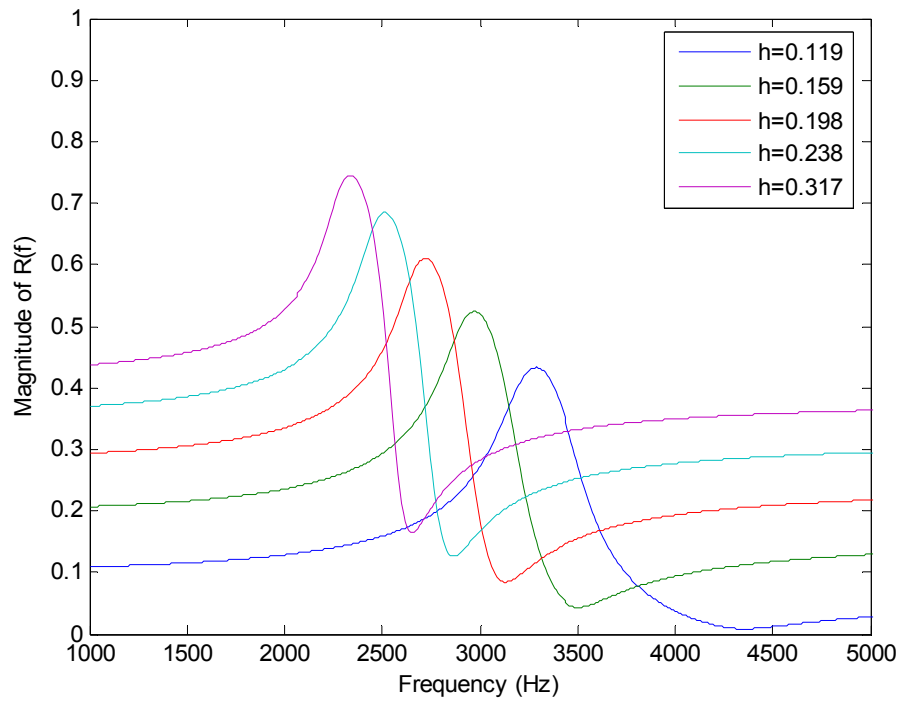


Fig. 3.2 Reflection coefficient $R(f)$ for different inner diameters.

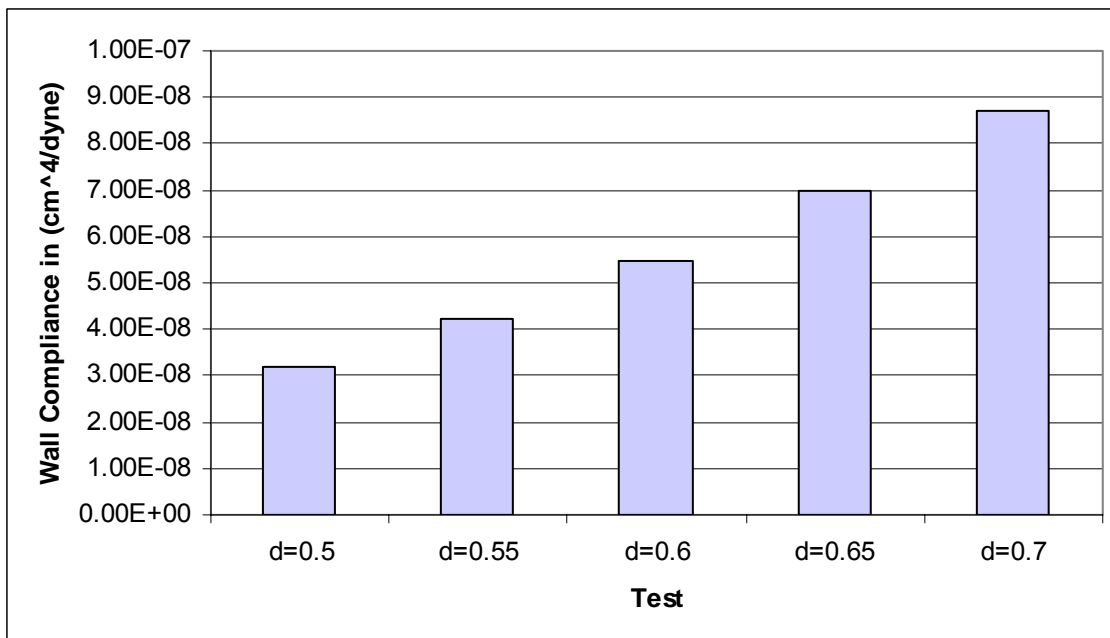


Fig. 3.3 Wall compliance (C_w) values for different tests.

3.2.1.2 Wall thickness effects

The tube wall thickness was varied in order to observe its effects on wall compliance, characteristic acoustic impedance and reflection coefficient. Uniform latex tubes with length $l=1\text{cm}$ and the parameters lists on Table V were considered for the diameter analysis.

Fig. 3.4 depicts the characteristic acoustic impedances as a function of frequency in Hz . From this plot, it can be observed that the curves exhibit similar behavior, however, when the wall thickness increases, the amplitude at $f = 1000 \text{ Hz}$ increases while at $f = 5000$ tend to remain constant, the transverse frequency f_{res} remains constant while f_2 decreases, the difference between the maximum and minimum peak decreases and the ratio f_2/f_{res} decreases.

Fig. 3.5 depicts the reflection coefficient as a function of frequency in Hz . From this plot, it can be observed that the curves exhibit a similar behavior, however, when the wall thickness increases, the amplitude at $f = 1000 \text{ Hz}$ decreases while at $f = 5000$ remain constant.

The wall compliance values for different diameters shown in Fig. 3.3 were computed using the equation of the Table II. By observing the equation and Fig. 3.6, it can be noted that the larger the wall thickness, the lower the compliance value.

Analyzing specifically the characteristic acoustic impedance equation of the transmission line model when the wall thickness increases, it can be noted that the wall resistance and wall inertance increases, while mechanical wall compliance decreases.

When $\omega \rightarrow 0$, the characteristic acoustic impedance is equal to the square root of the viscous friction by wall resistance over the heat conductance by wall resistance plus one. Wall resistance increases due to an increase in the wall thickness, while viscous friction and heat conductance remains constant because does not depend of the wall thickness. Thus the characteristic acoustic impedance amplitude decreases.

When $\omega \rightarrow \infty$, the characteristic acoustic impedance is equal to the square root of the medium inertance divided by the medium compliance. The medium inertance and the medium compliance remain constant because both do not depend of the thickness change. The characteristic acoustic impedance amplitude remain constant at frequencies $f=\infty$ when the wall thickness change.

Between $1000 < \omega < 5000$, the characteristic acoustic impedance exhibits two peaks, the maximum and minimum attenuation that are located in two frequencies that are known as transversal frequencies f_{res} and f_2 . When the wall thickness increases, f_r and f_2 increases.

TABLE V RUBBER PIPE PHYSICAL PROPERTIES VALUES USED FOR SIMULATION USED TO DETERMINE WALL THICKNESS EFFECTS.

PROPERTY	SYMBOL/UNITS	RUBBER
Density	$\rho_w (g / cm^3)$	0.92
Wall Internal Viscosity	$\eta (dyne \cdot s / cm^2)$	100
Young's Modulus of Elasticity	$E (dyne / cm^2)$	$2.3 \cdot 10^7$
Wall Thickness (Test 1-5)	$h (cm)$	0.119, 0.159, 0.198, 0.238, 0.317
Wall Radius	$r (cm)$	0.65

The transversal frequencies were computed from the transmission line model particular solution, and were compared with the observed values f_{res}^* and f_2^* of the characteristic acoustic impedance. Table VI lists the obtained values, where it can be seen that the transversal frequencies do not exhibit any differences between the visual obtained and calculated.

TABLE VI QUALITY FACTOR, DAMPING RATIO AND RESONANT FREQUENCIES OBTAINED FROM SIMULATION.

Test	Q	ζ	f_{res} (Hz)	f_2 (Hz)	f_{res}^* (Hz)	f_2^* (Hz)
h = 0.119	158	0.0031	2603	2956	2603	2956
h = 0.159	158	0.0031	2603	2871	2603	2871
h = 0.198	158	0.0031	2603	2821	2603	2821
h = 0.238	158	0.0031	2603	2785	2603	2785
h = 0.317	158	0.0031	2603	2404	2603	2404

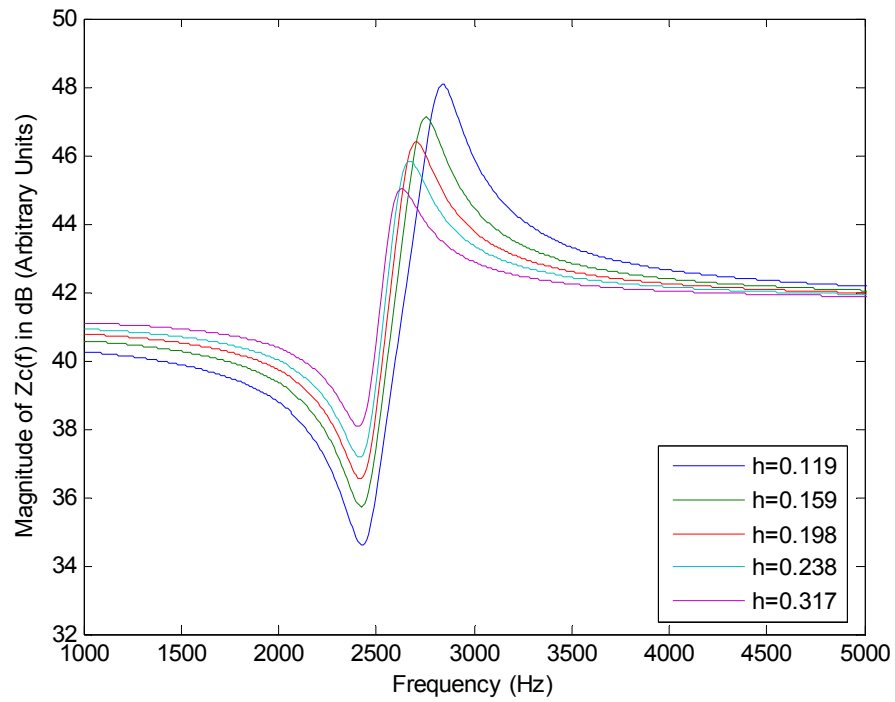


Fig. 3.4 Characteristic acoustic impedance $Z_c(f)$ for different thicknesses in cm.

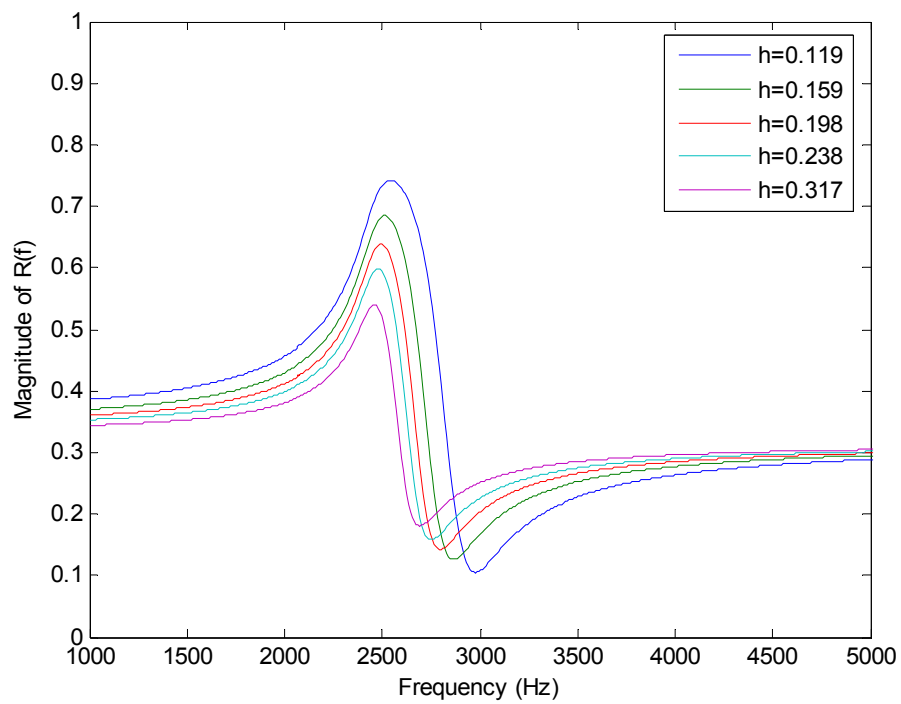


Fig. 3.5 Reflection coefficient $R(f)$ for different thicknesses in cm.

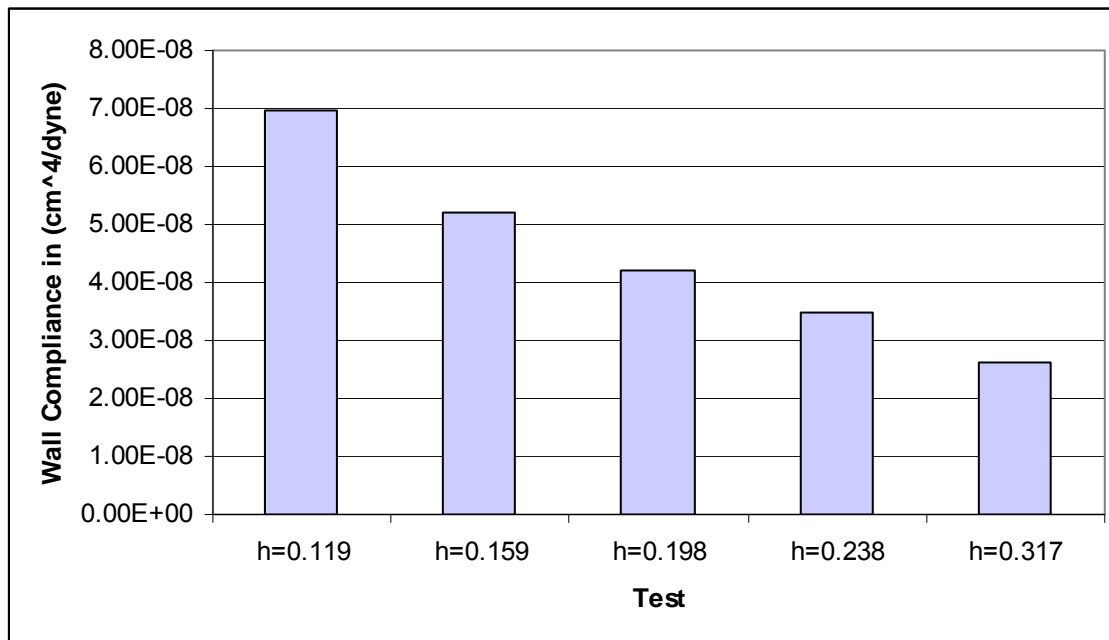


Fig. 3.6 Wall compliance (C_w) values for different thicknesses.

3.2.1.3 Wall density effects

The tube wall density was varied in order to observe its effects on wall compliance, characteristic acoustic impedance and reflection coefficient. Uniform latex tubes with length $l=1\text{cm}$ and the parameters lists on Table VII were considered for the wall density analysis.

Fig. 3.7 depicts the characteristic acoustic impedances as a function of frequency in Hz . From this plot it can be observed that the curves exhibit similar behavior, however, when the wall density increases, the amplitude at $f = 1000 \text{ Hz}$ and $f = 5000$ remain constant, the transverse frequencies values of f_{res} and f_2 decreases, the difference between the maximum and minimum peak remain constant and the ratio f_2/f_{res} remain constant.

Fig. 3.8 depicts the reflection coefficient as a function of frequency in Hz . From this plot it can be observed that the curves exhibit a similar behavior, however, when the wall density increases, the amplitude at $f = 1000 \text{ Hz}$ and $f = 5000$ remain constant.

The wall compliance values for different diameters shown in Fig. 3.9 were computed using the equation of the Table II. Observing the equation and Fig. 3.9 it can be noted that the wall compliance does not exhibit any variation when the wall density was varied.

Analyzing specifically the characteristic acoustic impedance equation of the transmission line model when the wall density increases, it can be noted that the wall inertance increases, while all others does not depend of the density changes. This parameter affects the characteristic acoustic impedance.

When $\omega \rightarrow 0$, the characteristic acoustic impedance is equal to the square root of the viscous friction by wall resistance over the heat conductance by wall resistance plus one. The amplitude in this limit remains constant because wall resistance, wall density, viscous friction and heat conductance remains constant.

When $\omega \rightarrow \infty$, the characteristic acoustic impedance is equal to the square root of the medium inertance divided by the medium compliance. The medium inertance and the medium compliance remain constant because both do not depend of the thickness change. The characteristic acoustic impedance amplitude remains constant at higher frequencies when the wall density changes.

Between $1000 < \omega < 5000$, the characteristic acoustic impedance exhibits two peaks, the maximum and minimum attenuation, that are located in two frequencies that are known as transversal frequencies f_{res} and f_2 . When the wall density increases, f_r and f_2 decreases.

TABLE VII RUBBER PIPE PHYSICAL PROPERTIES VALUES USED FOR SIMULATION.

PROPERTY	SYMBOL/UNITS	RUBBER
Density (<i>Test 1-5</i>)	$\rho_w (g / cm^3)$	0.88,0.90,0.92,0.94,0.96
Wall Internal Viscosity	$\eta (dyne \cdot s / cm^2)$	100
Young's Modulus of Elasticity	$E (dyne / cm^2)$	$2.6 \cdot 10^7$
Wall Thickness	$h (cm)$	0.159
Wall Radius	$r (cm)$	0.65

The transversal frequencies were computed from the transmission line model particular solution, and were compared with the observed values f_{res}^* and f_2^* of the characteristic acoustic impedance. Table VIII lists the obtained values, where it can be

seen that the transversal frequencies do not exhibit any differences between the visual obtained and calculated.

TABLE VIII QUALITY FACTOR, DAMPING RATIO AND RESONANT FREQUENCIES OBTAINED FROM SIMULATION.

Test	Q	ζ	f_{res} (Hz)	f_2 (Hz)	f_{res}^* (Hz)	f_2^* (Hz)
$\rho_w = 0.88$	155	0.0032	2661	2936	2661	2936
$\rho_w = 0.90$	157	0.0031	2632	2903	2632	2903
$\rho_w = 0.92$	158	0.0031	2603	2871	2603	2871
$\rho_w = 0.94$	160	0.0031	2575	2841	2575	2841
$\rho_w = 0.96$	162	0.0030	2548	2811	2548	2811

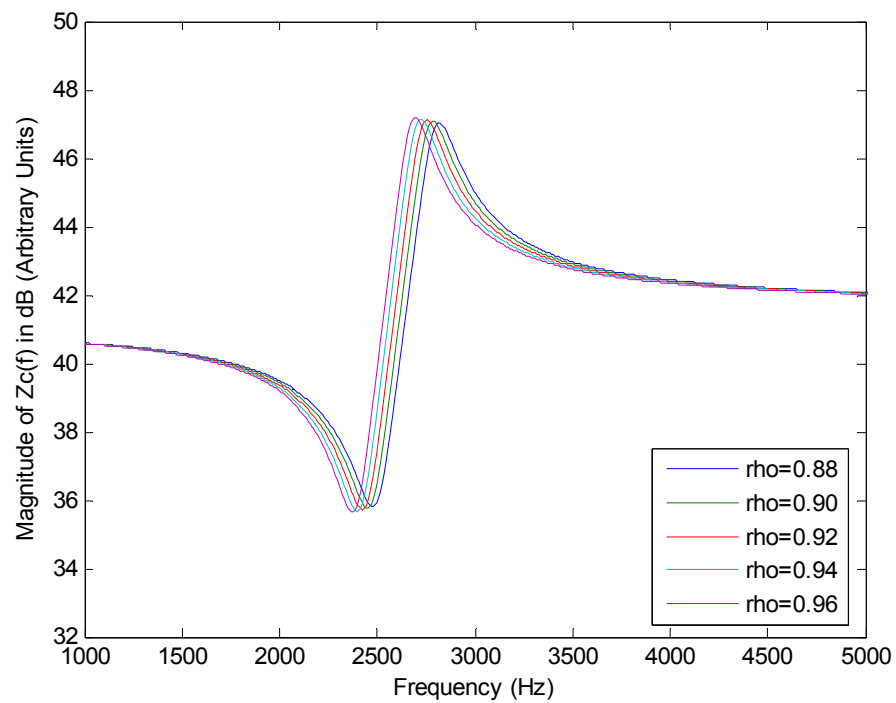


Fig. 3.7 Characteristic acoustic impedance $Z_c(f)$ for different wall densities in g/cm^3 .

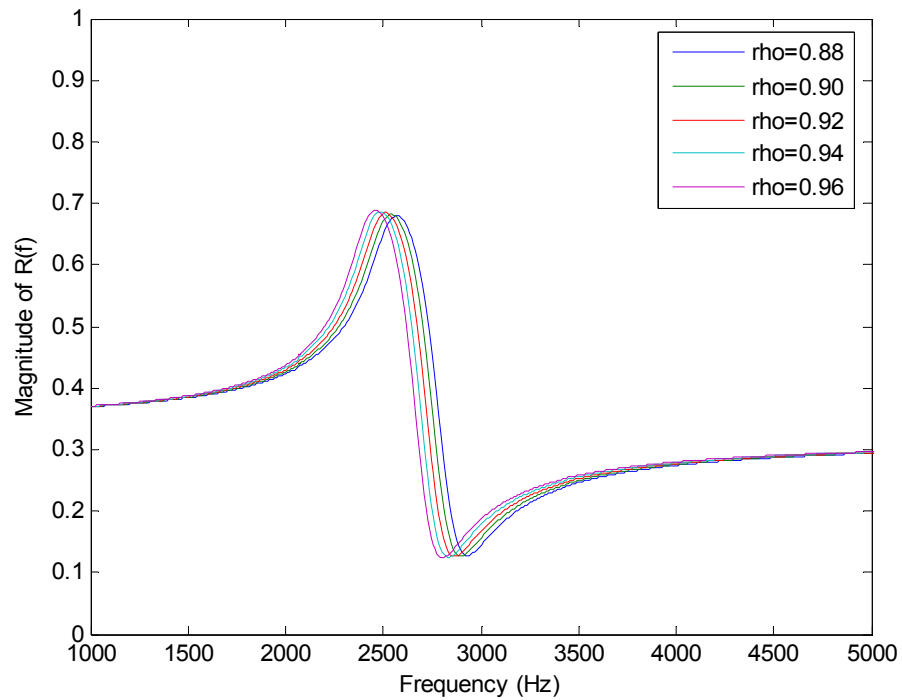


Fig. 3.8 Reflection coefficient $R(f)$ for different wall densities in g/cm^3 .

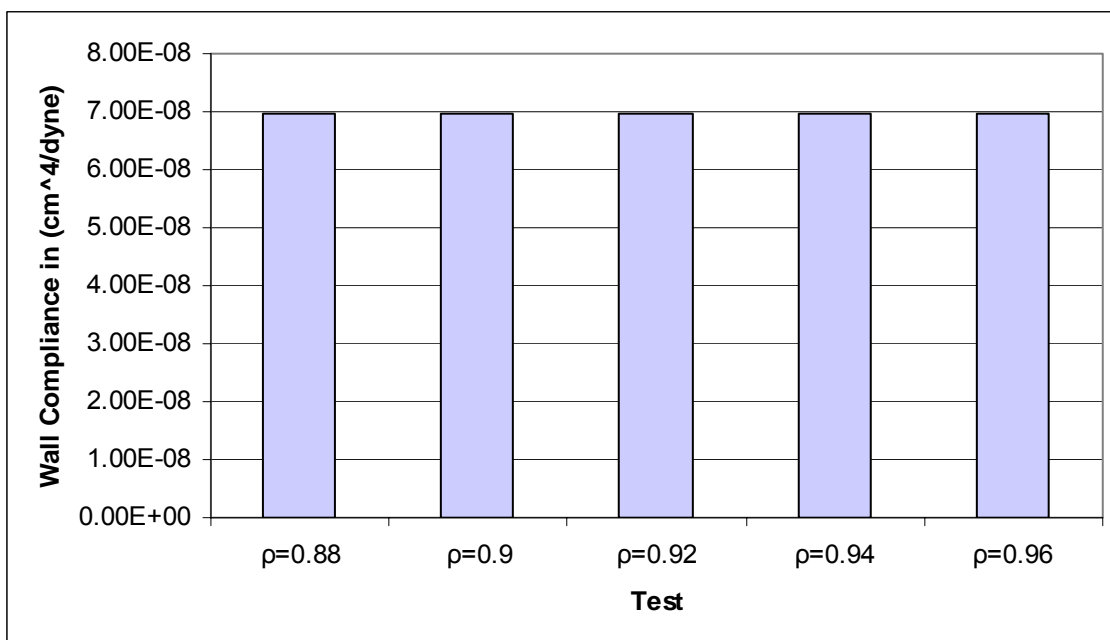


Fig. 3.9 Wall compliance (C_w) values for different wall densities in g/cm^3 .

3.2.1.4 Young's modulus effects

The Young's modulus was varied in order to observe its effects on wall compliance, characteristic acoustic impedance and reflection coefficient. Uniform latex tubes with length $l=1\text{cm}$ and the parameters lists on Table IX were considered for the wall Young's modulus analysis.

Fig. 3.10 depicts the characteristic acoustic impedances as a function of frequency in Hz . From this plot it can be observed that the curves exhibit similar behavior, however, when the Young's modulus increases, the amplitude at $f=1000\text{ Hz}$ increases while at $f=5000$ tend to remain constant, the transverse frequencies f_{res} and f_2 increases, the difference between the maximum and minimum peak decreases and the ratio f_2/f_{res} decreases.

Fig. 3.11 depicts the reflection coefficient as a function of frequency in Hz . From this plot it can be observed that the curves exhibit a similar behavior, however, when the Young's modulus increases, the amplitude at $f=1000\text{ Hz}$ decreases while at $f=5000$ tend to remain constant.

The wall compliance values for different diameters shown in Fig. 3.12 were computed using the equation of the Table II. Observing the equation and Fig. 3.12 it can be noted that the wall compliance decreases when the Young's modulus increases.

Analyzing specifically the characteristic acoustic impedance equation of the transmission line model when the Young's modulus increases, it can be noted that the wall compliance increases, while all others does not depend of the Young's modulus changes. This parameter affects the characteristic acoustic impedance.

When $\omega \rightarrow 0$, the characteristic acoustic impedance is equal to the square root of the viscous friction by wall resistance over the heat conductance by wall resistance plus one. The amplitude in this limits remains constant because wall resistance, wall density, viscous friction and heat conductance remains constant.

When $\omega \rightarrow \infty$, the characteristic acoustic impedance is equal to the square root of the medium inertance divided by the medium compliance. The medium inertance and the medium compliance remain constant because both do not depend of the young's modulus change. The characteristic acoustic impedance amplitude remains constant at higher frequencies, when the young's modulus changes.

Between $1000 < \omega < 5000$, the characteristic acoustic impedance exhibits two peaks, the maximum and minimum attenuation, that are located in two frequencies that are known as transversal frequencies f_{res} and f_2 . When the Young's modulus increases, f_r and f_2 increases.

TABLE IX RUBBER PIPE PHYSICAL PROPERTIES VALUES USED FOR SIMULATION.

PROPERTY	SYMBOL/UNITS	RUBBER
Density	$\rho_w (g / cm^3)$	0.92
Wall Internal Viscosity	$\eta (dyne \cdot s / cm^2)$	100
Young's Modulus of Elasticity (Test I-5)	$E (dyne / cm^2)$	$1.8 \cdot 10^7, 1.9 \cdot 10^7, 2.1 \cdot 10^7, 2.3 \cdot 10^7, 2.6 \cdot 10^7$
Wall Thickness	$h (cm)$	0.159
Wall Radius	$r (cm)$	0.65

The transversal frequencies were computed from the transmission line model particular solution, and were compared with the observed values f_{res}^* and f_2^* of the characteristic acoustic impedance. Table X lists the obtained values, where it can be seen that the transversal frequencies do not exhibit any differences between the visual obtained and calculated.

TABLE X QUALITY FACTOR, DAMPING RATIO AND RESONANT FREQUENCIES OBTAINED FROM SIMULATIONS.

Test	Q	ζ	$f_{res} (Hz)$	$f_2 (Hz)$	$f_{res}^* (Hz)$	$f_2^* (Hz)$
$E = 1.8E7$	132	0.0037	2166	2482	2166	2482
$E = 1.9E7$	135	0.0036	2225	2534	2225	2534
$E = 2.1E7$	142	0.0035	2339	2635	2339	2635
$E = 2.3E7$	149	0.0033	2448	2732	2448	2732
$E = 2.6E7$	158	0.0031	2603	2871	2603	2871

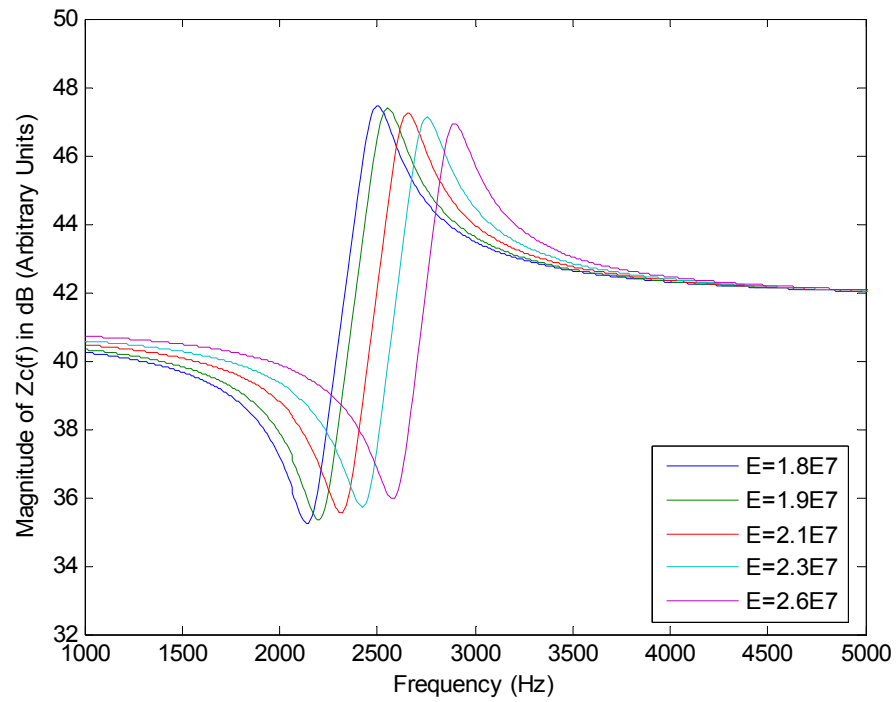


Fig. 3.10 Characteristic acoustic impedance $Z_c(f)$ for different Young's modulus in dyne/cm^2 .

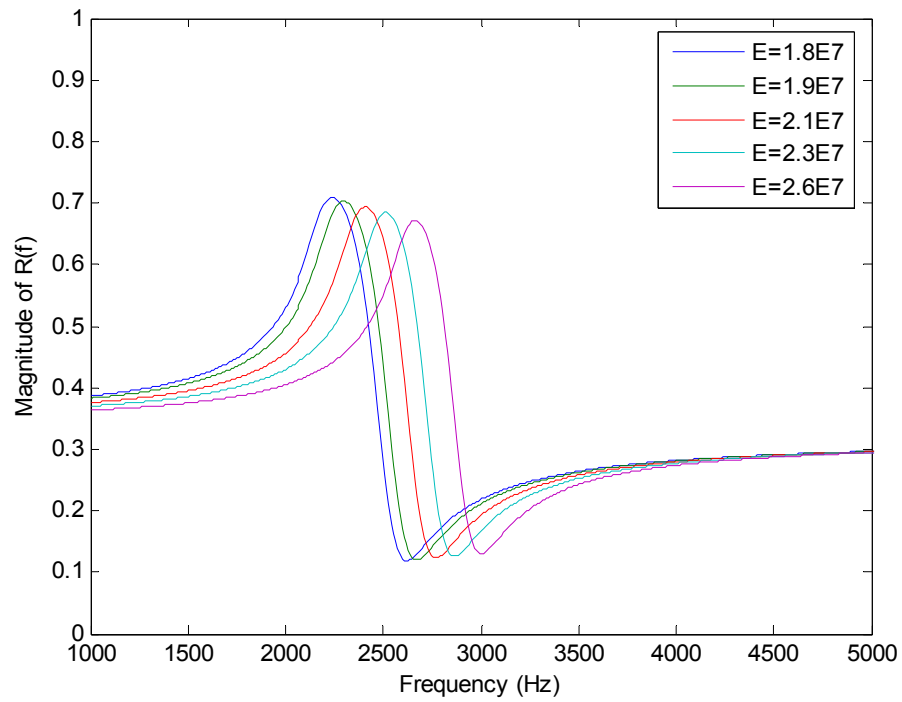


Fig. 3.11 Reflection coefficient $R(f)$ for different Young's modulus in dyne/cm^2 .

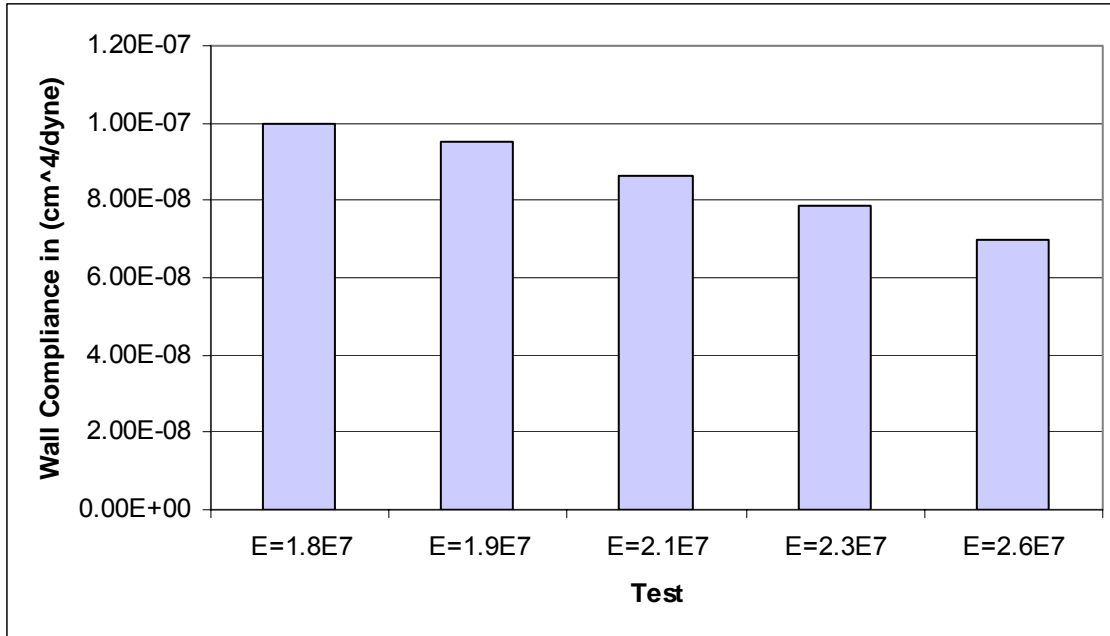


Fig. 3.12 Wall compliance (C_w) values for different Young's modulus in dyne/cm^2 .

3.2.1.5 Wall viscosity effects

The tube wall viscosity was varied in order to observe its effects on wall compliance, characteristic acoustic impedance and reflection coefficient. Uniform latex tubes with length $l=1\text{cm}$ and the parameters lists on Table XI were considered for the wall viscosity analysis.

Fig. 3.13 depicts the characteristic acoustic impedances as function of frequency in Hz . From this plot it can be observed that the curves exhibit similar behavior, however, when the wall viscosity increases, the amplitude at $f = 1000 \text{ Hz}$ and $f = 5000$ remains constant, the transverse frequencies f_{res} increases while f_2 decreases, the difference between the maximum and minimum peak decreases and the ratio f_2/f_{res} decreases.

Fig. 3.14 depicts the reflection coefficient as function of frequency in Hz . From this plot it can be observed that the curves exhibit a similar behavior, however, when the wall viscosity increases, the amplitude at $f = 1000 \text{ Hz}$ decreases while at $f = 5000$ remains constant.

The wall compliance values for different diameters shown in Fig. 3.15 were computed using the equation of Table II. Observing the equation and Fig. 3.15 it can be noted that the wall compliance remains constant.

Analyzing specifically the characteristic acoustic impedance equation of the transmission line model when the wall viscosity increases, it can be noted that the wall resistance increase; while all others do not depend of the wall viscosity changes. This parameter affects the characteristic acoustic impedance.

When $\omega \rightarrow 0$, the characteristic acoustic impedance is equal to the square root of the viscous friction by wall resistance over the heat conductance by wall resistance plus one. The amplitude in these limits remains constant because wall resistance, wall density, viscous friction and heat conductance remain constant.

When $\omega \rightarrow \infty$, the characteristic acoustic impedance is equal to the square root of the medium inertance over the medium compliance. The medium inertance and the medium compliance remain constant because neither depends on the wall viscosity change. The characteristic acoustic impedance amplitude remains constant at frequencies $f = \infty$ when the wall viscosity changes.

Between $1000 < \omega < 5000$, the characteristic acoustic impedance exhibits two peaks the maximum and minimum attenuation that are located in two frequencies that are known as transversal frequencies f_{res} and f_2 . When the wall viscosity increases, f_r and f_2 remain constant. From the graphic curves, it can be observed that the transversal resonant changes when the wall viscosity changes. This occurs because when the wall inertance increases the quality factor decreases. This change in the quality factor generates a displacement in the transversal frequencies as can be appreciated in Fig. 3.13.

TABLE XI RUBBER PIPE PHYSICAL PROPERTIES VALUES USED FOR SIMULATION.

PROPERTY	SYMBOL/UNITS	RUBBER
Density	$\rho_w (g / cm^3)$	0.92
Wall Internal Viscosity (Test 1-5)	$\eta (dyne \cdot s / cm^2)$	100,150,200,250,300
Young's Modulus of Elasticity	$E (dyne / cm^2)$	$2.3 \cdot 10^7$
Wall Thickness	$h (cm)$	0.159
Wall Radius	$r (cm)$	0.65

The transversal frequencies were computed from the transmission line model particular solution, and were compared with the observed values f_{res}^* and f_2^* of the

characteristic acoustic impedance. Table XII lists the obtained values, where it can be seen that the transversal frequencies exhibit differences between the visual obtained and calculated. Notice that the quality factor increases when the wall viscosity increases.

TABLE XII QUALITY FACTOR, DAMPING RATIO AND RESONANT FREQUENCIES OBTAINED FROM SIMULATIONS.

Test	Q	ζ	f_{res} (Hz)	f_2 (Hz)	f_{res}^* (Hz)	f_2^* (Hz)
$\eta = 100$	158	0.0031	2603	2871	2603	2871
$\eta = 150$	129	0.0038	2603	2871	2546	2916
$\eta = 200$	112	0.0044	2603	2871	2520	2942
$\eta = 250$	100	0.0049	2603	2871	2469	2968
$\eta = 300$	91	0.0054	2603	2871	2431	2980

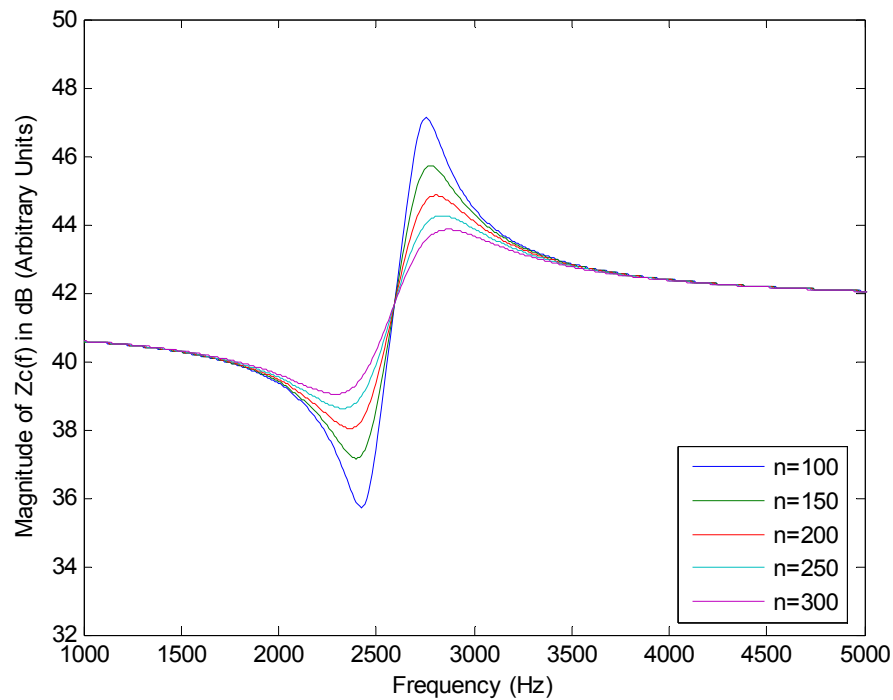


Fig. 3.13 Characteristic acoustic impedance $Z_I(f)$ for different wall viscosity values in $\text{dyne}\cdot\text{s}/\text{cm}^2$.

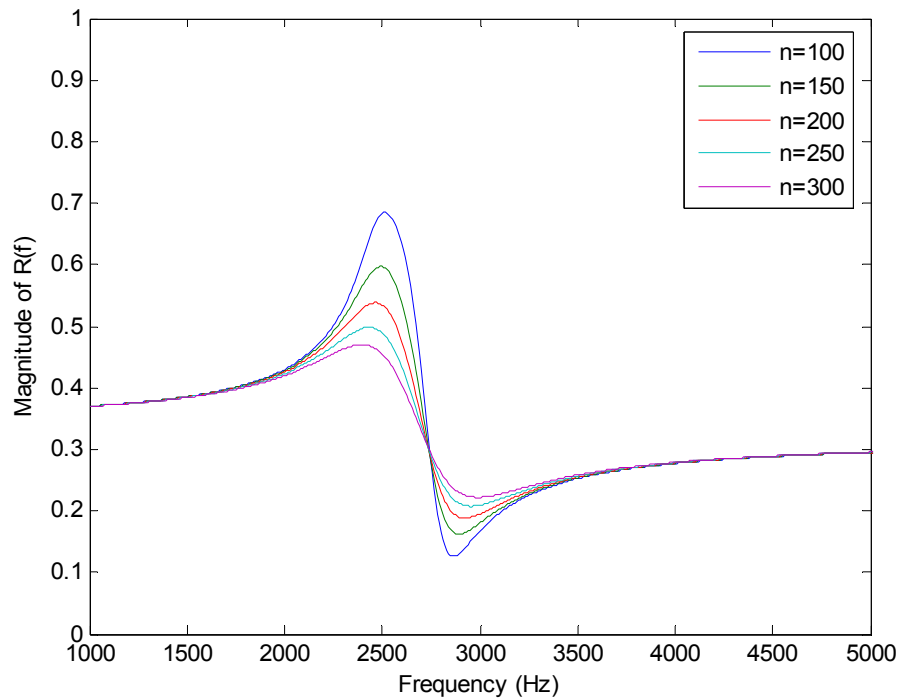


Fig. 3.14 Reflection coefficient $R(f)$ for different wall viscosity values in $\text{dyne}\cdot\text{s}/\text{cm}^2$.

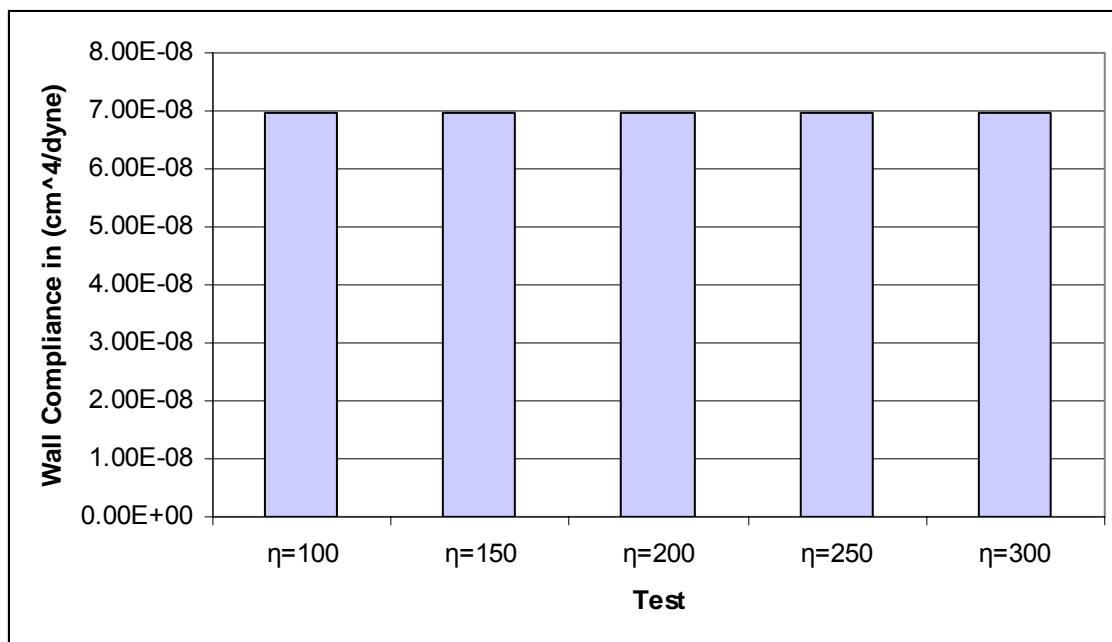


Fig. 3.15 Wall compliance (C_w) for different wall viscosity values. Test 1 $\eta = 300 \text{ dyne}\cdot\text{s}/\text{cm}^2$, Test 2 $\eta = 250 \text{ dyne}\cdot\text{s}/\text{cm}^2$, Test 3 $\eta = 200 \text{ dyne}\cdot\text{s}/\text{cm}^2$, Test 4 $\eta = 150 \text{ dyne}\cdot\text{s}/\text{cm}^2$, Test 5 $\eta = 100 \text{ dyne}\cdot\text{s}/\text{cm}^2$.

3.2.1.6 Young's modulus and wall thickness effects

Since the tube wall thickness was varied *in-vitro* and the Young's modulus is frequency dependant for rubber tubes, they were varied together in order to observe their effects on wall compliance, characteristic acoustic impedance and reflection coefficient. Uniform latex tubes with length $l=1\text{cm}$ and the parameters lists on Table XIII were considered for the wall thickness and Young's modulus analysis.

Fig. 3.16 depicts the characteristic acoustic impedances as a function of frequency in Hz . From this plot it can be observed that the curves exhibit similar behavior, however, when the Young's modulus increases and the wall thickness decreases, the amplitude at $f = 1000 \text{ Hz}$ decreases while at $f = 5000 \text{ Hz}$ remains constant, the transverse frequencies f_{res} and f_2 increase, the difference between the maximum and minimum peak increases and the ratio f_2/f_{res} increases.

Fig. 3.17 depicts the reflection coefficient as a function of frequency in Hz . From this plot it can be observed that the curves exhibit a similar behavior, however, when the Young's modulus increases and the wall thickness decreases, the amplitude at $f = 1000 \text{ Hz}$ increases while at $f = 5000 \text{ Hz}$ remains constant.

The wall compliance values for different Young's modulus and wall thickness shown in Fig. 3.18 were computed using Table II. Observing the equation and Fig. 3.12 it can be noted that the wall compliance increases when the Young's modulus increase and the wall thickness decreases.

Analyzing specifically the characteristic acoustic impedance equation of the transmission line model when the Young's modulus increases, it can be noted that the wall compliance increases, while all others do not depend on the Young's modulus changes. Now when the wall thickness decreases, it can be noted that the wall resistance and wall inertance decrease, while the wall compliance increases. This parameter affects the characteristic acoustic impedance.

When $\omega \rightarrow 0$, the characteristic acoustic impedance is equal to the square root of the viscous friction by wall resistance divided by the heat conductance times wall resistance plus one. The amplitude changes in these limits, because the wall thickness changes affect the wall resistance.

When $\omega \rightarrow \infty$, the characteristic acoustic impedance is equal to the square root of the medium inertance divide by the medium compliance. The medium inertance and the medium compliance remain constant because neither depends on the Young's modulus change. The characteristic acoustic impedance amplitude remains constant at higher frequencies, when the Young's modulus changes.

Between $1000 < \omega < 5000$, the characteristic acoustic impedance exhibits two peaks the maximum and minimum attenuation that are located in two frequencies, known as transversal frequencies f_{res} and f_2 . When the Young's modulus increases f_r and f_2 increase.

TABLE XIII RUBBER PIPE PHYSICAL PROPERTIES VALUES USED FOR SIMULATION.

PROPERTY	SYMBOL/UNITS	RUBBER
Density	$\rho_w (g / cm^3)$	0.92
Wall Internal Viscosity	$\eta (dyne \cdot s / cm^2)$	100
Young's Modulus of Elasticity (Test 1-5)	$E (dyne / cm^2)$	$1.8 \cdot 10^7, 1.9 \cdot 10^7, 2.1 \cdot 10^7, 2.3 \cdot 10^7, 2.6 \cdot 10^7$
Wall Thickness (Test 1-5)	$h (cm)$	0.317, 0.238, 0.198, 0.159, 0.119
Wall Radius	$r (cm)$	0.65

The transversal frequencies were computed utilizing the transmission line model particular solution, and were compared with the observed values f_{res}^* and f_2^* of the characteristic acoustic impedance. Table XIV lists the obtained values, where it can be seen that the transversal frequencies do not exhibit any differences between the visual obtained and calculated.

TABLE XIV QUALITY FACTOR, DAMPING RATIO AND RESONANT FREQUENCIES OBTAINED FROM SIMULATION.

Test	Q	ζ	$f_{res} (Hz)$	$f_2 (Hz)$	$f_{res}^* (Hz)$	$f_2^* (Hz)$
$E = 2.6E7$ $h = 0.119$	158	0.0031	2603	2956	2603	2956
$E = 2.3E7$ $h = 0.159$	149	0.0032	2448	2732	2448	2732
$E = 2.1E7$ $h = 0.198$	142	0.0035	2339	2579	2339	2579
$E = 1.9E7$ $h = 0.238$	135	0.0036	2225	2436	2225	2436
$E = 1.8E7$ $h = 0.317$	132	0.0037	2166	2330	2166	2330

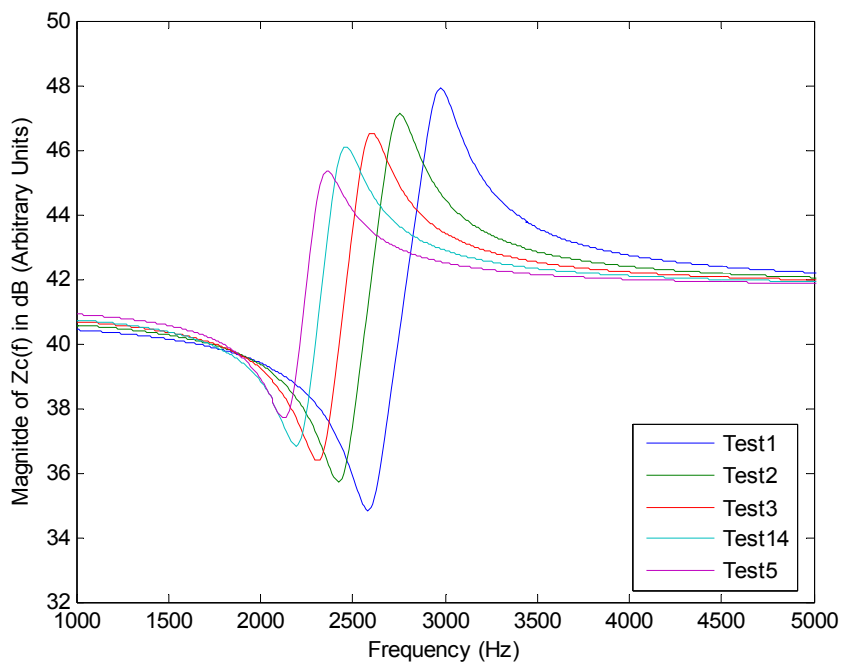


Fig. 3.16 Characteristic acoustic impedance $Z_c(f)$ for different Young's modulus and thickness values. Test 1, $E = 1.8E7$ dyne/cm², $h = 0.317$ cm; Test 2, $E = 1.9E7$ dyne/cm², $h = 0.238$ cm; Test 3, $E = 2.1E7$ dyne/cm², $h = 0.198$ cm; Test 4, $E = 2.3E7$ dyne/cm², $h = 0.159$ cm; Test 5, $E = 2.6E7$ dyne/cm², $h = 0.159$ cm.

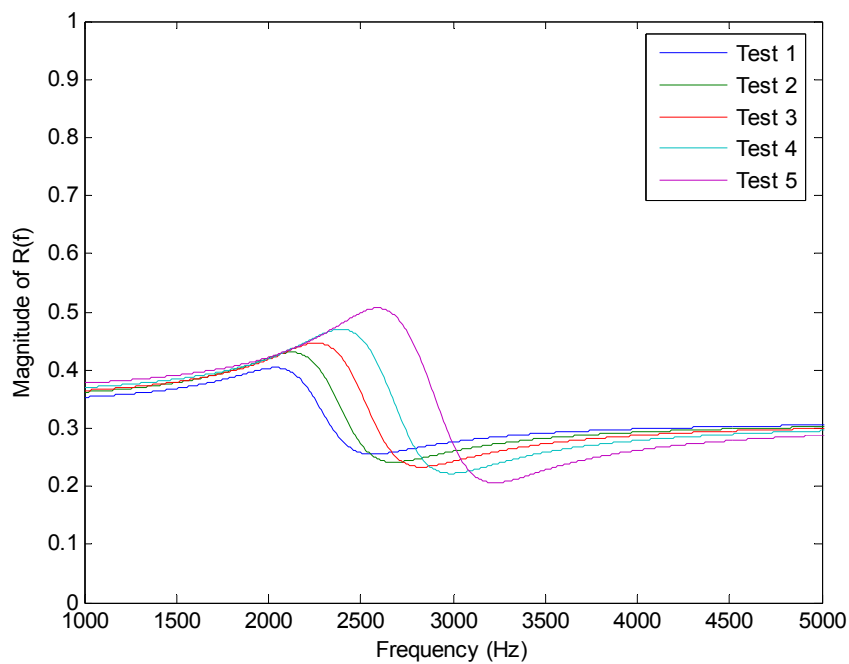


Fig. 3.17 Reflection coefficient $R(f)$ for different Young's modulus and thickness values. Test 1, $E = 1.8E7$ dyne/cm², $h = 0.317$ cm; Test 2, $E = 1.9E7$ dyne/cm², $h = 0.238$ cm; Test 3, $E = 2.1E7$ dyne/cm², $h = 0.198$ cm; Test 4, $E = 2.3E7$ dyne/cm², $h = 0.159$ cm; Test 5, $E = 2.6E7$ dyne/cm², $h = 0.159$ cm.

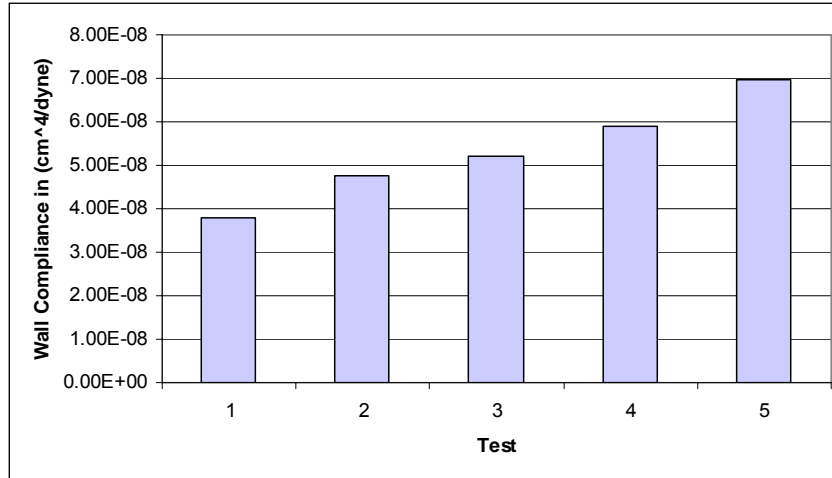


Fig. 3.18 Wall compliance for different Young's modulus and thickness values. Test 1, $E = 1.8E7$ dyne/cm², $h = 0.317$ cm; Test 2, $E = 1.9E7$ dyne/cm², $h = 0.238$ cm; Test 3, $E = 2.1E7$ dyne/cm², $h = 0.198$ cm; Test 4, $E = 2.3E7$ dyne/cm², $h = 0.159$ cm; Test 5, $E = 2.6E7$ dyne/cm², $h = 0.159$ cm.

3.2.2 Pulse echo acoustic reflectometry assessment.

This section describes how the pulse-echo acoustic reflectometry technique is used to estimate the wall compliance. Since error in the transversal frequencies increases when the quality factor decreases, two examples were considered to observe the transversal frequencies. Additionally, the reflected signal length N was varied to observe the effect on the characteristic acoustic impedance and reflection coefficient.

To obtain the sequence $y(t)$, an acoustic Hanning pulse was considered with a bandwidth from 0 Hz to 14 kHz (see Fig. 3.19 (a)) and a reflection coefficient $R(f)$. The acoustic pulse was created considering planar propagation in the tube, when the tube has a diameter of 0.647 cm, and the cutoff frequency $f_{cutoff} = 27.357$ kHz. Then, pulse-echo acoustic reflectometry method was applied to the sequence $y[n]$ computed from the transmission line model.

The reflection coefficient $R_{Sim}^*(\omega)$ and the characteristic acoustic impedances $Z_{1\ Sim}^*(\omega)$ were computed from 0 Hz to 20 kHz at 10 Hz increments. The reflection coefficient was calculated using the FFT of the incident and reflected signals, and the time delay was computed considering the implemented reflectometer dimension.

The wall compliances $C_w^*_{Sim}$ and $C_w^{**}_{Sim}$ were computed using the natural frequency and the transversal frequencies observed from the characteristic acoustic impedance.

Both, wall compliance were compared with the computed wall compliance C_w from the transmission line model, to observe the differences. The resonant frequency f_{res} , f_2 and f_r were computed to compare the values observed to f_{res}^* , f_2^* and f_r^* .

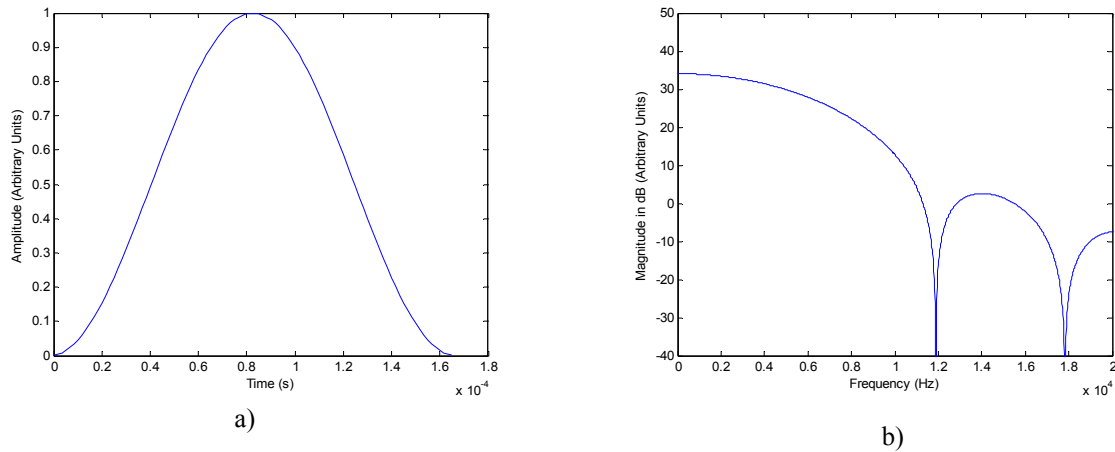


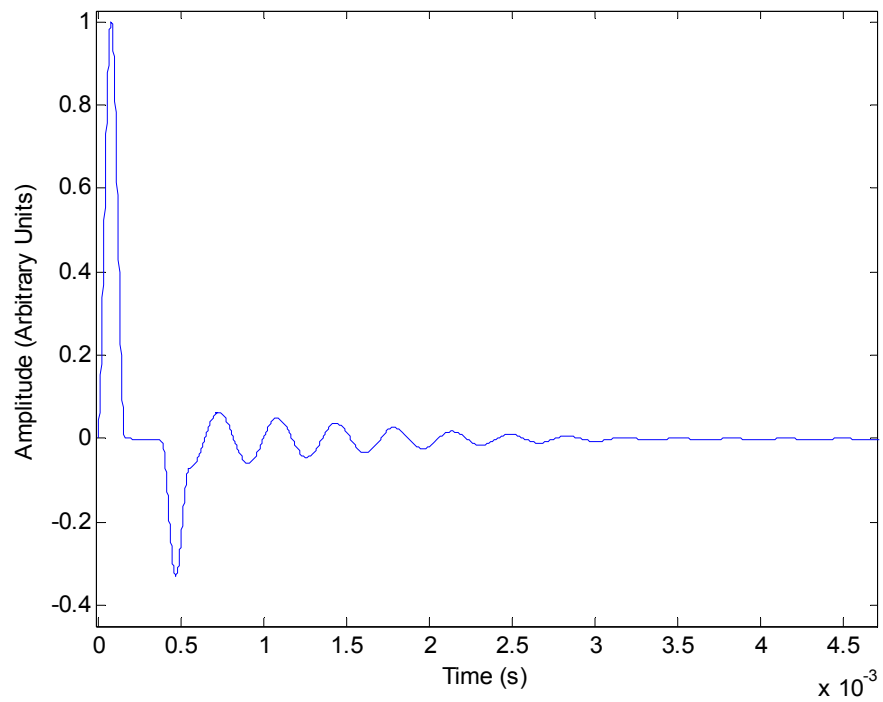
Fig. 3.19 Example of the incident pulse used to interrogate the systems (a) Example of the Hanning pulse at a cutoff frequency of 6 kHz in time domain. (b) FFT of the Hanning pulse.

3.2.2.1 Analysis of a signal whose quality factor $Q = 149.5$

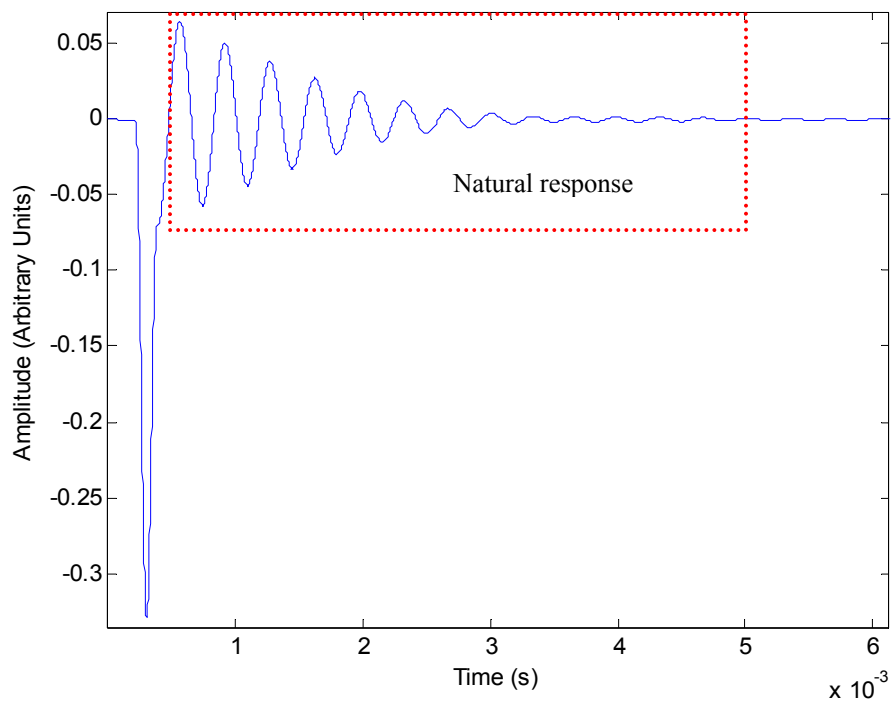
Table XV lists the parameters used in the simulation. The sequence $y[n]$ is depicted in Fig. 3.20 (a), while the cropped reflected signal is sketched in Fig. 3.20 (b). Fig. 3.21 shows the reflection coefficient curves obtained from pulse echo acoustic reflectometry analysis.

TABLE XV RUBBER PIPE PHYSICAL PROPERTIES VALUES USED FOR SIMULATION.

PROPERTY	SYMBOL/UNITS	RUBBER
Density	$\rho_w(g/cm^3)$	0.92
Wall Internal Viscosity	$\eta(\text{dyne} \cdot s/cm^2)$	100
Young's Modulus of Elasticity	$E(\text{dyne}/cm^2)$	2.3E7
Wall Thickness	$h(cm)$	0.159
Wall Radius	$r(cm)$	0.65



a)



b)

Fig. 3.20 (a) Example of the obtained sequence $y[n]$ when a Hanning pulse interrogates the system. (b) Reflected acoustic pulse in time domain.

The characteristic acoustic impedance was studied using different sample lengths in the reflected signal. From this analysis it can be observed that the transversal frequencies $f_{res}^*_{Sim}$ and $f_{2}^*_{Sim}$ vary when the length in the reflected signal changes (see Fig. 3.21). These differences occur because to represent such sequences by a discrete-time Fourier transform, it is necessary to consider a mean-square convergence of incident and reflected pulse $P_i(\omega)$ and $P_r(\omega)$; in both cases the total energy of the error must approach zero. Examining the plot of the characteristic acoustic impedance, it can be seen that the mean square converges properly when the number of samples is over 800 for this particular case.

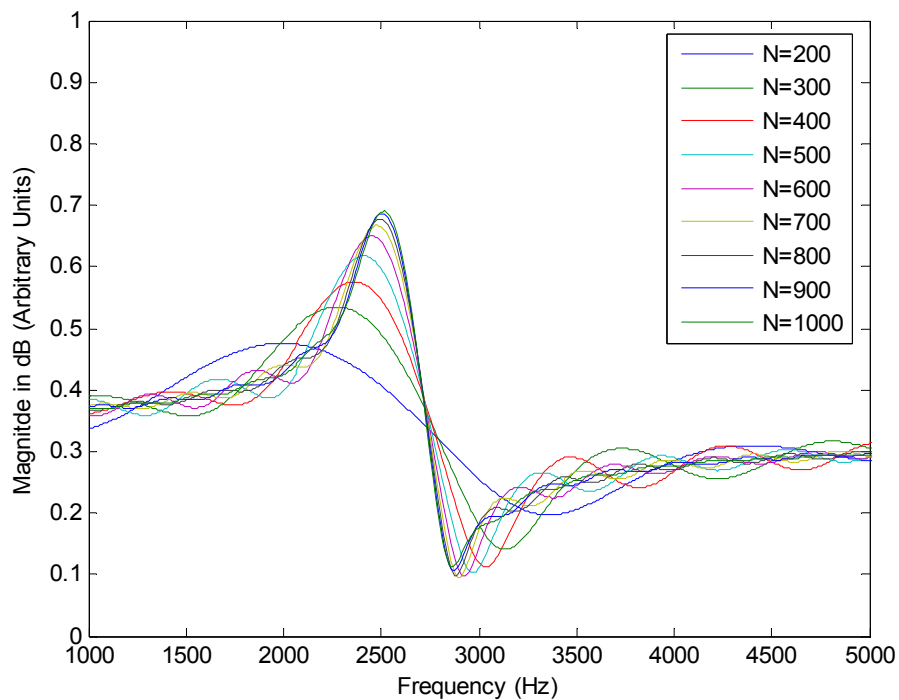


Fig. 3.21 Reflection coefficient $R^*(f)$ when length N in the reflection signal was varied.

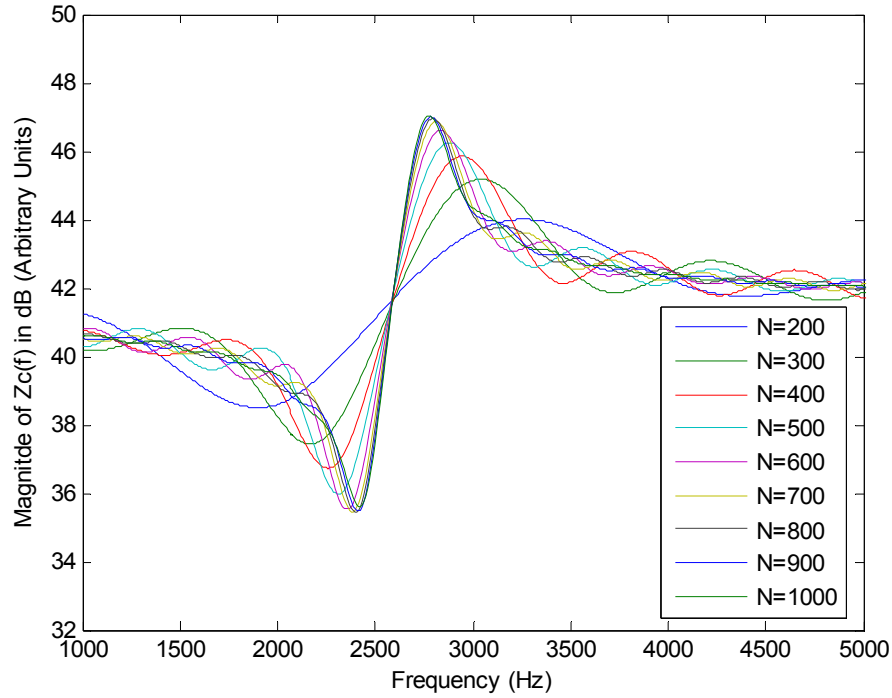


Fig. 3.22 Characteristic acoustic impedance $Z_1^*(f)$ when length N in the reflection signal was varied.

Table XVI lists the transversal frequencies observed from the characteristic acoustic impedance in Fig. 3.22. Notice from Table XVI that the transversal frequencies $f_{res}^*_{Sim}$ and $f_2^*_{Sim}$ tend to a constant value over 800 samples. The observed transversal frequencies at 1000 samples were $f_{res}^*_{Sim} = 2444.46$ Hz and $f_2^*_{Sim} = 2755.74$ Hz, while the expected values based on the transmission line model were $f_{res} = 2448.54$ Hz and $f_2 = 2732.41$ Hz. The differences in the transversal frequencies were 1.45% and 8.61% respectively.

Considering the wall compliance in Table XVI, it can be noted that the wall compliance $C_w^*_{Sim}$ tends to an asymptote after 800 samples. The estimated wall compliance at 1000 samples, $C_w^*_{Sim}$ is equal to $0.585 \cdot 10^{-7} \text{ cm}^4/\text{dyne}$, while the computed $C_w = 0.645 \cdot 10^{-7} \text{ cm}^4/\text{dyne}$, giving a difference of 9.32%.

TABLE XVI TRANSVERSAL FREQUENCIES AND WALL COMPLIANCE FOR VARIOUS VALUES OF N .

Length	$f_{res}^*_{Sim}$ (Hz)	$f_2^*_{Sim}$ (Hz)	$C_w^*_{Sim}$ ($cm^4/dyne$)	Difference (%)
N = 200	1904.3	3268.4	$4.6352 \cdot 10^{-7}$	686.96
N = 300	2169.8	3030.4	$2.2644 \cdot 10^{-7}$	284.45
N = 400	2252.2	2948	$1.6992 \cdot 10^{-7}$	188.49
N = 500	2307.1	2883.9	$1.3399 \cdot 10^{-7}$	127.49
N = 600	2352.9	2838.1	$1.0838 \cdot 10^{-7}$	84.01
N = 700	2380.4	2810.7	$0.93907 \cdot 10^{-7}$	59.43
N = 800	2444.46	2755.74	$0.645 \cdot 10^{-7}$	9.32
N = 900	2444.46	2755.74	$0.645 \cdot 10^{-7}$	9.32
N = 1000	2444.46	2755.74	$0.645 \cdot 10^{-7}$	9.32

Notice from Table XVII that the transversal frequencies $f_{res}^*_{Sim}$ tend to a constant value over 900 samples, while $f_r^*_{Sim}$ does not depend on the length N . Considering 1000 samples, the values obtained for the resonant and natural frequencies were $f_{res}^*_{Sim} = 2416.99$ Hz and $f_r^*_{Sim} = 2669.9$ Hz, while the expected values based on the transmission line model were $f_{res} = 2444.46$ Hz and $f_r = 2667$ Hz. The difference in the transversal frequency was 1.105% while the resonant frequency was 0.074%.

TABLE XVII TRANSVERSAL FREQUENCIES AND WALL COMPLIANCE FOR VARIOUS VALUES OF N .

Length	$f_{res}^*_{Sim}$ (Hz)	$f_r^*_{Sim}$ (Hz)	$C_w^{**}_{Sim}$ ($cm^4/dyne$)	Difference (%)
N = 200	1895.14	2644.01	$2.94 \cdot 10^{-7}$	399.15
N = 300	2178.96	2644.01	$1.47 \cdot 10^{-7}$	149.58
N = 400	2261.35	2644.01	$1.14 \cdot 10^{-7}$	93.55
N = 500	2316.28	2644.01	$0.942 \cdot 10^{-7}$	59.93
N = 600	2371.22	2644.01	$0.756 \cdot 10^{-7}$	28.35
N = 700	2389.53	2644.01	$0.697 \cdot 10^{-7}$	18.34
N = 800	2444.46	2644.01	$0.583 \cdot 10^{-7}$	1.02
N = 900	2444.46	2669.9	$0.605 \cdot 10^{-7}$	1.02
N = 1000	2444.46	2669.9	$0.605 \cdot 10^{-7}$	1.02

Now, considering the wall compliance in Table XVII, it can be noted that $C_w^{**}_{Sim}$ tends to an asymptote after 800 samples. The difference in the wall compliance estimation $C_w^*_{Sim}$ and $C_w^{**}_{Sim}$ were of 9.32% and 3.305% respectively. These differences are caused by the visual estimation of the transversal frequencies; additionally, the error

in the frequencies occurs because the FFT was computed with a $\Delta f = 10$ Hz. Therefore the difficulty in the estimation of the wall compliance from pulse-echo acoustic reflectometry technique was the visual location of the transversal frequencies.

3.2.2.2 Analysis of a signal with a known quality factor $Q = 88$.

Table XVIII lists the parameters used in the simulation. The sequence $y[n]$ is depicted in Fig. 3.23 (a), while the cropped reflected signal is sketched in Fig. 3.23 (b). Fig. 3.24 shows the reflection coefficient curves obtained from pulse echo acoustic reflectometry analysis.

TABLE XVIII RUBBER PIPE PHYSICAL PROPERTIES VALUES USED FOR SIMULATION.

PROPERTY	SYMBOL/UNITS	RUBBER
Density	$\rho_w (g / cm^3)$	0.92
Wall Internal Viscosity	$\eta (dyne \cdot s / cm^2)$	300
Young's Modulus of Elasticity	$E (dyne / cm^2)$	2.3E7
Wall Thickness	$h (cm)$	0.159
Wall Radius	$r (cm)$	0.65

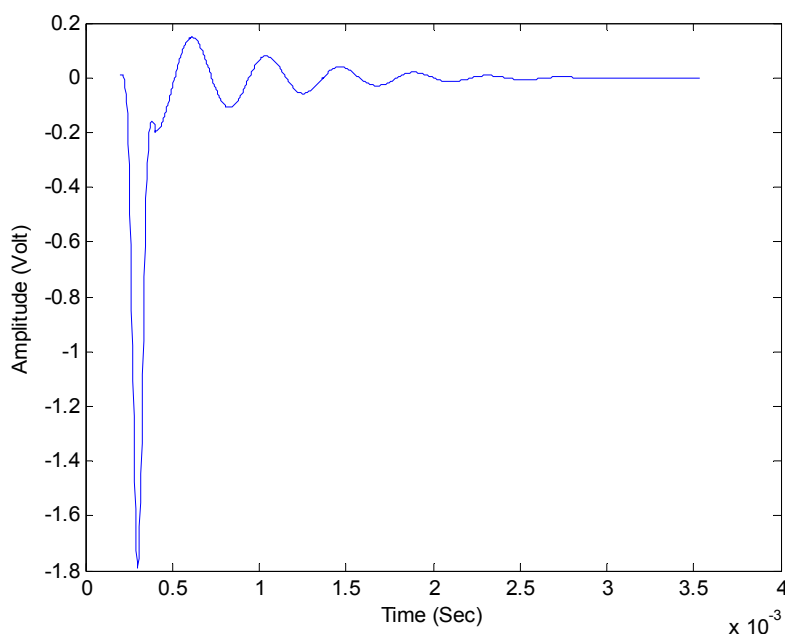


Fig. 3.23 Reflected acoustic pulse in time domain.

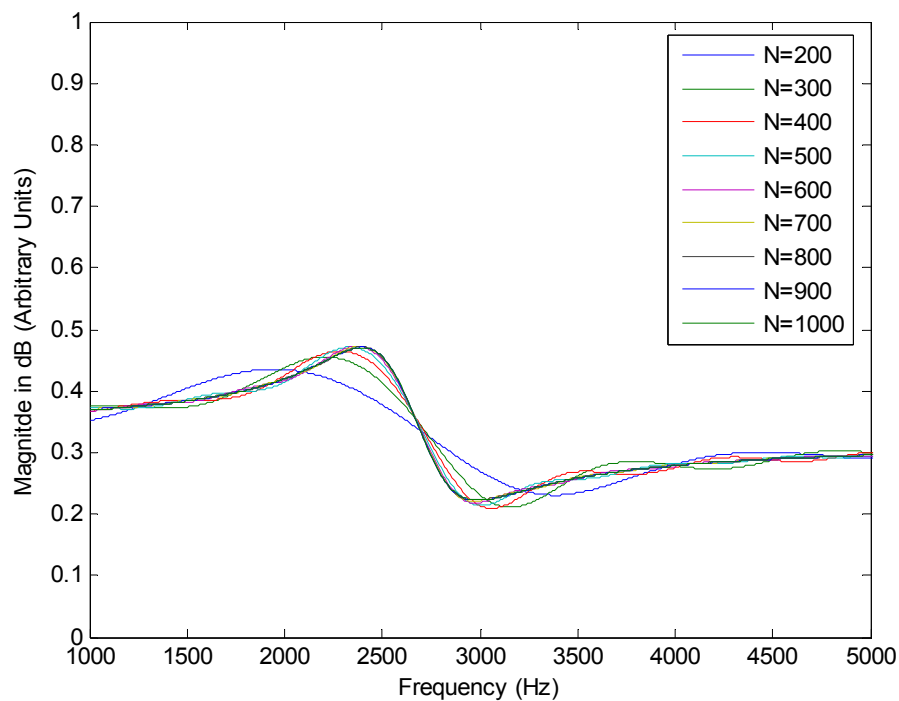


Fig. 3.24 Reflection coefficient $R^*(\omega)$ when length N in the reflection signal was varied.

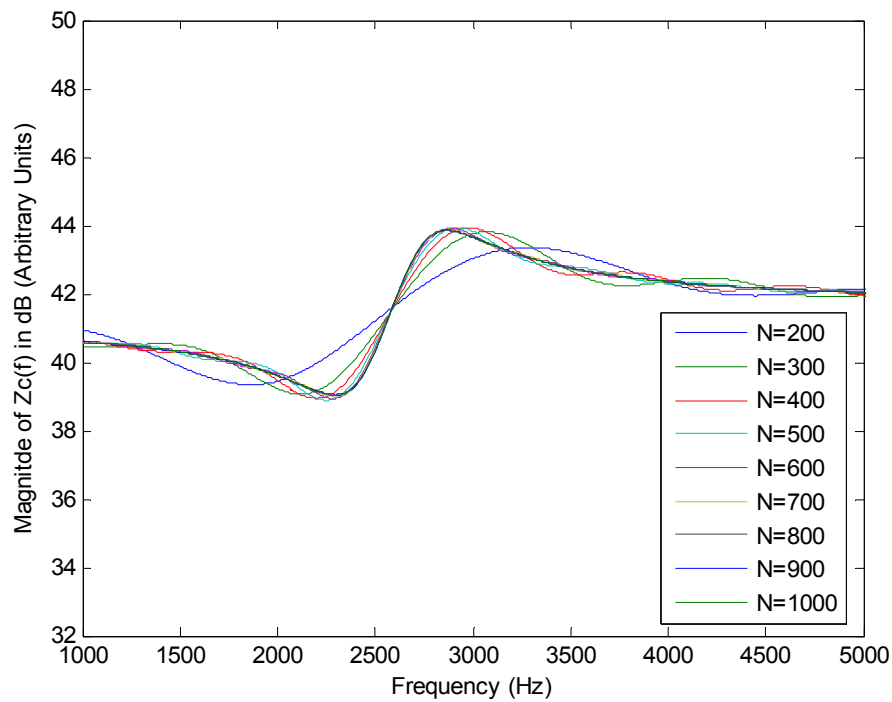


Fig. 3.25 Characteristic acoustic impedance $Z_1^*(\omega)$ when length N in the reflection signal was varied.

The characteristic acoustic impedance was studied using different samples lengths in the reflected signal. From this analysis it can be observed that the transversal frequencies $f_{res}^*_{Sim}$ and $f_2^*_{Sim}$ vary when the length N in the reflected signal changes (see Fig. 3.24 and Fig. 3.25). These differences occur because to represent such sequences by a discrete-time Fourier transform, it is necessary to consider a mean-square convergence of incident and reflected pulse $P_i(\omega)$ and $P_r(\omega)$; in both cases the total energy of the error must approach zero. Examining the plot of the characteristic acoustic impedance, it can be seen that the mean square converges properly when the number of samples is over 600 in this particular case.

Notice from the Table XIX that the transversal frequencies $f_{res}^*_{Sim}$ and $f_2^*_{Sim}$ tend to a constant value over the 600 samples. The transversal frequencies observed at 1000 samples were $f_{res}^*_{Sim} = 2325.4$ Hz and $f_2^*_{Sim} = 2874.8$ Hz, while the expected values based on the transmission line model were $f_{res} = 2448.54$ Hz and $f_2 = 2732.41$ Hz. The differences in the transversal frequencies were 5.19% and 5.04% respectively.

Considering the wall compliance in the Table XIX, it can be noted that the wall compliance $C_w^*_{Sim}$ tends to an asymptote after 600 samples. The estimated wall compliance at 1000 samples, $C_w^*_{Sim}$ is equal to $1.1205 \cdot 10^{-7} \text{ cm}^4/\text{dyne}$, while the computed $C_w = 0.589 \cdot 10^{-7} \text{ cm}^4/\text{dyne}$, giving a difference of 90.24%.

TABLE XIX TRANSVERSAL FREQUENCIES AND WALL COMPLIANCE FOR VARIOUS VALUES OF N .

Length	$f_{res}^*_{Sim}$ (Hz)	$f_2^*_{Sim}$ (Hz)	$C_w^*_{Sim}$ (cm^4/dyne)	Difference (%)
N = 200	1876.8	3286.7	$5.068 \cdot 10^{-7}$	760.44
N = 300	2087.4	3048.7	$2.6113 \cdot 10^{-7}$	343.34
N = 400	2215.6	2966.3	$2.0599 \cdot 10^{-7}$	249.73
N = 500	2252.2	2893.1	$1.5985 \cdot 10^{-7}$	171.39
N = 600	2325.4	2874.8	$1.1205 \cdot 10^{-7}$	90.24
N = 700	2325.4	2874.8	$1.1205 \cdot 10^{-7}$	90.24
N = 800	2325.4	2874.8	$1.1205 \cdot 10^{-7}$	90.24
N = 900	2325.4	2874.8	$1.1205 \cdot 10^{-7}$	90.24
N = 1000	2325.4	2874.8	$1.1205 \cdot 10^{-7}$	90.24

Notice from the Table XX, it can be observe that the transversal frequencies $f_{res}^*_{Sim}$ tend to a constant value over the 900 samples while $f_r^*_{Sim}$ does not depend of the length N . Considering 1000 samples, the values obtained for the resonant and natural frequencies were $f_{res}^*_{Sim} = 2416.99$ Hz and $f_r^*_{Sim} = 2669$ Hz respectively, while the expected values based on the transmission line model were $f_{res} = 2448.54$ Hz and $f_r = 2667.02$ Hz. The differences in the transversal frequencies were 1.3% and 0.074% respectively.

Now, considering the wall compliance in the Table XX, it can be noted that the wall compliance $C_w^{**}_{Sim}$ tends to an asymptote after 600 samples. The estimated wall compliance at 1000 samples, $C_w^{**}_{Sim}$ is equal to $0.691 \cdot 10^{-7} \text{ cm}^4/\text{dyne}$, while the computed wall compliance is $C_w = 0.589 \cdot 10^{-7} \text{ cm}^4/\text{dyne}$, giving a difference of 1.17%.

TABLE XX TRANSVERSAL FREQUENCIES AND WALL COMPLIANCE FOR VARIOUS VALUES OF N .

Length	$f_{res}^*_{Sim}$ (Hz)	$f_r^*_{Sim}$ (Hz)	$C_w^{**}_{Sim}$ (cm^4/dyne)	Difference (%)
N = 200	1940.92	2669	$2.73 \cdot 10^{-7}$	363.50
N = 300	2160.64	2669	$1.6 \cdot 10^{-7}$	171.65
N = 400	2224.73	2669	$1.33 \cdot 10^{-7}$	125.81
N = 500	2288.82	2669	$1.08 \cdot 10^{-7}$	83.36
N = 600	2416.99	2669	$0.691 \cdot 10^{-7}$	1.17
N = 700	2416.99	2669	$0.691 \cdot 10^{-7}$	1.17
N = 800	2416.99	2669	$0.691 \cdot 10^{-7}$	1.17
N = 900	2416.99	2669	$0.691 \cdot 10^{-7}$	1.17
N = 1000	2416.99	2669	$0.691 \cdot 10^{-7}$	1.17

4 Wall Compliance Estimation Using Pulse-Echo Acoustic Reflectometry

4.1 Methodology

This chapter provides a detailed description of the system constructed to experimentally measure the wall compliance of viscos-elastic air-filled tubes. Additionally, the algorithms implemented to generate the plane acoustic pulse and estimate the input characteristic acoustic impedance and local wall compliance are explained.

4.1.1 Compliance estimation via volumetric tests

The static total wall compliance of various latex tubes was experimentally measured using a volumetric test. The procedure consists of carefully injecting a known volume of incompressible fluid (water), being careful not to exceed the rubber's limit region of elasticity. The resulting internal change in pressure caused by the injecting liquid was recorded to obtain a pressure vs. volume curve. From the obtained curve, the inverse of the slope is known as static wall compliance, denoted C_{wMech} .

Fig. 4.1 shows the set up used to measure the mechanical compliance. This setup is composed by an injector, pressure gage, rigid pipe and compliant tube. The injector was used to insert a specific volume of water into the compliant tube, the gage was used to measure the pressure inside the pipe and the rigid tube was used to join the different instrument parts.

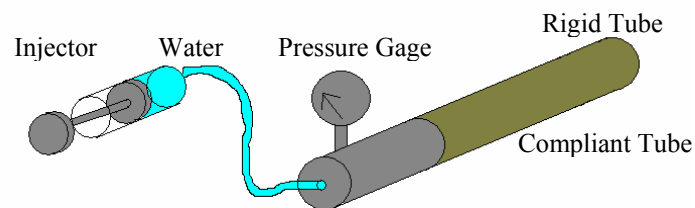


Fig. 4.1 Mechanical estimations setup

4.1.2 Acoustic reflectometer

Fig. 4.2 shows a block diagram of the pulse-echo acoustic reflectometer system used in the study. This is composed of a personal computer, analog filters, signal generator, sound amplifier, data acquisition, speaker and microphone. The reflectometer system component and how they work will be described below.

The system consisted of a loudspeaker (*Morel MDT 30*) that was connected at the end of a plastic pipe through the conic coupler. Foam material was added to the cone in order to attenuate the reflection caused by the incident pulse. As is shown in Fig. 4.2, a microphone (*Knowles EM-3046*) was connected in such a way that its pressure sensing port was flush with the inner wall of the copper pipe at 3.5 cm of the source tube end. This microphone records the reflections returning from the tubular object under test, which is coupled to the far end of the source tube. A photograph of the reflectometer is shown in Fig. 4.3.

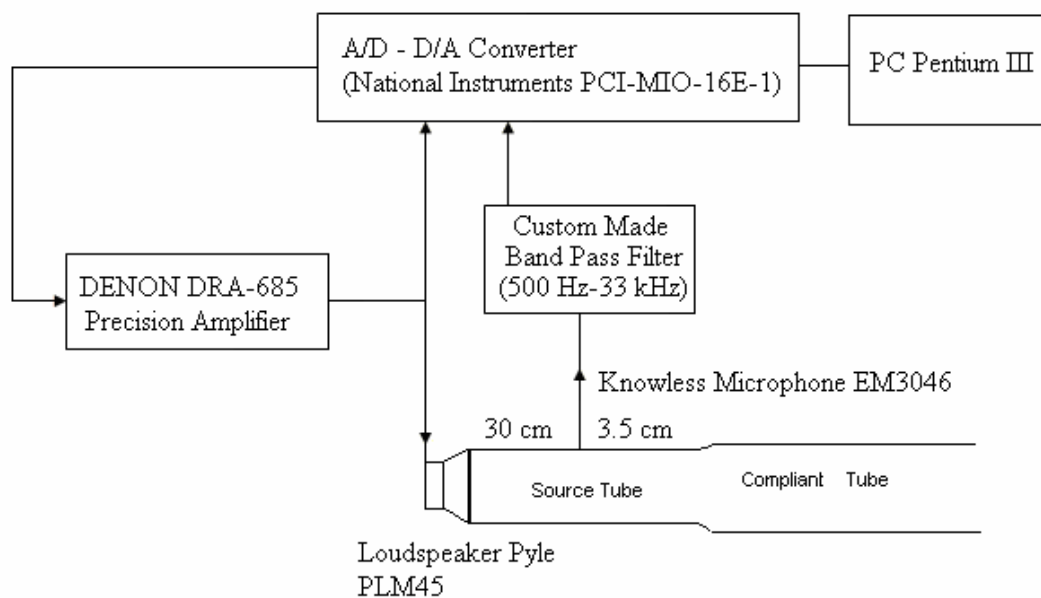


Fig. 4.2 Experimental setup utilized to perform the acoustic measurements.



Fig. 4.3 Pulse-echo acoustic reflectometry system

The electric signals used to drive the speaker were generated in a personal computer, and amplified by *Denon DRA-685* precision amplifier. Sound signals were recorded with the microphone and the electrical signal was amplified (*AC-coupled, 40 dB gain*) and filtered to prevent aliasing and noise. The obtained signal was digitized at a sampling rate of 300 S/s with a data acquisition board (*National Instruments PCI-MIO-16E-1*) that was installed on the computer. A virtual instrument (*VI*) was created using LabVIEW, and was used for signal generation, acquisition, analysis and display.

4.1.2.1 Loudspeaker/source tube coupling

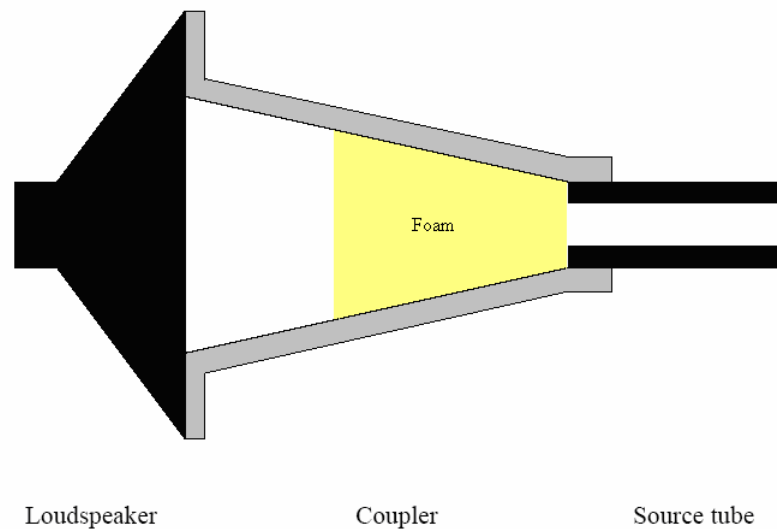


Fig. 4.4 Loudspeaker/source tube coupler.

The loudspeaker was coupled with the source tube through a plastic cone (Fig. 4.4). The conic coupler between the loudspeaker and source tube minimizes reflections; foam is placed inside the cone to minimize any ‘ringing’ from the loudspeaker. The coupler is bolted tightly to the loudspeaker and the source tube.

4.1.2.2 Source tube/test object coupling

The source tube (reflectometer) is coupled to the object under investigation (compliant tube) as shown in Fig. 4.5. The source tube was selected with an internal diameter $d = 0.45$ cm and an external diameter $d = 0.65$ cm. The selected object (compliant tube) had an internal diameter $d = 0.65$ cm and was placed tightly with the source tube. This coupling gave a large discontinuity at the joint between the source tube and the object, leading to a large reflection at the beginning.

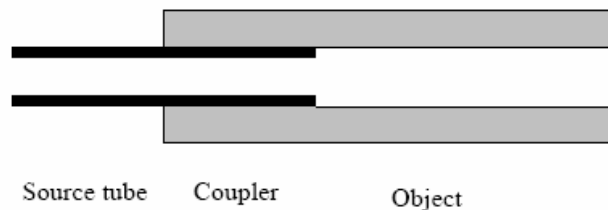


Fig. 4.5 Coupling between the source tube and object under investigation.

4.1.2.3 Analog Band pass Filter

An analog band pass filter and analog amplifier were designed to amplify, prevent aliasing, filter noise and cancel the DC component of the transducer. Fig. 4.6 sketches the block diagram used to design the filter, which is divided in different stages. The first stage was designed in order to have high input impedance and good common-mode rejection. A high pass filter was designed in the second stage with a cutoff frequency $f_c = 500$ Hz and unitary gain. The third stage was designed considering a low pass filter with a cutoff frequency $f_c = 30$ kHz and unitary gain. The last stage was designed to amplify the input signal by 40 dB with a non-inverting amplifier.

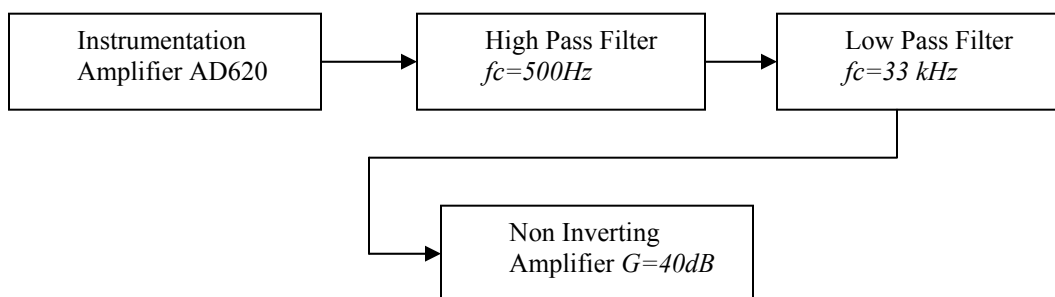


Fig. 4.6 Example of block diagram used in the design of the custom made analog filter.

4.1.3 Acoustic Pulse Generation

The compliant pipes experimental studies were based on acoustic plane wave propagation. When an acoustic pulse travels inside a tube, reflections occur due to impedance changes. In order to minimize the attenuation, dispersion and overlap of the reflected acoustic pulse the distance between the microphone and the end of the source tube was computed considering the length of the incident acoustic pulse.

The procedure of generating the acoustic pulse was performed in a long tube, in order to avoid any reflection interference with the incident pulse. An inverse filter technique was implemented to generate an acoustic Hanning pulse. After obtaining the plane acoustic wave, the long tube was removed from the end of the source tube in order to measure the time delay between the incident and reflected acoustic signals using a cross correlation technique.

There are two important reasons to generate an acoustic pulse: The only way to isolate and compare the desired reflections is if the incident sound wave has a known form easy to recognize in the received signal. The other reason is to compare the experimental acoustic impulse response with the simulated model acoustic response to a known input acoustic pulse.

4.1.3.1 Inverse filter technique

The problem with generating an acoustic pulse is that the system can be complex and that its output response to an input acoustic signal produces an unknown signal. Inverse filter technique [36] was implemented to identify the transfer function of the system and accurately generate the pulse. This was obtained by deconvolving the input electrical pulse signal with the output acoustic pulse. Then with the IIR, the required electrical signal to produce a desired acoustic sound signal pressure was computed.

The inverse filter technique was implemented as follows. An electrical signal $x(t)$ was the electrical pulse that was applied to the amplifier and loudspeaker, and the acoustic output signal $y(t)$ was recorded by a microphone. The system transfer function $H(\omega)$ can be determined by applying the Fourier transforms to the input and output signals, and taking their ratio as follow

$$H(\omega) = \frac{Y(\omega)X^*(\omega)}{X(\omega)X^*(\omega)} \quad (4.1-1)$$

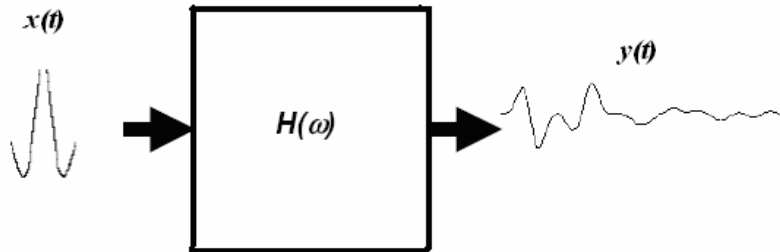


Fig. 4.7 Inverse procedure to obtain $H(j\omega)$

Once $H(\omega)$ is determined, then the needed electrical input is computed as follows

$$E(t) = FFT^{-1}\left(\frac{Y(\omega)}{H(\omega) + \zeta}W(\omega)\right), \quad (4.1-2)$$

where ζ is a small constraining factor to prevent division by zero or by a small number which would result in high magnitude frequency components. $Y(\omega)$ is the Fourier transform of the acoustic pulse that is to be designed. $W(\omega)$ is a digital band-pass filter with cut-off frequency to reject frequency components that are not present in $H(\omega)$. Fig. 4.8 depicts the computed electrical pulse $E(t)$ that generates the output acoustic pulse signal $p(t)$.

To create the acoustic pulse experimentally, a long plastic tube is coupled at the end of the reflectometer. This tube avoids the occurrence of near reflections and permits to interrogation of the system in order to create a Hanning pulse that will be used to interrogate the objects.

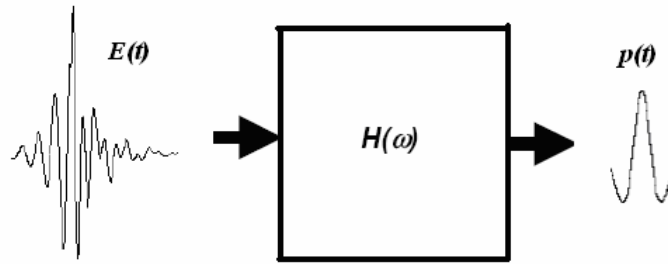


Fig. 4.8 Electrical pulse $E(t)$ that generates an acoustic pulse $p(t)$.

4.1.3.2 Cross-correlation

Cross-correlation is a measure of similarity between two signals, commonly used to find features in an unknown signal by comparing it to a known one. It is a function of the relative time between the signals, and it is sometimes called the *sliding dot product*.

For discrete functions f_i and g_i the cross-correlation is defined as

$$(f \otimes g)_i \equiv \sum_j f_j^* g_{i+j} \quad (4.1-3)$$

where the sum is over the corresponding values of the integer j and an asterisk indicates the complex conjugate.

The procedure to measure the time delay consisted in cutting the incident and reflected acoustic signal from the sequence recorded by the microphone. Then the cross correlation between the incident and reflected signals is computed. This mathematical procedure returns a vector of the lags indices at which the cross correlation was estimated. Then, the time delay was computed by the average of the lag vectors minus the length of the incident pulse times the sampling time produces the time delay.

$$T_d \equiv \frac{1}{M} \sum_{i=1}^M (f \otimes g)_i \frac{1}{f_s} \quad (4.1-4)$$

where f_s is the sampling frequency and M is the maximum number of samples after windowing of the incident and reflected pulses.

4.1.4 Wall compliance and characteristic acoustic impedance estimation

After synthesizing an acoustic Hanning plane pulse, it was used to interrogate rubber tubes with different thicknesses, through pulse-echo acoustic reflectometry. The resulting signals for the different cases were recorded and analyzed.

The incident and reflected acoustic signals were cropped from the recorded signal, in order to compute the reflection coefficient $R^*(\omega)$ using

$$R^*(\omega) = \frac{P_r(\omega) \cdot e^{j\omega T_d}}{P_i(\omega)} \quad (4.1-5)$$

where $P_r(\omega)$ and $P_i(\omega)$ are the spectra of the reflected and incident sound signals respectively. T_d is the time delay associated with the round-trip travel time of the acoustic pulse from the microphone to the tube boundary and back. Computed using cross correlation technique (4.1-4).

The input characteristic acoustic impedance $Z_1^*(\omega)$ was calculated considering the acoustic reflectometry theory in which

$$Z_1^*(\omega) = \frac{1 + R^*(\omega)}{1 - R^*(\omega)} \cdot Z_0 \quad (4.1-6)$$

where Z_0 is the characteristic impedance of the source tube. The acoustic characteristic impedance is assumed to be constant between the audible range since the source tube is rigid, therefore its impedance can be computed as

$$Z_0 = \frac{\rho_0 c}{S} \quad (4.1-7)$$

where ρ_0 is the air density, c is the air sound speed, and S is the cross-sectional area. The obtained results of the characteristic acoustic impedance $Z_1^*(\omega)$ will be used to find the transversal frequencies f_{res} and f_2 . Finally, the local wall compliance was computed using the transversal resonant obtained from the characteristic acoustic impedance C_{wAc}

$$C_{wAc} = \left(\left(\frac{f_2}{f_r} \right)^2 - 1 \right) * C_a \quad (4.1-8)$$

where C_a is the medium compliance and was computed using the equation on Table II. Additionally, the wall compliance C_w^{**Ac} was computed using the natural frequency f_r and the transversal frequency f_{res} in which the maximum reflection occur.

$$C_w^{**Ac} = \frac{\left(1 - \left(\frac{f_r}{f_{res}}\right)^2\right)}{C_a L_a (2\pi f_r)^2 - 1} C_a, \quad (4.1-9)$$

where C_a and L_a is the medium compliance and it was computed using equation on Table II.

4.2 Complex Modulus of rubber like material

It is demonstrated from sensitivity analysis in chapter two, that the characteristic acoustic impedance is related to the Young's modulus. In order to justify the values used in the transmission line model vs. pulse-echo acoustic reflectometry section, this section discusses how the Young's modulus was obtained.

4.2.1 Dynamic Young's modulus

Knowledge of the complex modulus, particularly their components such as dynamic modulus, loss modulus and their frequency dependence, have been of interest to scientists and engineers for a long time and can be expressed as

$$H_w(\omega) = E_{dyn}(\omega) + j\omega\eta_w(\omega) \quad [38] \quad (4.2-1)$$

where $E_{dyn}(\omega)$ is the dynamic Young's modulus in $dyne/cm^2$, and $\eta_w(\omega)$ is the internal wall viscosity in $dyne*s/cm^2$. This information is important in predicting the wave propagation through the material, in order to control vibration, taking the dynamic properties into account when calculating vibration response and in the analysis of acoustic propagation. Furthermore, such information is absolutely necessary to understand the material's behavior.

The dynamic properties can be determined by experimental measurement using the appropriate instruments. Most available experimental data cover a wide frequency range

using different polymers [38-41], it can be observed that the frequency dependence is most significant when the loss factor is high. This behavior is one characteristic of rubbers and rubber-like materials in shear and uniaxial tension-compression deformation [38].

Considering that the dynamic Young's modulus of rubber is variable and frequency dependent, it was measured at frequency $f = 0$. Therefore, a stress-strain test was implemented to experimentally measure the static modulus magnitude. However, since the tubes used vibrate at different frequencies and the magnitude of the modulus is frequency dependant, the selected values were modified based on the value measured from static stress-strain test, and subsequently varied considering the observed behavior on related papers [38-41].

4.2.2 Stress-strain test

The tension test is widely used to provide basic design information on materials. In the tension test, a specimen is subjected to a continually increasing uniaxial tensile force while simultaneous observations are made such as the specimen elongation. An engineering stress-strain curve is constructed from the load elongation measurements as is depicted in Fig 2.4.

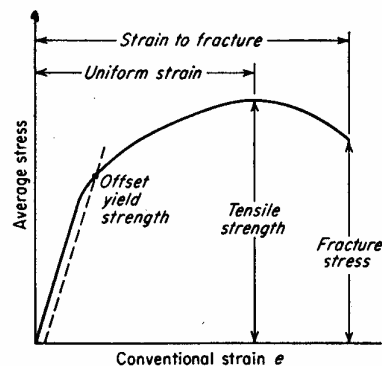


Fig. 4.9 Engineering stress-strain curve [42]

The mathematical static Young's modulus describes the tendency to be deformed when a force is applied to it. The elastic modulus of an object is defined as the slope of its stress-strain curve:

$$E = \frac{\text{stress}}{\text{strain}} \quad (4.2-2)$$

where E is the elastic modulus; stress is the force causing the deformation divided by the area to which the force is applied; and strain is the ratio of the change caused by the stress to the original state of the object [43].

TABLE XXI APPROXIMATE YOUNG'S MODULUS OF RUBBER

	Young's Modulus	Unit
Rubber	$1 \cdot 10^7 - 100 \cdot 10^7$	<i>dyne / cm²</i>

4.3 Noise Removal

A source of error in the characteristic acoustic impedance estimation is the noise caused by electrical systems and low acoustic signals not captured by the transducer. These noises generate error in the characteristic acoustic impedance estimated. System identification was used to predict a time domain sequence signal from the noisy recorded signal.

The noise was modulated using the following mathematic expression

$$y(t) = A \cdot e^{-\alpha t} \cdot \sin(\omega t - \phi) + DC \quad (4.3-1)$$

where A is amplitude in *volts*, α is the attenuation constant, ω is the damped frequency in *rad/s* and DC is the offset in *Volt* of the signal.

Nonlinear least mean square parameter estimation identification techniques were used to determine the parameters. Gauss-Newton algorithm was implemented since it is an iterative procedure that is used typically to solve nonlinear least squares problems. The algorithm for m given functions f_1, \dots, f_m of n parameters p_1, \dots, p_n with $m \geq n$, want to minimize the sum

$$S(p) = \sum_{i=1}^m (f_i(p))^2 \quad (4.3-2)$$

Where, p stands for the vector (p_1, \dots, p_n) .

$$\hat{p}^{k+1} = \hat{p}^k - (J_f(p^k)^T J_f(p^k))^{-1} J_f(p^k)^T f(p^k) \quad (4.3-3)$$

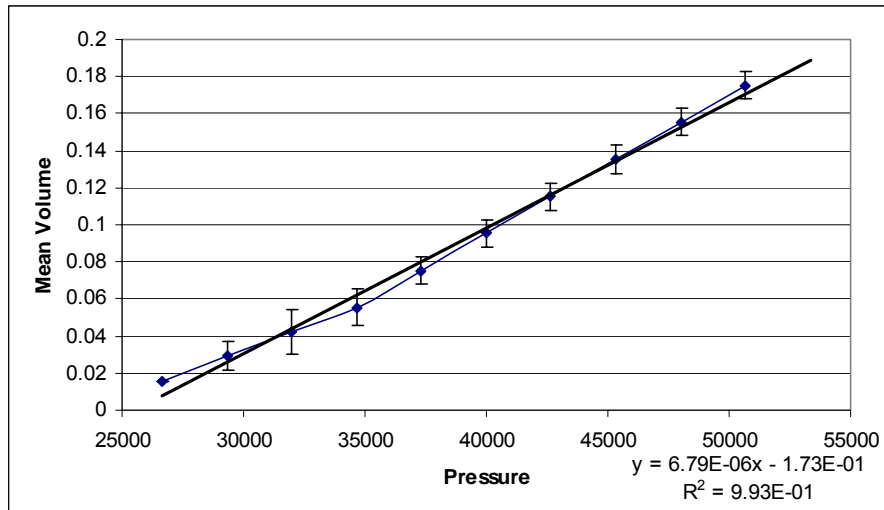
where $f=(f_1, \dots, f_m)$ and J_f denotes the Jacobian of f and \hat{p} the parameters to estimate. In this algorithm, the user has to provide an initial guess for the parameter vector p , which is called \hat{p}^0 .

4.4 Results and Discussion

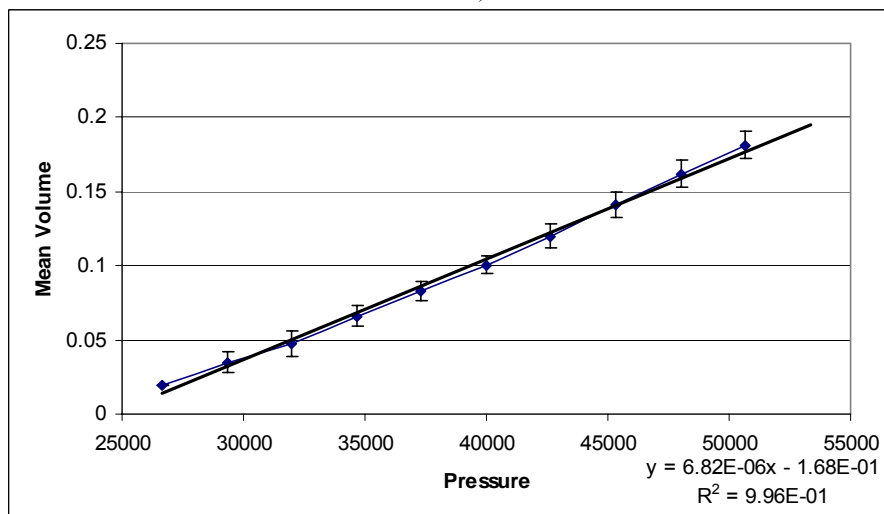
This section presents the results of the experiments performed to understand how the input characteristic acoustic impedance and the wall compliance change when the tube wall thickness is varied. The first part shows the results obtained with the volumetric test technique. The second part shows the results of using inverse filtering technique. The third part shows the results obtained from using acoustic reflectometry technique to estimate the characteristic acoustic impedance in tubes without foreign materials and with foreign materials on the outer walls. The fourth part of this section shows and discusses the results obtained from modeling with acoustic reflectometry. The last part presents the results obtained when the system identification technique is used to reconstruct the natural system response.

4.4.1 Volumetric Test

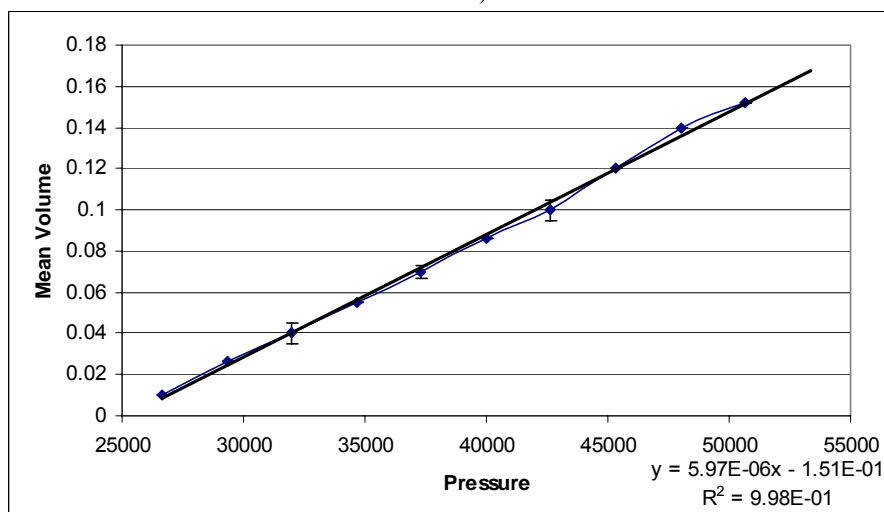
The volumetric test was used to determine the tubes wall compliance. Water at temperature $T = 25$ °C was injected into five latex tubes with different wall thickness and lengths of 22cm. Fig. 4.10 depicts the volume output in function of pressure for five different latex tubes. A linear fitting was computed for each case, where the total wall compliance is the curve's slope. To obtain an approximation of per unit length wall compliance or local wall compliance, the total wall compliance was divided by the tube length l .



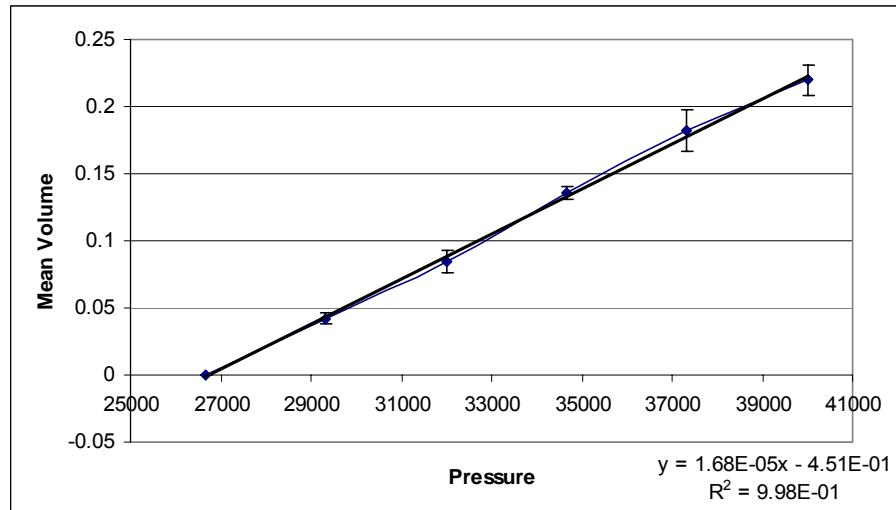
a)



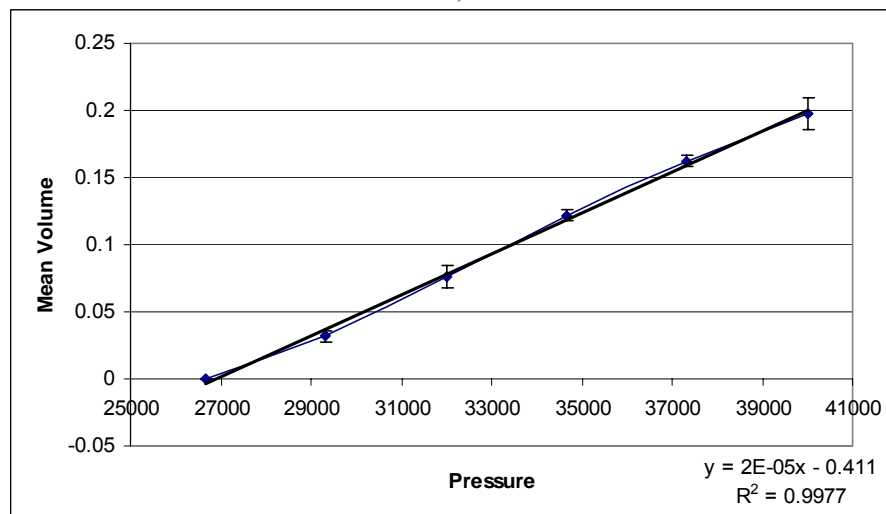
b)



c)



d)



e)

Fig. 4.10 Volume vs. pressure. Curves include linear fitting with its mathematical expressions for latex tubes. a) $h = 0.159$ cm, b) $h = 0.159$ cm, c) $h = 0.198$ cm, d) $h = 0.238$ cm, e) $h = 0.317$ cm.

TABLE XXII WALL COMPLIANCE MEASUREMENTS FOR DIFFERENT RUBBER PIPES USING VOLUMETRIC TESTS

Thickness (cm)	Measured Compliance	Units
0.119	$1.79 \cdot 10^{-7}$	$cm^5/dyne$
0.159	$1.71 \cdot 10^{-7}$	$cm^5/dyne$
0.198	$1.55 \cdot 10^{-7}$	$cm^5/dyne$
0.238	$1.36 \cdot 10^{-7}$	$cm^5/dyne$
0.317	$1.31 \cdot 10^{-7}$	$cm^5/dyne$

Fig. 4.11 depicts the behavior of the local wall compliance when the wall thickness increases. It can be observed that the latex tube stored capacity decreased when the wall thickness increased.

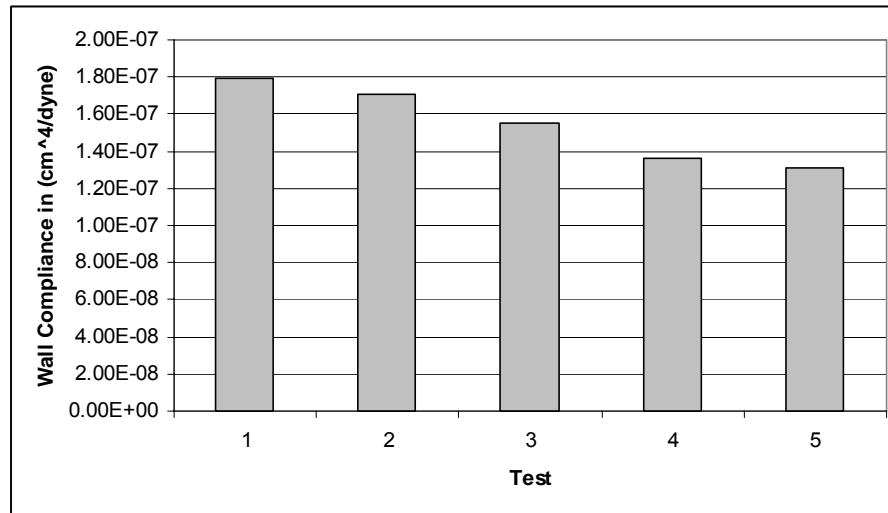


Fig. 4.11 Local wall compliance for latex tubes. Test 1 $h = 0.159$ cm, Test 2 $h = 0.159$ cm, Test 3 $h = 0.198$ cm, Test 4 $h = 0.238$ cm, Test 5 $h = 0.317$ cm.

4.4.2 Acoustic Hanning pulse created using inverse filtering technique

An acoustic Hanning pulse was created using inverse filter technique. The frequency content of this pulse had to be less than the cut-off frequency in order to ensure plane wave propagation. The cut-off frequency was computed considering the tube inner diameter $d = 0.647$ cm by which the obtained frequency was $f_{cuff} = 31.057$ kHz. Therefore, considering the transducer and the speaker frequency response, a Hanning acoustic pulse with a bandwidth of 0-14 kHz was created.

According to the procedure described in the previous section, to avoid nearby reflections caused by bounces in the source tube boundary, an extension tube was connected at the end of the source tube as Fig. 4.12 shows. Afterward, the inverse filtering technique was applied taking into consideration an electric Hanning pulse $x(t)$ of approximately 50 μ s (see Fig. 4.13 (a)) to interrogate the system. This signal was sent to the speaker and then the acoustic signal $y(t)$ was recorded (see Fig. 4.13 (b)). These signals allow computing the system response $H(\omega)$ in frequency domain. After obtaining the frequency response, the sequence $y_f(t)$ is computed using equation 4.2-2 with a digital

band pass filter $W(\omega)$ with cut-on and cut-off frequencies of $f_{cut-on} = 500 \text{ Hz}$ and $f_{cut-off} = 1500 \text{ Hz}$ respectively.

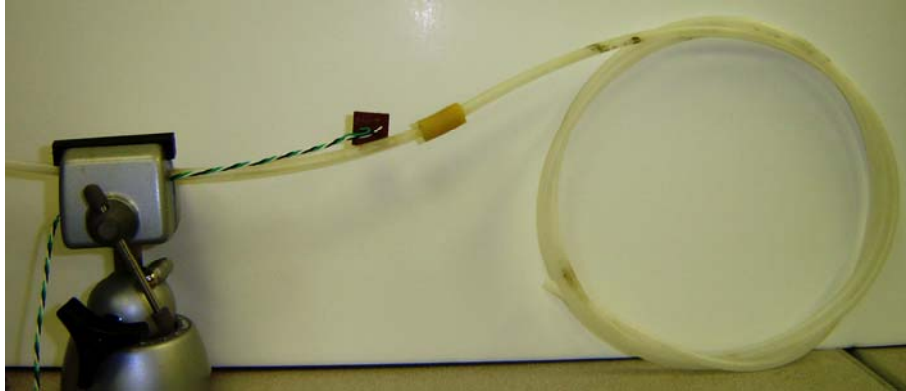
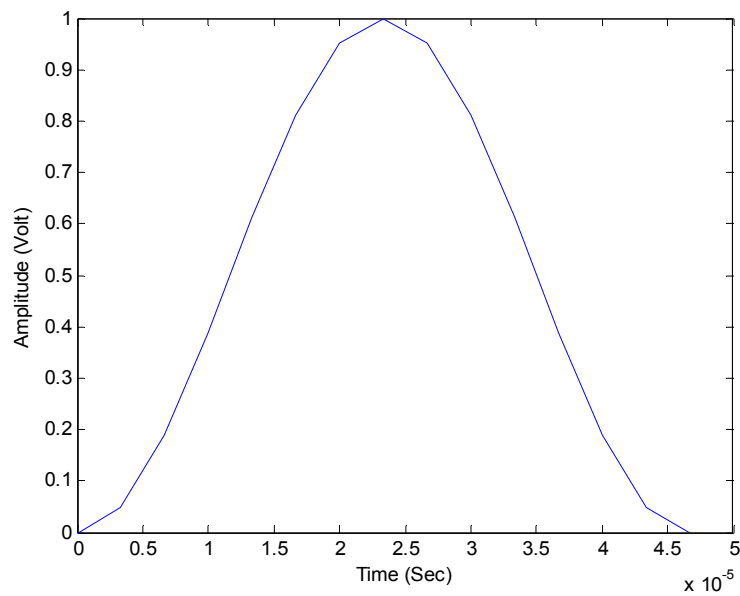


Fig. 4.12 Reflectometer and extension tube used to generate an acoustic pulse to interrogate the latex tubes.

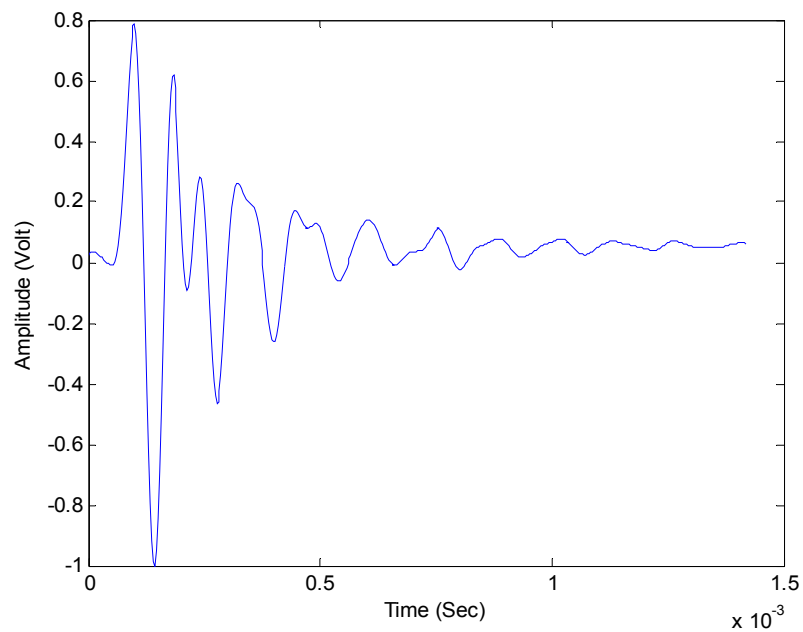
Fig. 4.14 sketches the resulting signal $y_f(t)$ which shows an incident pulse of $100 \mu\text{s}$ duration and its respective reflection when the extension tube was retired. Notice that the reflection is inverted; this occurs because there is not a tube connected at the end of the source tube.

Once the inverse filtering was applied, the extension tube was removed from the end of the reflectometer. A cap was placed on the end of the reflectometer and the incident and reflected pulses were analyzed applying the inverse fast Fourier transform. Fig. 4.15 depicts the magnitude of the incident and reflected acoustic pulses as a function of frequency in Hz . It can be observed that the reflected pulse exhibits a bandwidth between 0-14k Hz . Notice that the incident pulse also exhibits this same bandwidth. The only difference is the magnitude.

The time delay between the acoustic incident pulse and its acoustic reflected pulse was studied with an open ended reflectometer, using cross correlation. The acoustic incident and reflected signals were cropped from ten different tests and applying equation 4.1-4 the time delay was $T_d = 2.2 \text{ ms}$ with a standard deviation of zero.



a)



b)

Fig. 4.13 Input and output pulses used to determine the frequency response $H(\omega)$ of the system (referring to the DENON amplifier, preamplifier and reflectometer). a) Electric pulse $x[n]$ of $50 \mu\text{s}$ designed in order to interrogate the system. b) Output signal $y[n]$ resulting from the perturbation $x(t)$.

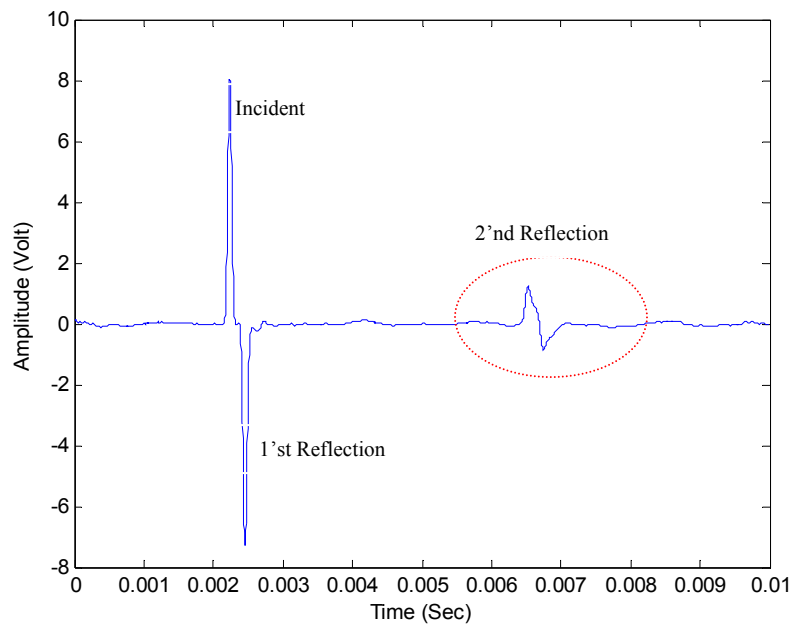


Fig. 4.14 Signal obtained after deconvolution. It contains three acoustic pulses: the incident, first reflection and second reflection. The incident pulse is a positive Hanning and the reflected, a negative Hanning pulse.

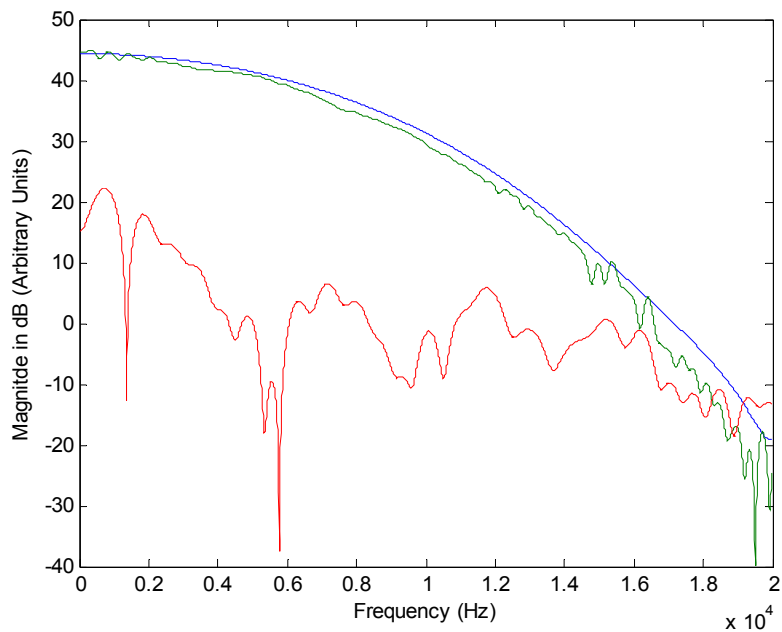


Fig. 4.15 Fourier transform of the incident pulse, reflected pulse and noise. The incident pulse is represented by the color blue. The reflected pulse is represented by the color green. The noise is represented by the color red.

A critical part of this experiment was the connection between the reflectometer and the extension tube. Additionally, the foam had to be placed in a position in front of the source tube and coupler. This was needed to ensure that the inverse filter would generate the correct signal.

4.4.3 Acoustic characteristic impedance results

In this section, the results of the experiments performed using acoustic reflectometry to compute characteristic acoustic impedances are presented. These experimentations were implemented using five different rubber tubes with wall thicknesses of $h = 0.115$ cm, $h = 0.159$ cm, $h = 0.198$ cm, $h = 0.238$ cm, $h = 0.317$ cm and with an inner diameter of $d = 0.647$ cm. These tubes were selected considering the highest frequency that the transducer can sense ($f = 10$ kHz) and the speaker can generate ($f = 15$ kHz), therefore the tubes transversal frequencies should be in these ranges.

The input characteristic acoustic impedances were computed from experimental data in the range of 0 Hz to 20 kHz, using pulse-echo acoustic reflectometry. The latex tubes were interrogated using a Hanning pulse with a bandwidth of 0-14 kHz considering planar wave propagation. The acoustic signals inside the source tube were recorded using a sampling frequency of 300 S/s.

4.4.3.1 Tubes experimentation without foreign material

These tests were made connecting the compliant tubes to the source tubes. The acoustic response to an incident acoustic Hanning pulse was recorded by the microphone as is depicted in the Fig. 4.16. Then the incident (Fig. 4.16 (a)) and reflected (Fig. 4.17 (b)) acoustic pulse were cropped from the recorded signal. Notice from the Fig. 4.17 (b) that the reflected signals exhibit differences between them, such as damping, magnitude and frequency.

The Fast Fourier Transforms (*FFT*) of the incident, reflected and background noise signals were computed (see Fig. 4.18). From these curves it can be observed that the spectra of the reflected contains information between 0-12 kHz and exhibits two peaks between the 2-5 kHz and the spectra of the incident pulse contains information between

0-14 kHz. On the other hand, the signal to noise ratio for frequencies below 1.5 kHz is low; therefore, acoustic information contained at this lower frequency range is not suitable for analysis.

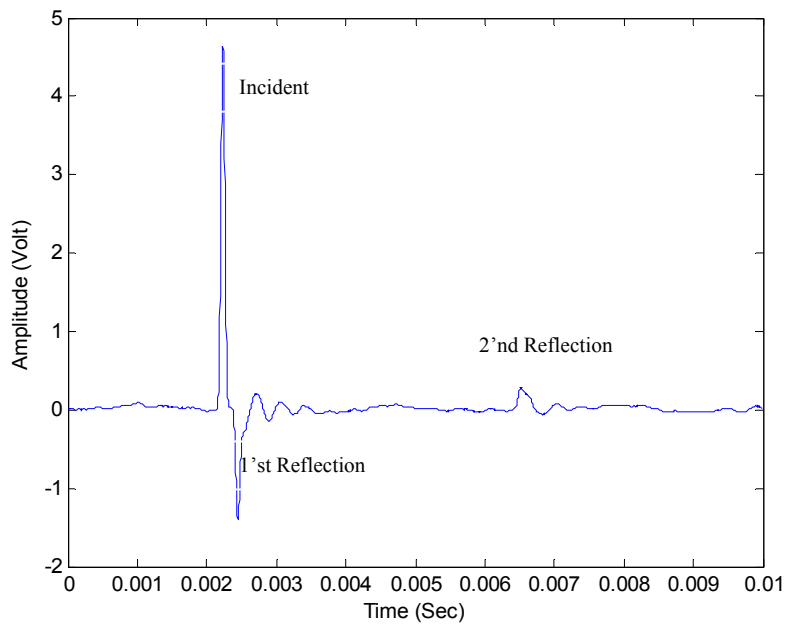
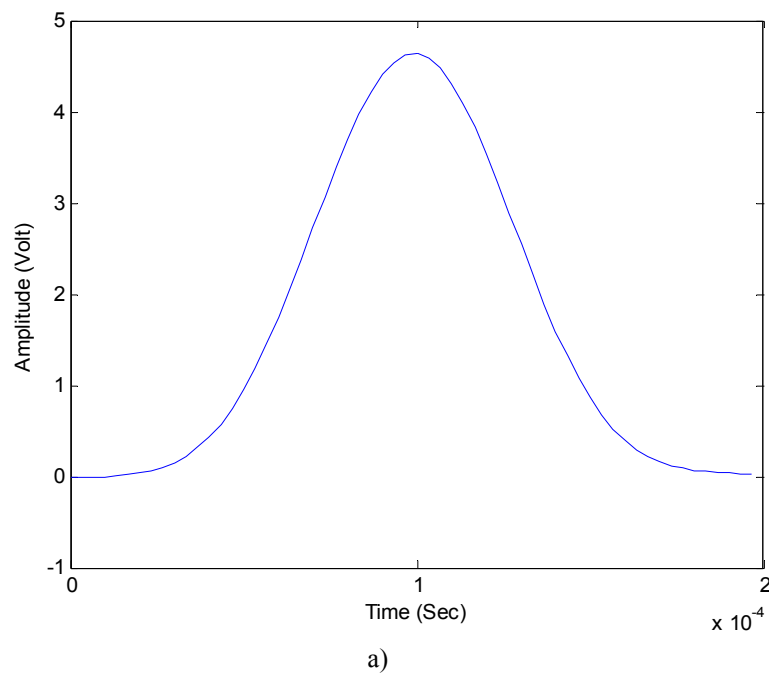
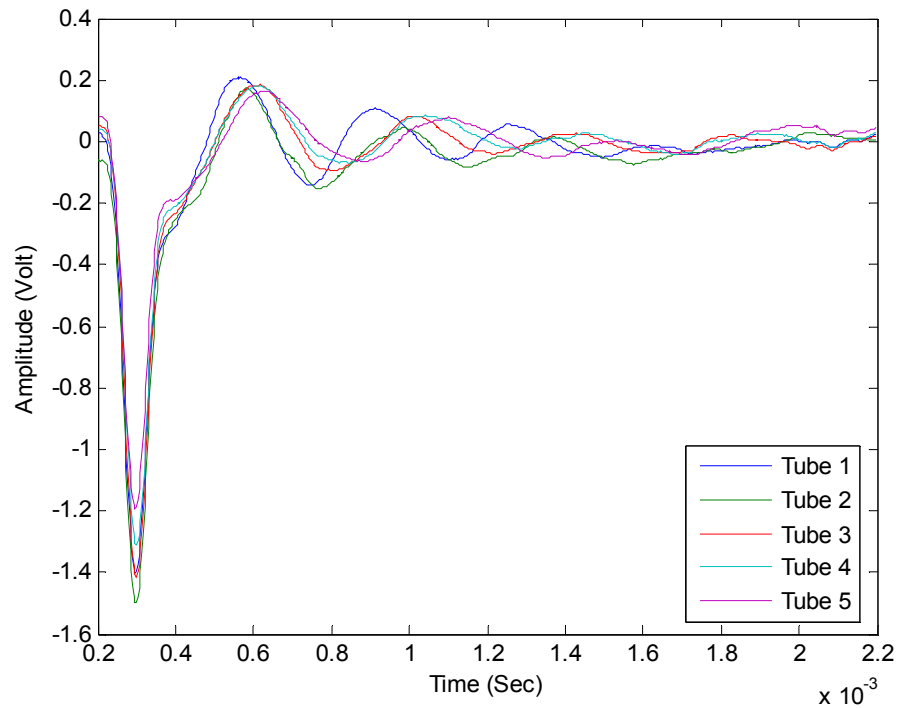


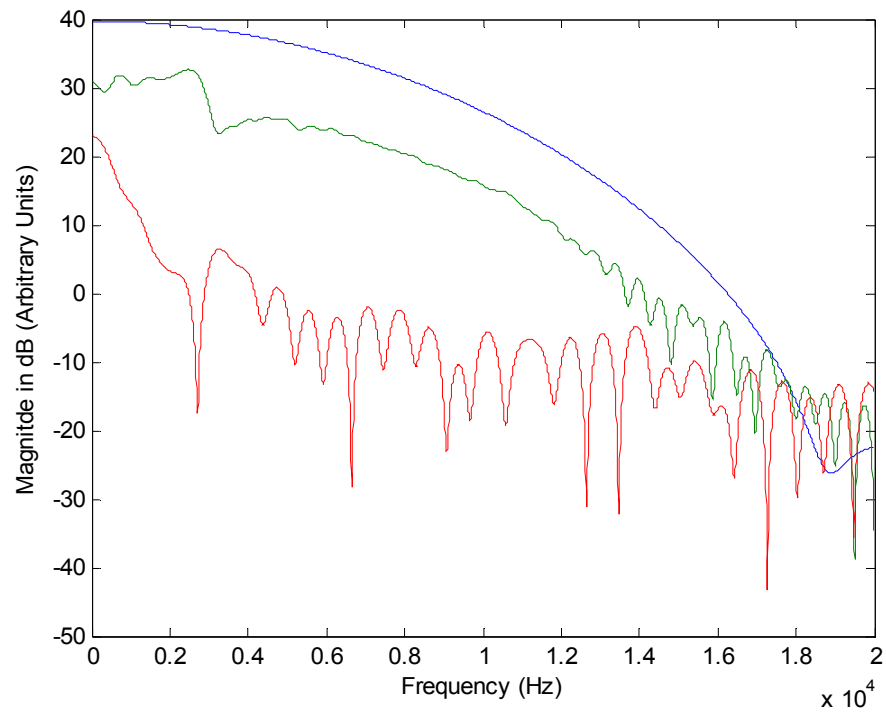
Fig. 4.16 Signal recorded at a sampling rate of 300 kS/s for a tube with an inner diameter of 0.647 cm and wall thickness of 0.119 cm.



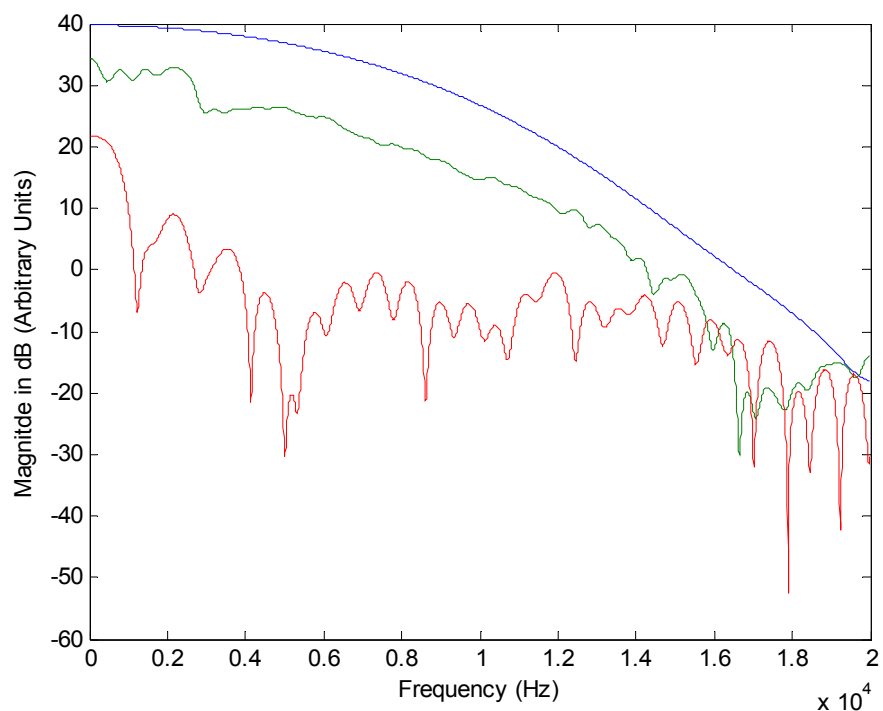


b)

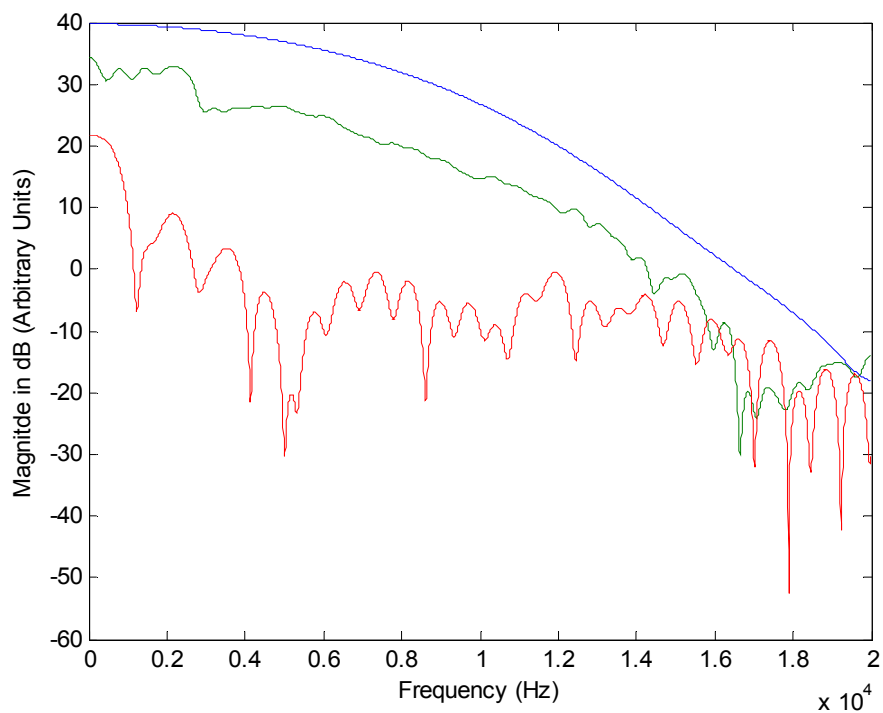
Fig. 4.17 a) Incident signal of 50 μ s of duration, recorded at a sampling rate of 300 kS/s. b) Reflected signal recorded at a sampling rate of 300 kS/s.



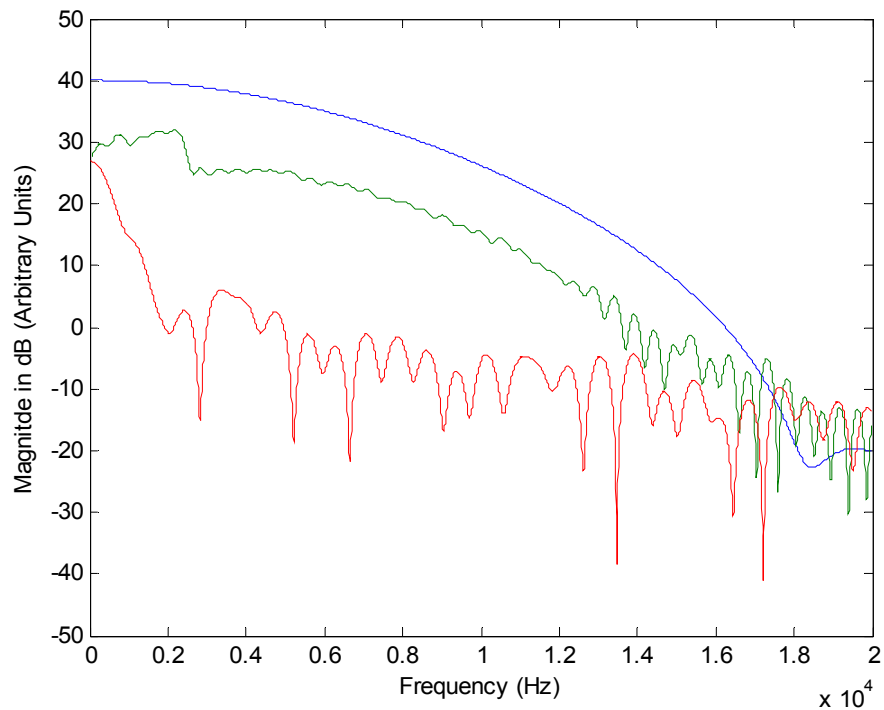
a)



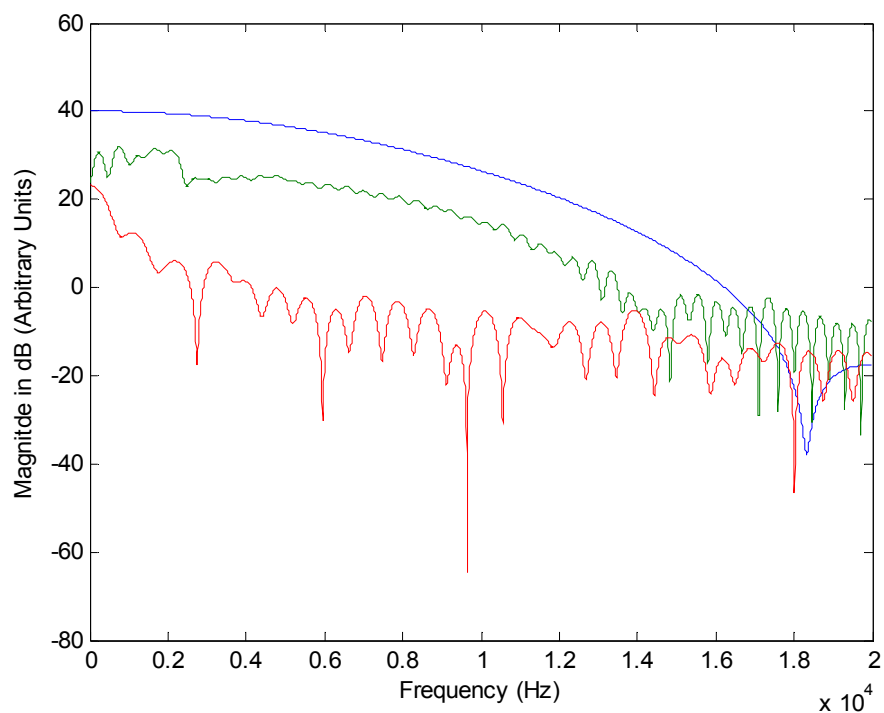
b)



c)



d)



e)

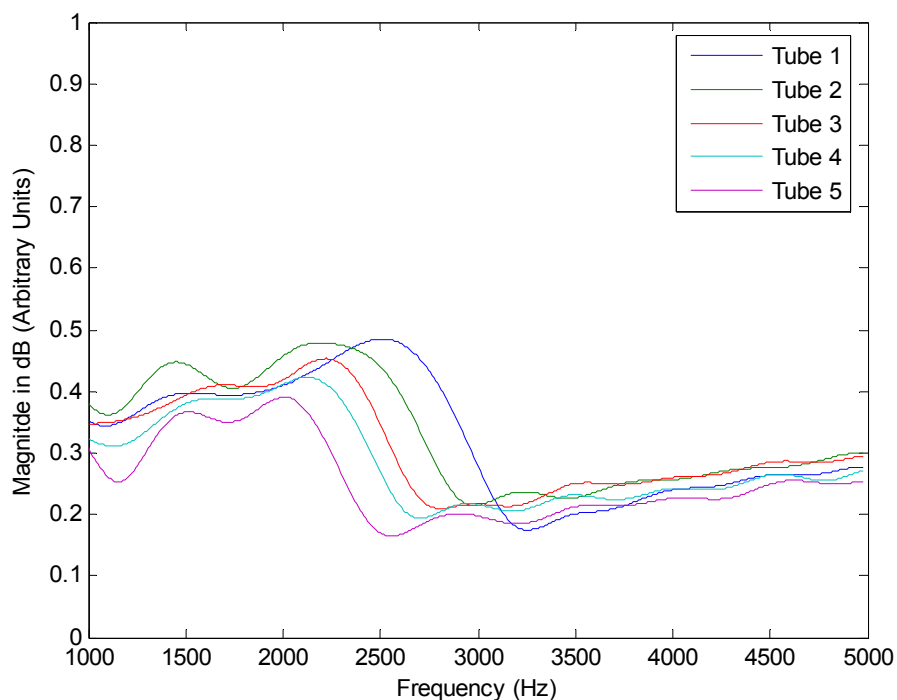
Fig. 4.18 Fast Fourier Transforms of the incident, reflected and noise signals experimentally measured for latex tubes with different wall thicknesses. a) $h = 0.159$ cm, b) $h = 0.159$ cm, c) $h = 0.198$ cm, d) $h = 0.238$ cm, e) $h = 0.317$ cm.

The reflection coefficient and characteristic acoustic impedances were computed with equation 4.1-5 and 4.1-6 respectively. A length of 600 samples was considered to compute the characteristic acoustic impedances and reflection coefficients.

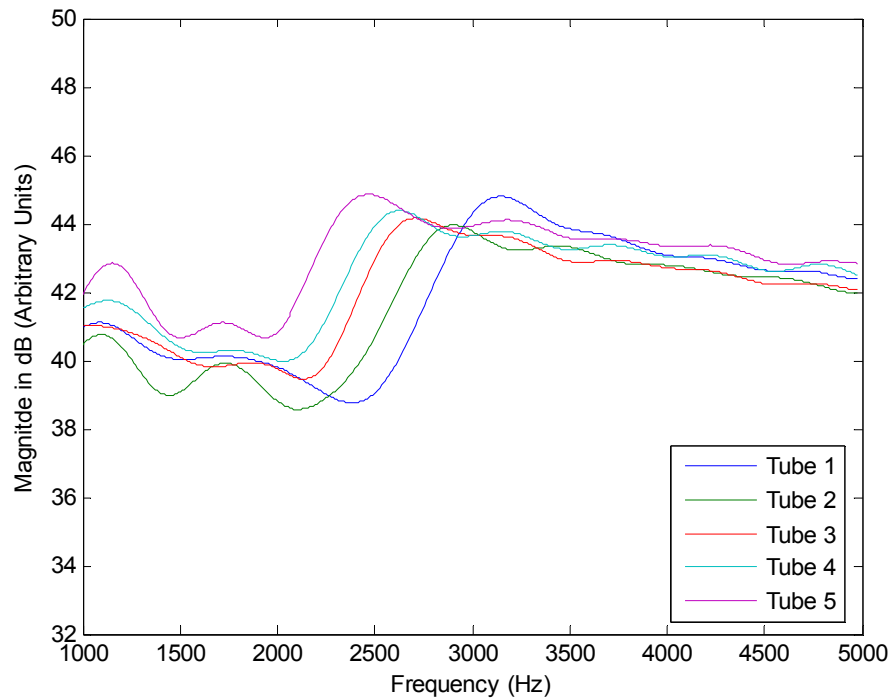
Fig. 4.19 (a) shows the experimental reflection coefficients as a function of frequency in Hz , while Fig. 4.19 (b) depicts the experimental characteristic acoustic impedances as a function of frequency in Hz . From the characteristic acoustic impedance analysis it can be observed that the transversal resonant frequencies are dependent on the tubes wall thickness. Table XXIII lists the transversal frequencies experimentally observed from the characteristic acoustic impedance curves, obtained for the five compliant tubes.

TABLE XXIII EXPERIMENTAL TRANSVERSAL FREQUENCIES OBTAINED FROM THE CHARACTERISTIC IMPEDANCE.

	$f_{res} (Hz)$	$f_2 (Hz)$
Tube 1	2380	3149
Tube 2	2243	2893
Tube 3	2124	2700
Tube 4	2032	2618
Tube 5	1922	2453



a)



b)

Fig. 4.19 Characteristic acoustic impedance for latex tubes with different wall thicknesses. Test 1 $h = 0.159$ cm, Test 2 $h = 0.159$ cm, Test 3 $h = 0.198$ cm, Test 4 $h = 0.238$ cm, Test 5 $h = 0.317$ cm.

4.4.3.2 Tubes experimentation with foreign material

Masking tape was added to the tubes wall in order to observe the effect in the characteristic acoustic impedances. The acoustic response to an incident acoustic Hanning pulse was recorded by the microphone as is depicted in Fig. 4.20. Then, the incident (Fig. 4.21 (a)) and reflected (Fig. 4.21 (b)) acoustic pulses were cropped from the recorded signal. Notice from Fig. 4.21 (b) that the reflected signal exhibit differences between them, such as damping, magnitude and frequency.

The Fast Fourier Transforms (*FFT*) of the incident, reflected and background noise signals were computed and shown in Fig. 4.21. From these curves it can be observed that the spectra of the reflected signal contains information between 0-12 kHz and exhibits two peaks between the 2-5 kHz and the spectra of the incident pulse contains information between 0-14 kHz. On the other hand, the signal to noise ratio for frequencies below 1.5 kHz is low; therefore, acoustic information contained at this lower frequency range is not suitable for analysis.

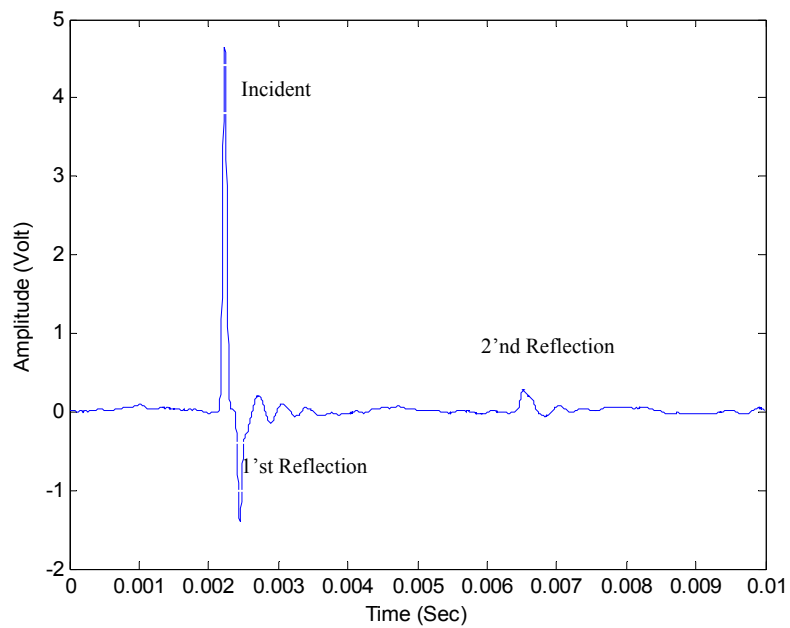
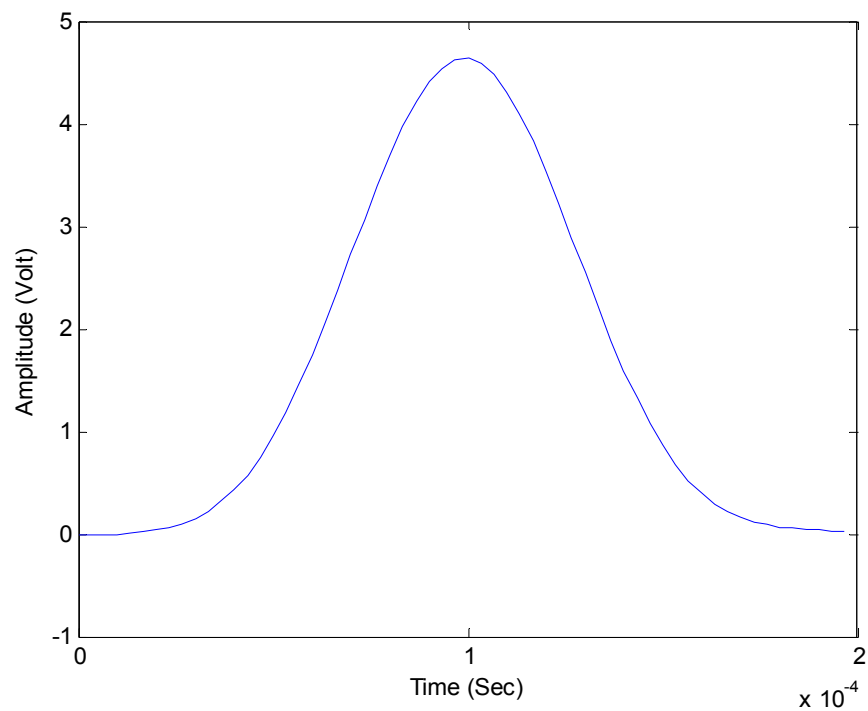


Fig. 4.20 Signal recorded at a sampling rate of 300 kS/s for a tube with a inner diameter of 0.647 cm and wall thickness of 0.119 cm.



a)

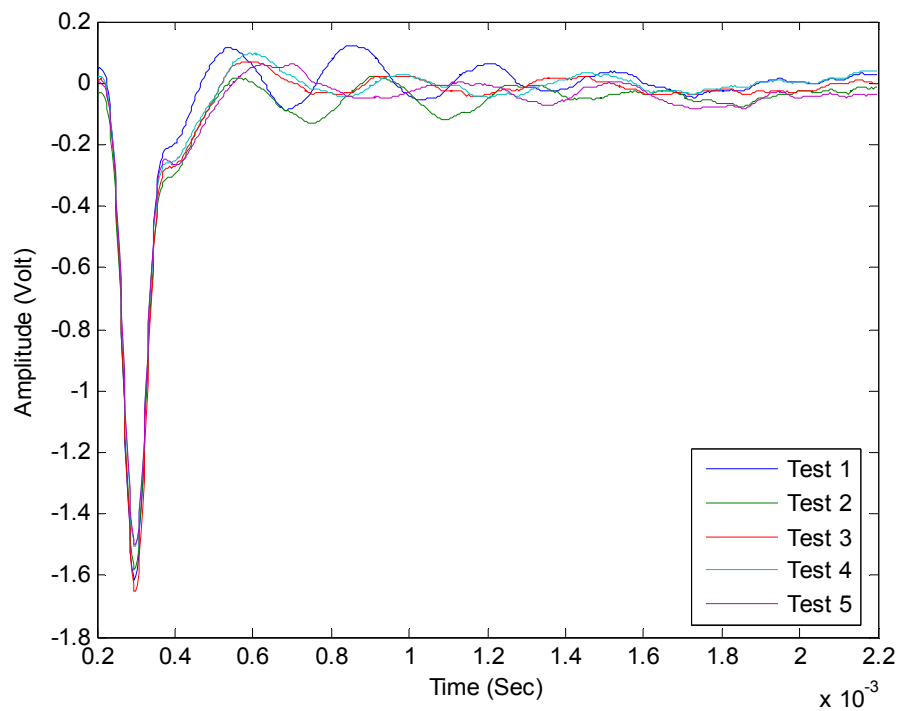
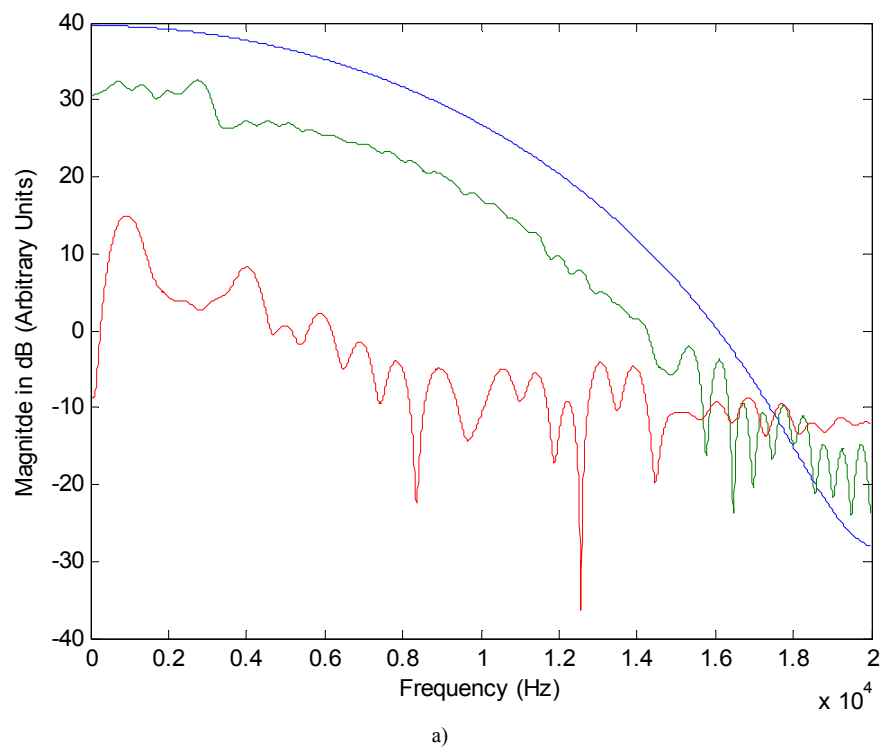
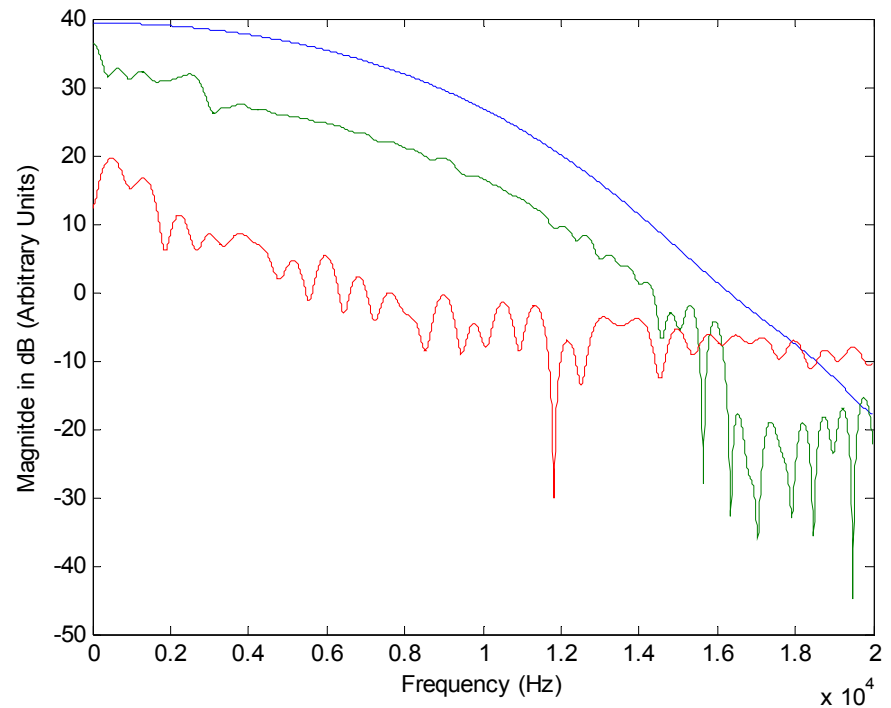
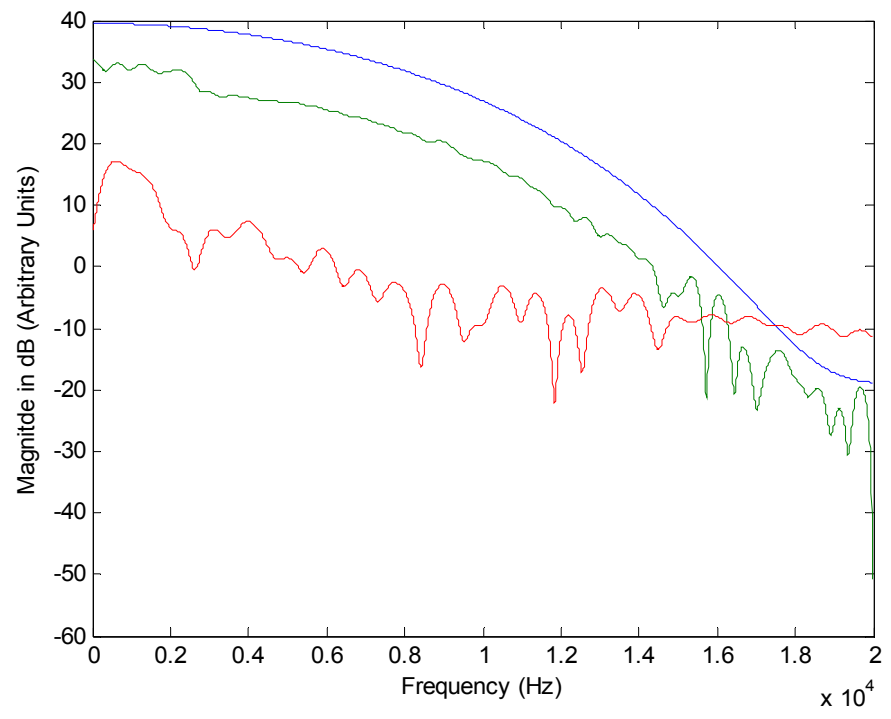


Fig. 4.21 a) Incident signal of 50 μs of duration, recorded at a sampling rate of 300 kS/s. b) Reflected signal recorded at a sampling rate of 300 kS/s.

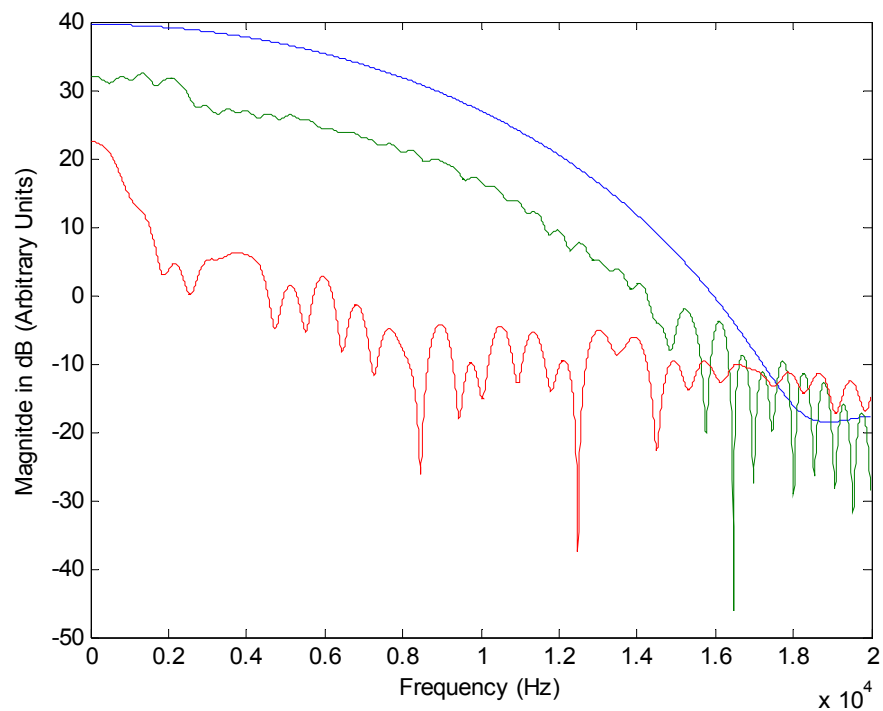




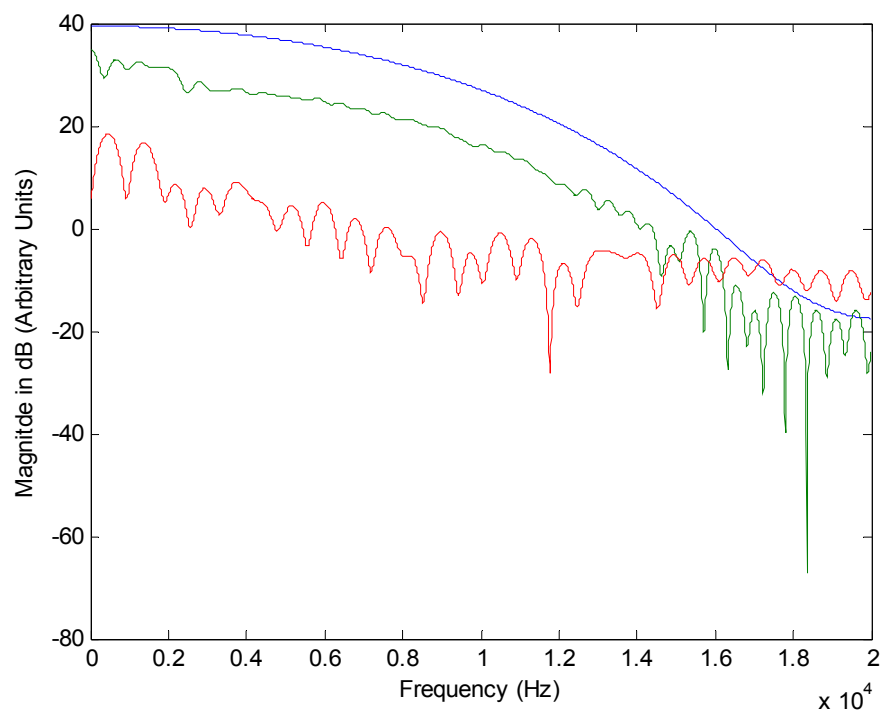
b)



c)



d)



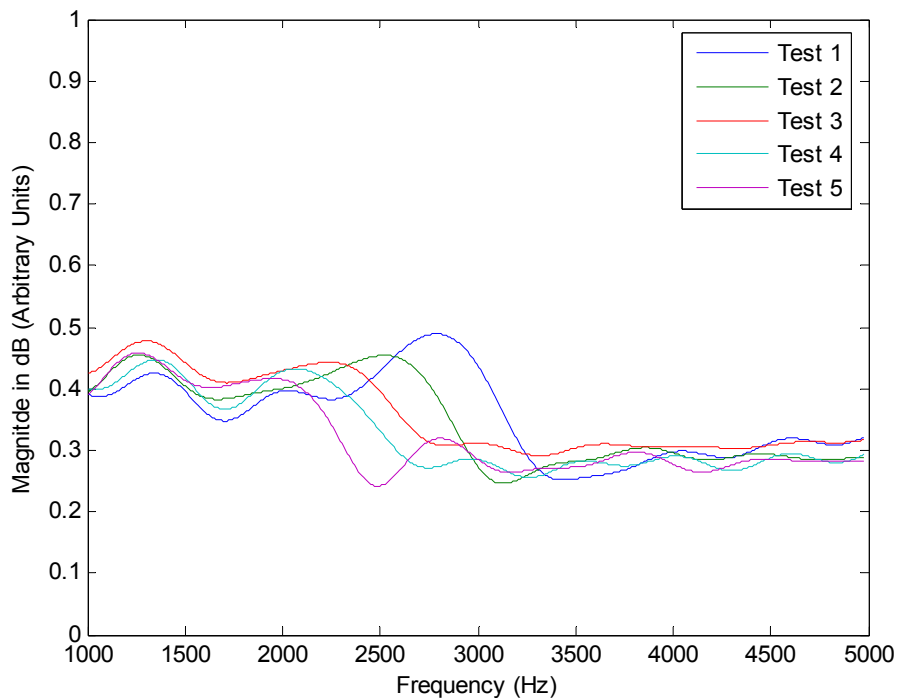
e)

Fig. 4.22 Fast Fourier Transforms of the incident, reflected and noise signals experimentally measured for latex tubes with different wall thickness values. a) $h = 0.159$ cm, b) $h = 0.159$ cm, c) $h = 0.198$ cm, d) $h = 0.238$ cm, e) $h = 0.317$ cm.

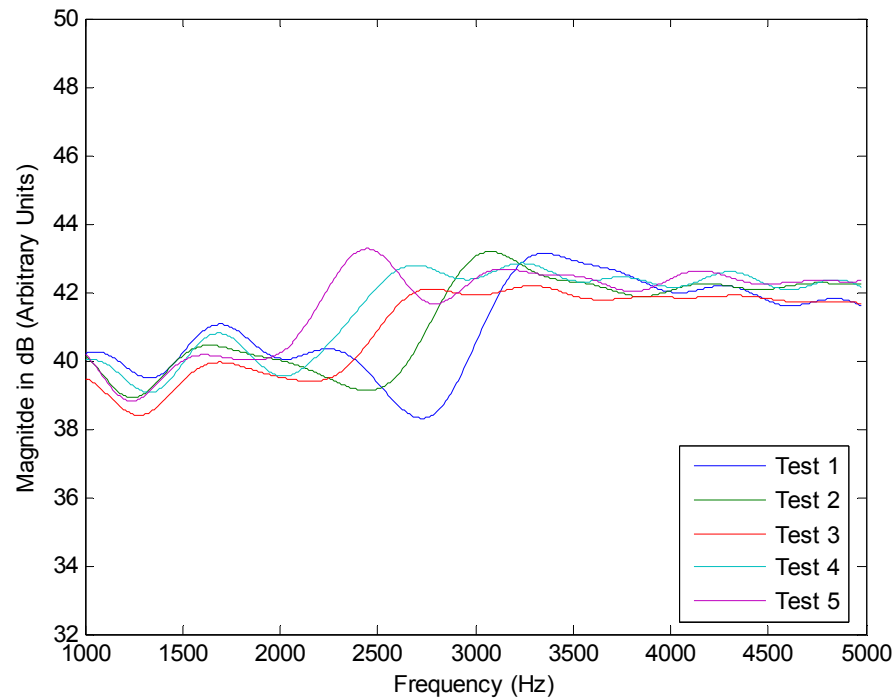
The reflection coefficient and characteristic acoustic impedances were computed with equations 4.1-5 and 4.1-6 respectively. A length of 600 samples was considered to compare the behavior of the characteristic acoustic impedances and reflection coefficients. Fig. 4.23 (a) shows the experimental reflection coefficients as function of frequency in Hz , while Fig. 4.23 (b) depicts the experimental characteristic acoustic impedances as function of frequency in Hz . From the characteristic acoustic impedance analysis it can be observed that the transversal resonant frequencies are dependent on the reflection vector length. Table XXIV lists the transversal frequencies experimentally observed from the characteristic acoustic impedances obtained for the five compliant tubes.

TABLE XXIV EXPERIMENTAL TRANSVERSAL FREQUENCIES OBTAINED FROM THE CHARACTERISTIC IMPEDANCE.

	$f_{res} (Hz)$	$f_2 (Hz)$
Tube 1	2728	3314
Tube 2	2453	3057
Tube 3	2178	2764
Tube 4	2023	2691
Tube 5	1885	2453



a)



b)

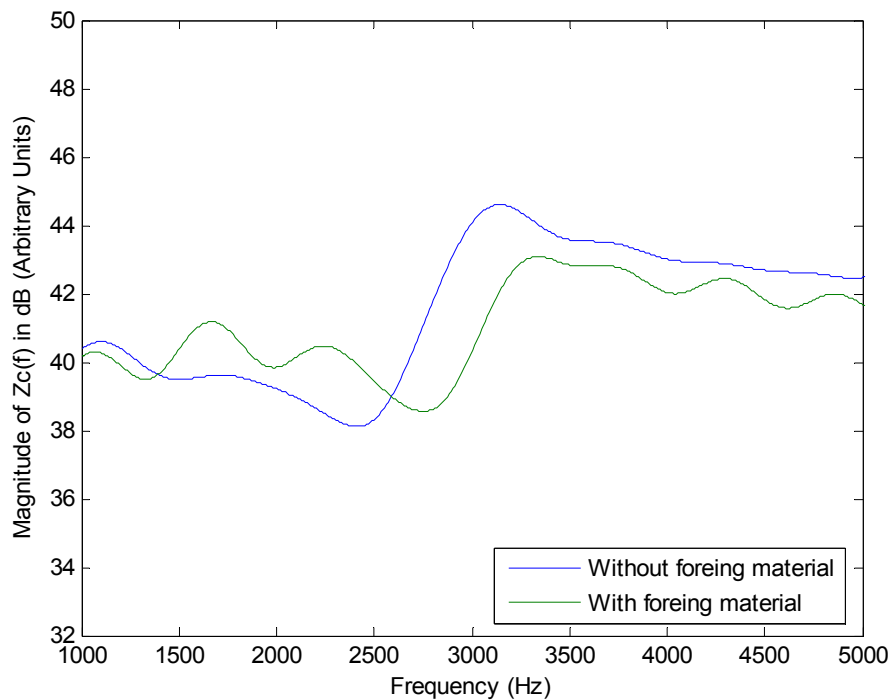
Fig. 4.23 Characteristic acoustic impedance for latex tubes with different wall thicknesses. Test 1 $h = 0.159$ cm, Test 2 $h = 0.159$ cm, Test 3 $h = 0.198$ cm, Test 4 $h = 0.238$ cm, Test 5 $h = 0.317$ cm.

4.4.3.3 With vs. without foreign material discussion

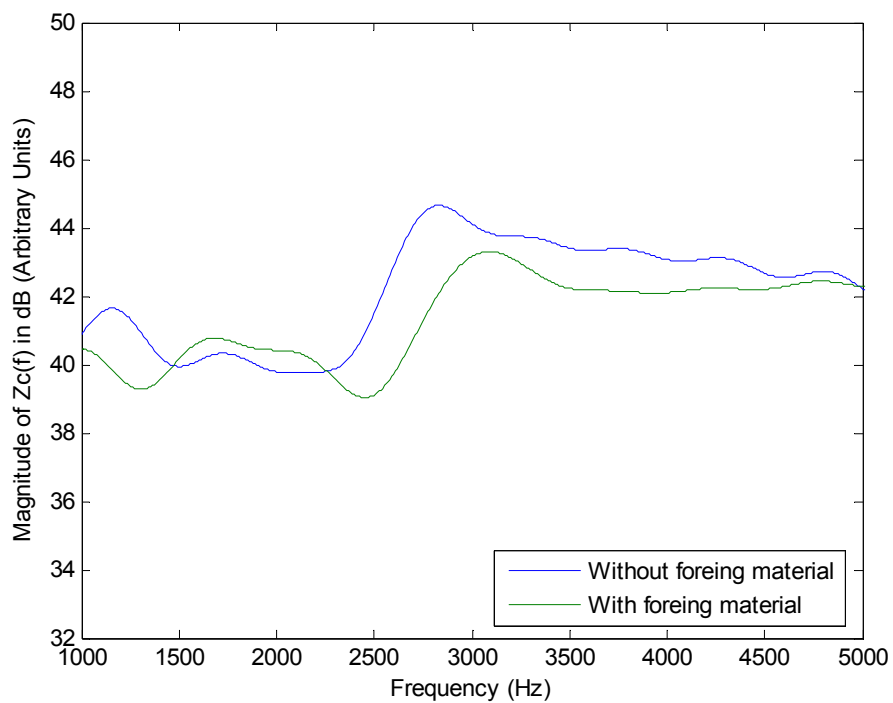
When a foreign material is fixed to the tubes, it can be observed that the transversal frequencies increase. This behavior occurs because the fact that the Young's modulus increases when a foreign material is added, making the tubes harder. Table XXV lists the obtained values for f_{res}^* and f_2^* that represent transversal frequencies without foreign material, and f_{res}^{**} and f_2^{**} represent the obtained transversal frequencies with foreign material.

The characteristic acoustic impedance of latex tubes were compared, for the cases with and without foreign material. Notice from Fig. 4.24 that the characteristic acoustic impedance curves are similar, but they have different amplitudes and different transversal frequencies. For the cases when the wall thicknesses were 0.119 cm and 0.159 cm, it was observed that the characteristic impedance amplitude and its transversal frequencies are affected dramatically, however when the wall thickness was over 0.238 cm, the

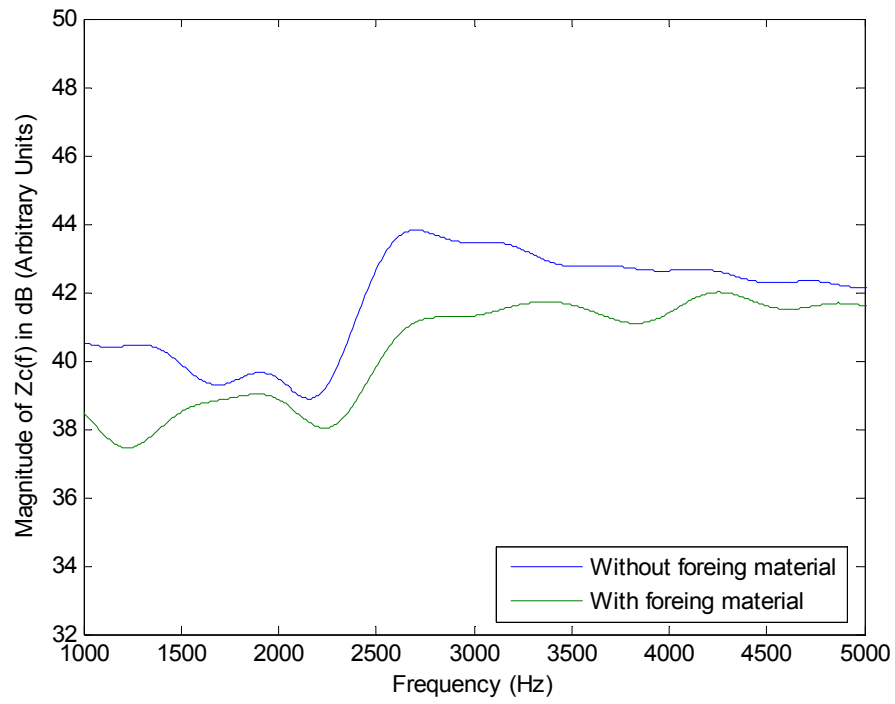
amplitude changes, but the transversal frequencies are not modified. Notice that for both cases, when $f = 1000$ and $f = 5000$, the amplitude tends to the same amplitude.



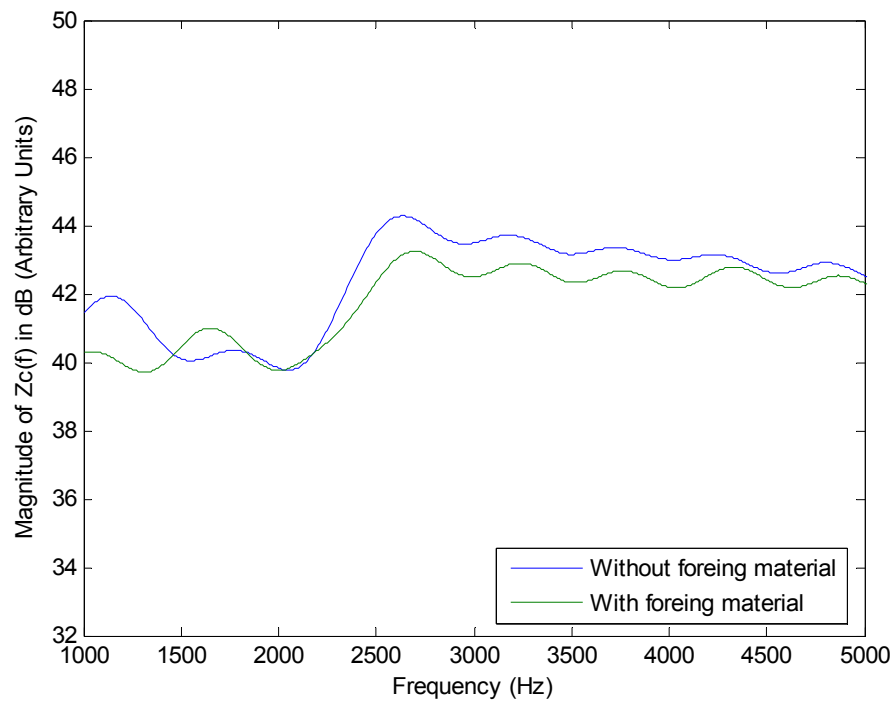
a)



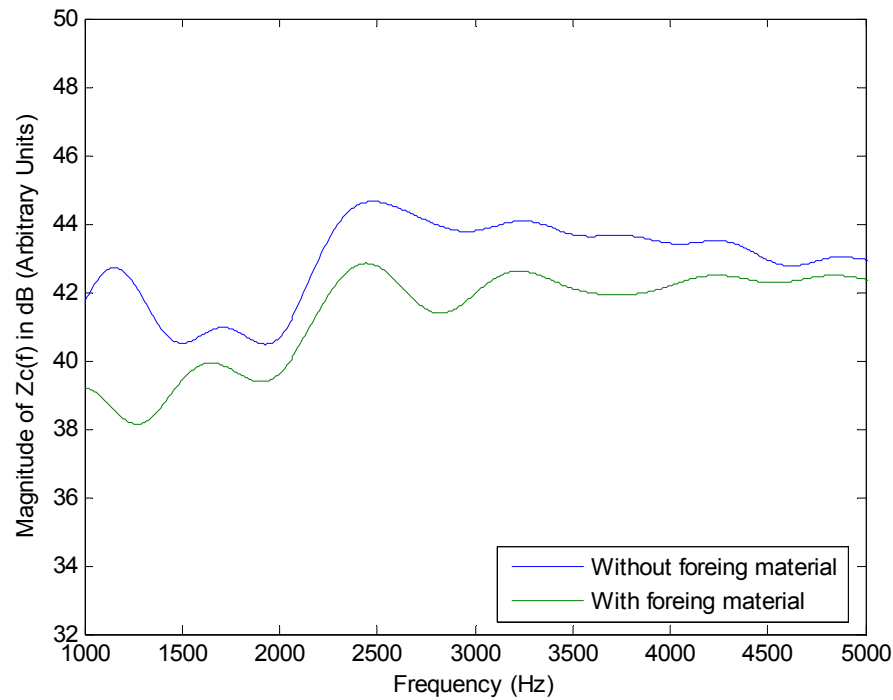
b)



c)



d)



e)

Fig. 4.24 Characteristic acoustic impedance for latex tubes with different wall thickness, with foreign materials and without foreign materials. a) $h = 0.159$ cm, b) $h = 0.159$ cm, c) $h = 0.198$ cm, d) $h = 0.238$ cm, e) $h = 0.317$ cm.

TABLE XXV EXPERIMENTAL TRANSVERSAL FREQUENCIES OBTAINED FROM THE CHARACTERISTIC IMPEDANCE.

Thickness	f_{res}^* (Hz)	f_{res}^{**} (Hz)	f_2^* (Hz)	f_2^{**} (Hz)
Tube 1	2380	2728	3149	3314
Tube 2	2243	2453	2893	3057
Tube 3	2124	2178	2700	2764
Tube 4	2032	2040	2618	2691
Tube 5	1922	1930	2453	2490

4.5 Transmission Line Model vs. Echo-Acoustic Reflectometry

In this section, the experimental results obtained for the five tubes were compared with a lumped transmission line model results. The experimental latex tubes were considered to simulate the acoustic response to an incident Hanning pulse. Representative curves are presented with the modeled and experimental reflected acoustic

pulse signal and the characteristic acoustic impedance. Local wall compliance obtained in simulation C_{wSim} and experiments C_{wExp} are compared to observe their relations.

As was previously mentioned, the transmission line model depends on different parameters that represent the tube wall and the medium. Although different methods to experimentally obtain these properties have been published, these techniques are difficult to reproduce and the exact values of the parameters were difficult to obtain, making the analysis more complex. The Young's modulus was selected following patterns observed in related papers [38-41], considering the values range and its dependency on frequency. The density was measured using a density kit and the diameter and thickness were measured using a caliper.

In the analysis it can be observed that at frequencies higher than 1.5 kHz, where the signal to noise ratio was high, the experimental characteristic impedance curve closely resembled the one predicted by the acoustic transmission line model. In particular, the location of the valley and peak associated with the frequencies f_{res} and f_2 , respectively, were comparable in both cases.

4.5.1 Tube of 0.119 cm of thickness with inner wall of 0.647 cm

Substitution of wall parameters (listed in Table XXVI) into the transmission line model produce a response in time domain to an acoustic Hanning pulse, which was compared with the experimental acoustic response as it is illustrated in Fig. 4.25. From this figure, it can be observed that the experimental signals are similar to the simulated, exhibit the same behavior and the damping ratio for the simulation is 0.0037. Notice that the acoustic signal over the time $t = 1.5$ ms can not be measured by the microphone, because the low pressure can not be sensed.

Also, the characteristic acoustic impedances estimated experimentally and by simulation were compared in Fig. 4.26. The experimental and simulated characteristic acoustic impedances were computed from 1-5 k Hz at increments of 10 Hz, using equation 4.1-6 and 3.1-5, respectively. The reflected signal length used was of $l = 600$ samples. From these characteristic impedance curves, it can be observed that the minimum value of Z_c occurred at a frequency $f_{res}=2.38$ kHz, while the maximum value occurred at a frequency of $f_2=3.149$ kHz.

The experimental wall compliance was calculated using equation 2.3-1, yielding a wall compliance value of $C_{wExp} = 1.62 \cdot 10^{-7} \text{ cm}^5/\text{dyne}$. Substitution of wall parameters into the TLM expression for C_w yielded a per unit length wall compliance $C_{wSim} = 0.69 \cdot 10^{-7} \text{ cm}^5/\text{dyne}$.

TABLE XXVI TRANSMISSION LINE MODEL PARAMETERS USED IN SIMULATION FOR A TUBE WITH WALL THICKNESS OF 0.119 CM.

PROPERTY	SYMBOL/UNITS	TLM Parameter
Density	$\rho_w (\text{g} / \text{cm}^3)$	0.92
Wall Internal Viscosity	$\eta (\text{dyne} \cdot \text{s} / \text{cm}^2)$	300
Young's Modulus of Elasticity	$E (\text{dyne} / \text{cm}^2)$	2.6E7
Wall Thickness	$h (\text{cm})$	0.119
Wall Radius	$r (\text{cm})$	0.65

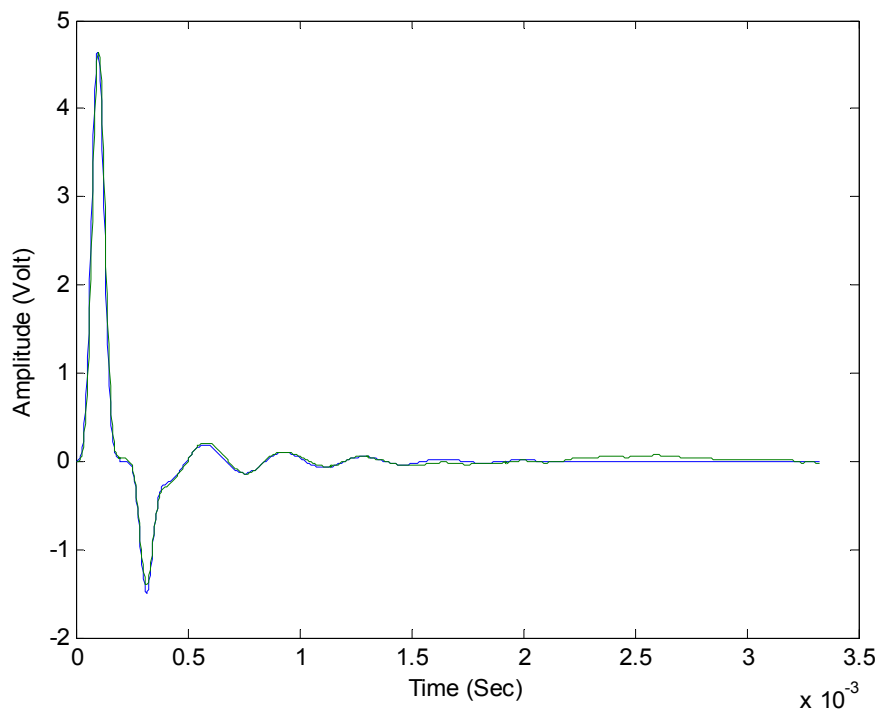


Fig. 4.25 Comparison of simulated reflected signal (blue) with acoustically obtained (green) for a latex tube with wall thickness of 0.119 cm.

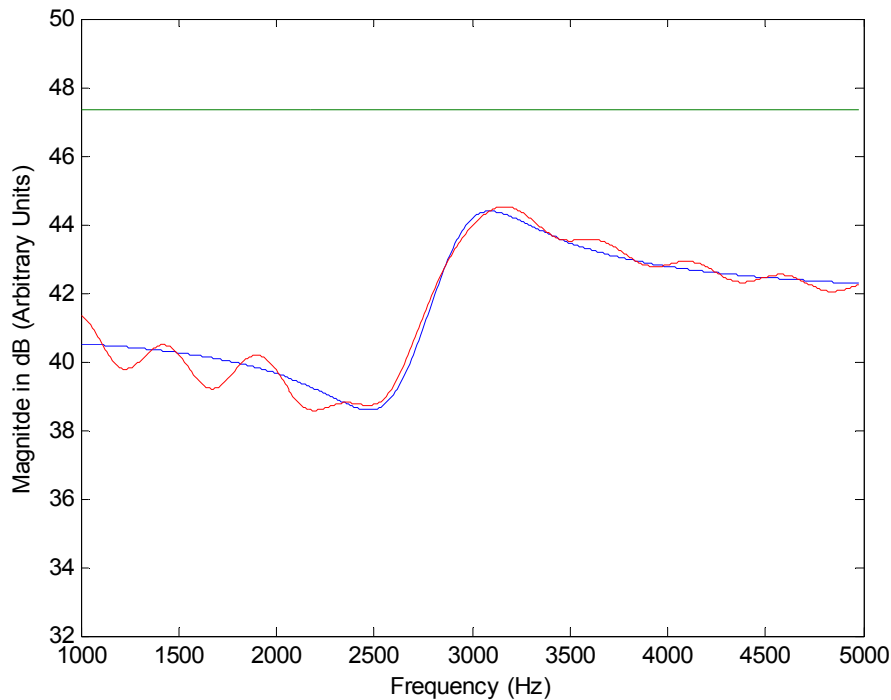


Fig. 4.26 Comparison of characteristic acoustic impedances obtained by simulation (blue) with the acoustically measured (red) for a latex tube with wall thickness of 0.119 cm. The reflectometer impedance is plotted in green.

4.5.2 Tube of 0.159 cm of thickness with inner wall of 0.647 cm

Substitution of wall parameters (listed in Table XXVII) into the transmission line model produce a response in time domain to an acoustic Hanning pulse, which was compared with the experimental acoustic response as it is illustrated in Fig. 4.27. From this figure, it can be observed that the experimental signals are similar to the simulated, exhibit the same behavior and the damping ratio for the simulation is 0.0036. Notice that the acoustic signal over the time $t = 1.2$ ms can not be measured by the microphone, because the low pressure can not be sensed.

Also, the characteristic acoustic impedances estimated experimentally and by simulation were compared in Fig. 4.28. The experimental and simulated characteristic acoustic impedances were computed from 1-5 kHz at increments of 10 Hz, using equations 4.1-6 and 3.1-5, respectively. The reflected signal length used was of $l = 600$ samples. From these characteristic impedance curves, it can be observed that the

minimum value of Z_c occurred at a frequency $f_{res}=2.243$ kHz, while the maximum value occurred at a frequency of $f_2 = 2.893$ kHz.

The experimental wall compliance was calculated using equation 2.3-1, yielding a wall compliance value of $C_{wExp} = 1.46 \cdot 10^{-7}$ cm⁵/dyne. Substitution of wall parameters into the TLM expression for C_w yielded a per unit length wall compliance $C_{wSim} = 0.608 \cdot 10^{-7}$ cm⁵/dyne.

TABLE XXVII TRANSMISSION LINE MODEL PARAMETERS USED IN SIMULATION FOR A TUBE WITH WALL THICKNESS OF 0.159 CM.

PROPERTY	SYMBOL/UNITS	TLM Parameter
Density	$\rho_w (g / cm^3)$	0.92
Wall Internal Viscosity	$\eta (dyne \cdot s / cm^2)$	300
Young's Modulus of Elasticity	$E (dyne / cm^2)$	2.3E7
Wall Thickness	$h (cm)$	0.159
Wall Radius	$r (cm)$	0.65

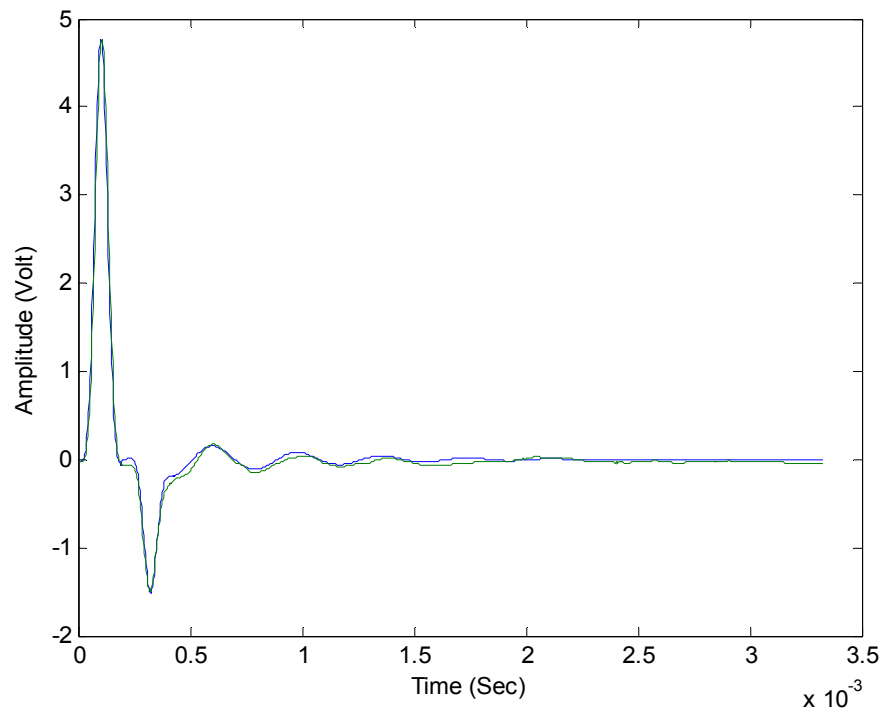


Fig. 4.27 Comparison of simulated reflected signal (blue) with acoustically obtained (green) for a latex tube with wall thickness of 0.159 cm.

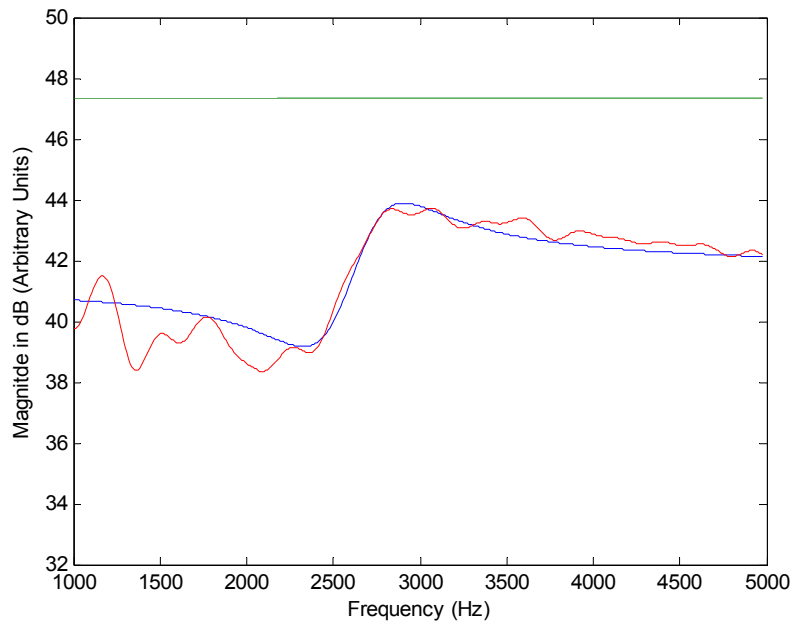


Fig. 4.28 Comparison of characteristic acoustic impedances obtained by simulation (blue) with acoustically measured (red) for a latex tube with wall thickness of 0.159 cm. The reflectometer impedance is plotted in green.

4.5.3 Tube of 0.198 cm of thickness with inner wall of 0.647 cm

Substitution of wall parameters (listed in Table XXVIII) into the transmission line model produce a response in time domain to an acoustic Hanning pulse, which was compared with the experimental acoustic response as it is illustrated in Fig. 4.29. From this figure, it can be observed that the experimental signals are similar to the simulated, exhibit the same behavior and the damping ratio for the simulation is 0.0035. Notice that the acoustic signal over the time $t = 2$ ms can not be measured by the microphone, because the low pressure can not be sensed.

Also, the characteristic acoustic impedances estimated experimentally and by simulation were compared in Fig. 4.30. The experimental and simulated characteristic acoustic impedances were computed from 1-5 kHz at increments of 10 Hz, using equations 4.1-6 and 3.1-5, respectively. The reflected signal length used was of $l = 600$ samples. From these characteristic impedance curves, it can be observed that the minimum value of Z_c occurred at a frequency $f_{res} = 2.24$ kHz, while the maximum value occurred at a frequency of $f_2 = 2.7$ kHz.

The experimental wall compliance was calculated using equation 2.3-1, yielding a wall compliance value of $C_{wExp} = 1.37 \cdot 10^{-7} \text{ cm}^5/\text{dyne}$. Substitution of wall parameters into the TLM expression for C_w yielded a per unit length wall compliance $C_{wSim} = 0.51 \cdot 10^{-7} \text{ cm}^5/\text{dyne}$.

TABLE XXVIII TRANSMISSION LINE MODEL PARAMETERS USED IN SIMULATION FOR A TUBE WITH WALL THICKNESS OF 0.198 CM.

PROPERTY	SYMBOL/UNITS	RUBBER
Density	$\rho_w(\text{g} / \text{cm}^3)$	0.92
Wall Internal Viscosity	$\eta(\text{dyne} \cdot \text{s} / \text{cm}^2)$	300
Young's Modulus of Elasticity	$E(\text{dyne} / \text{cm}^2)$	2.1E7
Wall Thickness	$h(\text{cm})$	0.198
Wall Radius	$r(\text{cm})$	0.65

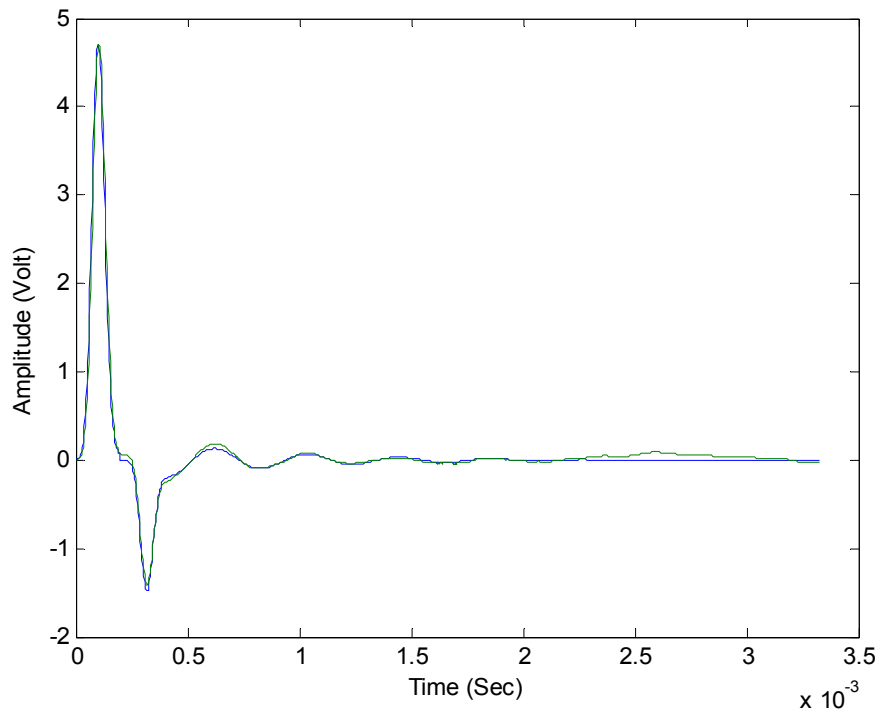


Fig. 4.29 Comparison of simulated reflected signal (blue) with acoustically obtained (green) for a latex tube with wall thickness of 0.198 cm.

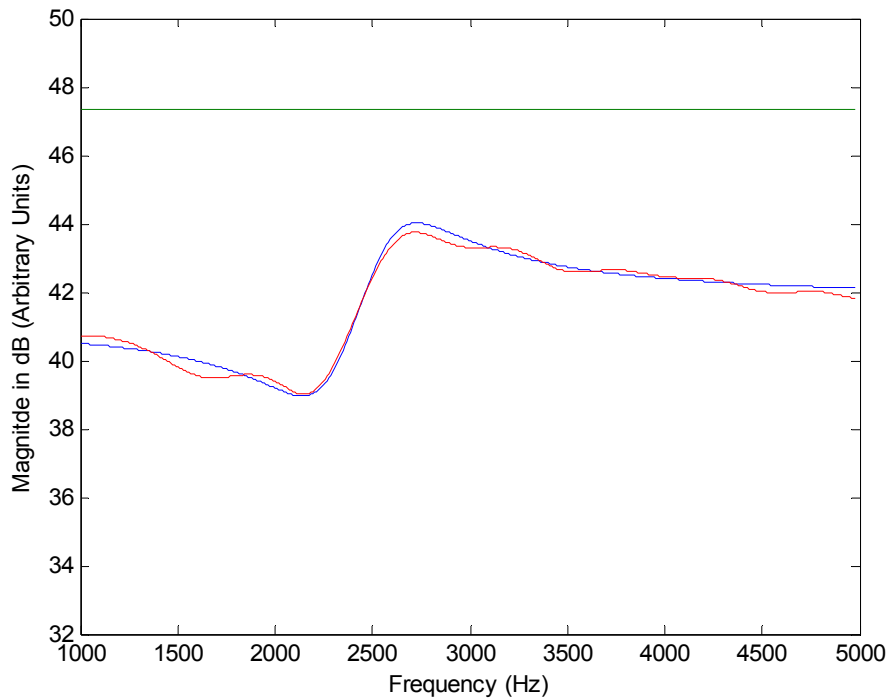


Fig. 4.30 Comparison of characteristic acoustic impedances obtained by simulation (blue) with acoustically measured (red) for a latex tube with wall thickness of 0.198 cm. The reflectometer impedance is plotted in green.

4.5.4 Tube of 0.238 cm of thickness with inner wall of 0.647 cm

Substitution of wall parameters (listed in Table XXIX) into the transmission line model produce a response in time domain to an acoustic Hanning pulse, which was compared with the experimental acoustic response as it is illustrated in Fig. 4.31. From this figure, it can be observed that the experimental signals are similar to the simulated, exhibit the same behavior and the damping ratio for the simulation is 0.0035. Notice that the acoustic signal over the time $t = 1.7$ ms can not be measured by the microphone, because the low pressure can not be sensed.

Also, the characteristic acoustic impedances estimated experimentally and by simulation were compared in Fig. 4.32. The experimental and simulated characteristic acoustic impedances were computed from 1-5 kHz at increments of 10 Hz, using equations 4.1-6 and 3.1-5, respectively. The reflected signal length used was of $l = 600$ samples. From these characteristic impedance curves, it can be observed that the

minimum value of Z_c occurred at a frequency $f_{res} = 2.032$ kHz, while the maximum value occurred at a frequency of $f_2 = 2.618$ kHz.

The experimental wall compliance was calculated using equation 2.3-1, yielding a wall compliance value of $C_{wExp} = 1.31 \cdot 10^{-7} \text{ cm}^5/\text{dyne}$. Substitution of wall parameters into the TLM expression for C_w yielded a per unit length wall compliance $C_{wSim} = 0.470 \cdot 10^{-7} \text{ cm}^5/\text{dyne}$.

TABLE XXIX TRANSMISSION LINE MODEL PARAMETERS USED IN SIMULATION FOR A TUBE WITH WALL THICKNESS OF 0.238 CM.

PROPERTY	SYMBOL/UNITS	RUBBER
Density	$\rho_w (\text{g} / \text{cm}^3)$	0.92
Wall Internal Viscosity	$\eta (\text{dyne} \cdot \text{s} / \text{cm}^2)$	300
Young's Modulus of Elasticity	$E (\text{dyne} / \text{cm}^2)$	1.9E7
Wall Thickness	$h (\text{cm})$	0.238
Wall Radius	$r (\text{cm})$	0.65

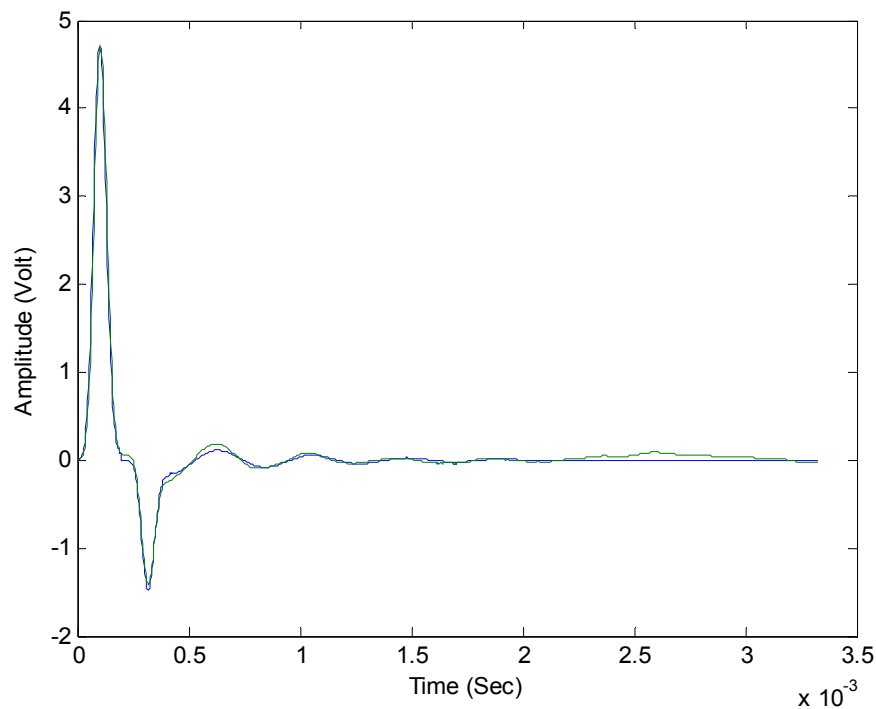


Fig. 4.31 Comparison of simulated reflected signal (blue) with acoustically obtained (green) for a latex tube with wall thickness of 0.238 cm.

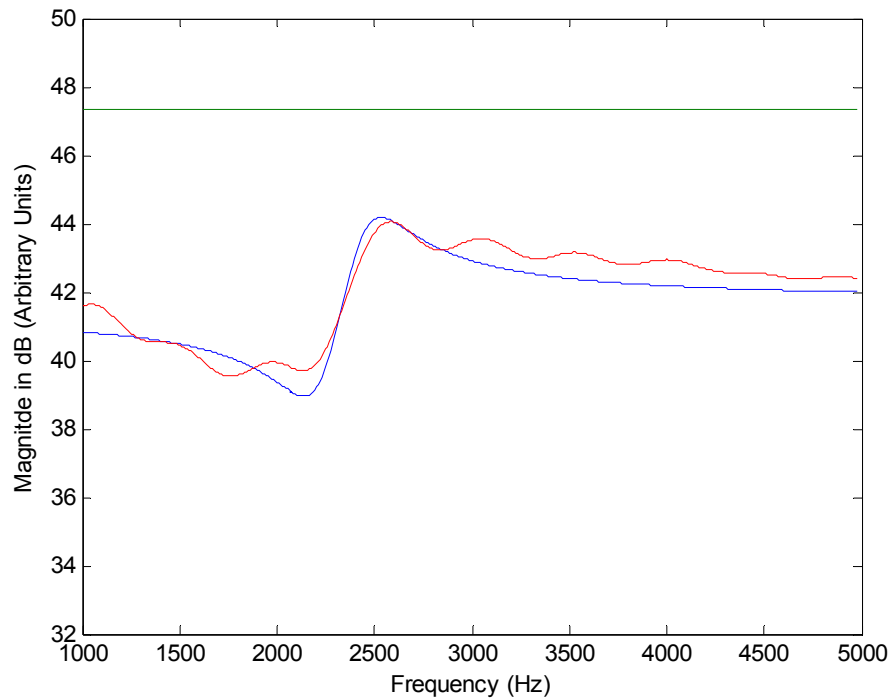


Fig. 4.32 Comparison of characteristic acoustic impedances obtained by simulation (blue) with acoustically measured (red) for a latex tube with wall thickness of 0.238 cm. The reflectometer impedance is plotted in green.

4.5.5 Tube of 0.317 cm of thickness with inner wall of 0.647 cm

Substitution of wall parameters (listed in Table XXX) into the transmission line model produce a response in time domain to an acoustic Hanning pulse, which was compared with the experimental acoustic response as it is illustrated in Fig. 4.33. From this figure, it can be observed that the experimental signals are similar to the simulated, exhibit the same behavior and the damping ratio for the simulation is 0.0035. Notice that the acoustic signal over the time $t = 1.3$ ms can not be measured by the microphone, because the low pressure can not be sensed.

Also, the characteristic acoustic impedances estimated experimentally and by simulation were compared in Fig. 4.34. The experimental and simulated characteristic acoustic impedances were computed from 1-5 kHz at increments of 10 Hz, using equations 4.1-6 and 3.1-5, respectively. The reflected signal length used was of $l = 600$ samples. From these characteristic impedance curves, it can be observed that the

minimum value of Z_c occurred at a frequency $f_{res} = 1.912$ kHz, while the maximum value occurred at a frequency of $f_2 = 2.453$ kHz.

The experimental wall compliance was calculated using equation 2.3-1, yielding a wall compliance value of $C_{wExp} = 1.36 \cdot 10^{-7} \text{ cm}^5/\text{dyne}$. Substitution of wall parameters into the TLM expression for C_w yielded a per unit length wall compliance $C_{wSim} = 0.37 \cdot 10^{-7} \text{ cm}^5/\text{dyne}$.

TABLE XXX TRANSMISSION LINE MODEL PARAMETERS USED IN SIMULATION FOR A TUBE WITH WALL THICKNESS OF 0.317 CM.

PROPERTY	SYMBOL/UNITS	RUBBER
Density	$\rho_w (\text{g} / \text{cm}^3)$	0.92
Wall Internal Viscosity	$\eta (\text{dyne} \cdot \text{s} / \text{cm}^2)$	300
Young's Modulus of Elasticity	$E (\text{dyne} / \text{cm}^2)$	1.8E7
Wall Thickness	$h (\text{cm})$	0.317
Wall Radius	$r (\text{cm})$	0.65

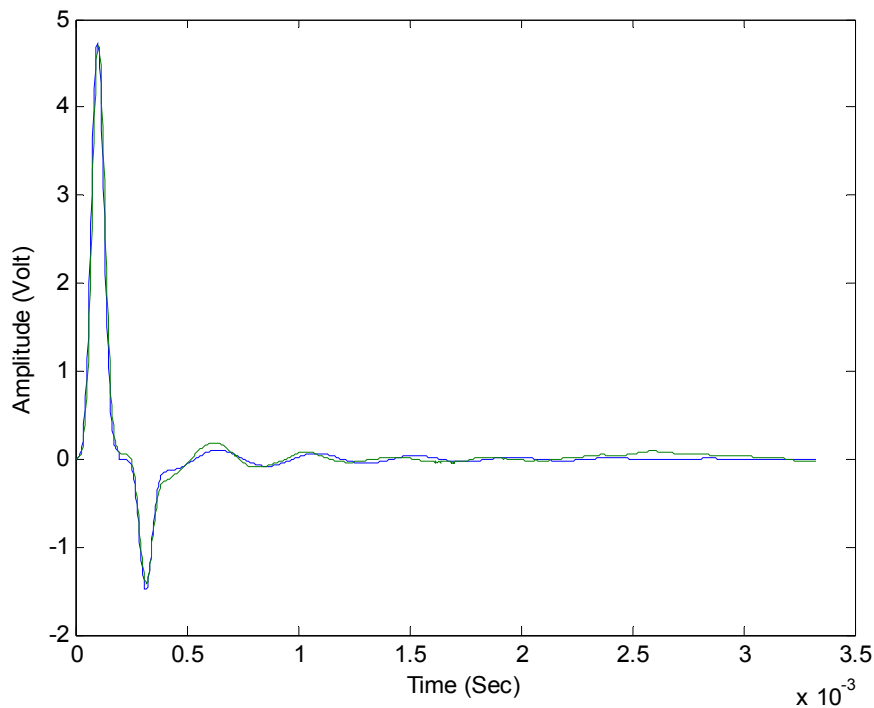


Fig. 4.33 Comparison of simulated reflected signal (blue) with acoustically obtained (green) for a latex tube with wall thickness of 0.317 cm.

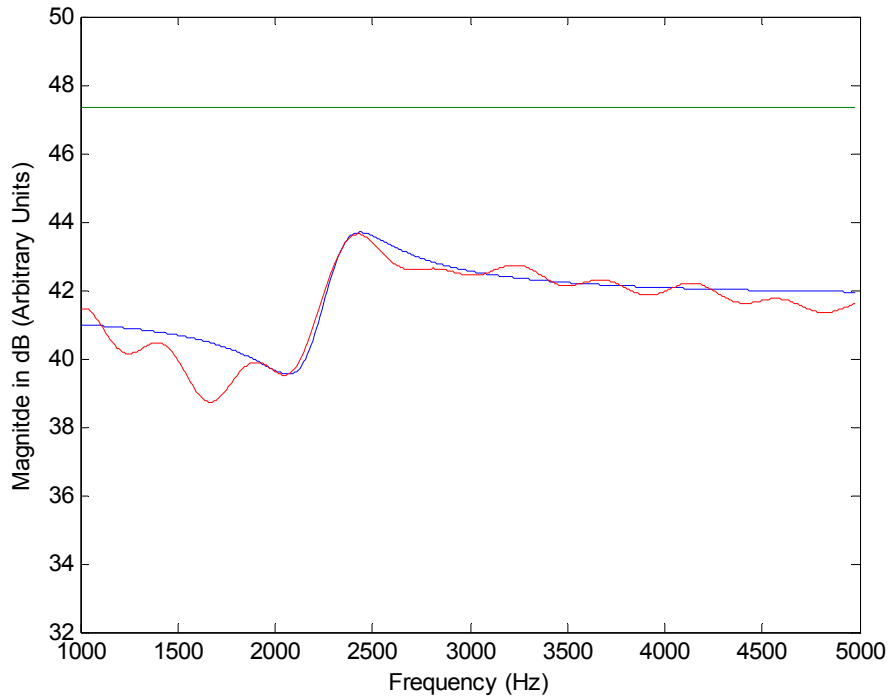


Fig. 4.34 Comparison of characteristic acoustic impedances obtained by simulation (blue) with acoustically measured (red) for a latex tube with wall thickness of 0.317 cm. The reflectometer impedance is plotted in green

4.6 Noise Removal

The resultant signal of an acoustic perturbation into the pipes is described in Fig. 4.35. This solution may be divided into two differential solutions: the forced response and natural response, as illustrated on Fig. 4.35. The interest for this case is the reconstruction of the experimental signal since part of the signal is noisy. By observation, the natural response has a behavior that could be mathematically described by

$$y(t) = A * e^{\alpha t} \cos(\omega \cdot t + \phi) + DC, \quad (4.6-1)$$

where A represents the amplitude attenuation, α represents the attenuation caused by the distance, t is the time in seconds, ω is the angular frequency in rad/s , ϕ is the phase and DC represents the constant value added to the signal.

The Gauss Newton algorithm was used to reconstruct the natural response from a part of the experimental data. A portion of the natural response was analyzed using initials

values ($A = 1000$, $DC = -0.01$, $\alpha = 0.1$, $\bar{\omega} = 2\pi f_{res}$, $\phi = \pi/4$) closed to the natural response values. An example of a particular solution of an acoustic natural response for a latex pipe when the wall thickness is 0.119 cm is presented on Fig. 4.37.

The Gauss Newton algorithm produces a suitable estimation of the reflected acoustic signal. Therefore, when the characteristic acoustic impedances were computed from the estimated data using acoustic reflectometry, it was obtained that curves of the characteristic acoustic impedance curve were closer to those predicted by the experimental characteristic acoustic. Fig. 4.40 shows the comparison between the experimental and estimated characteristic acoustic impedances.

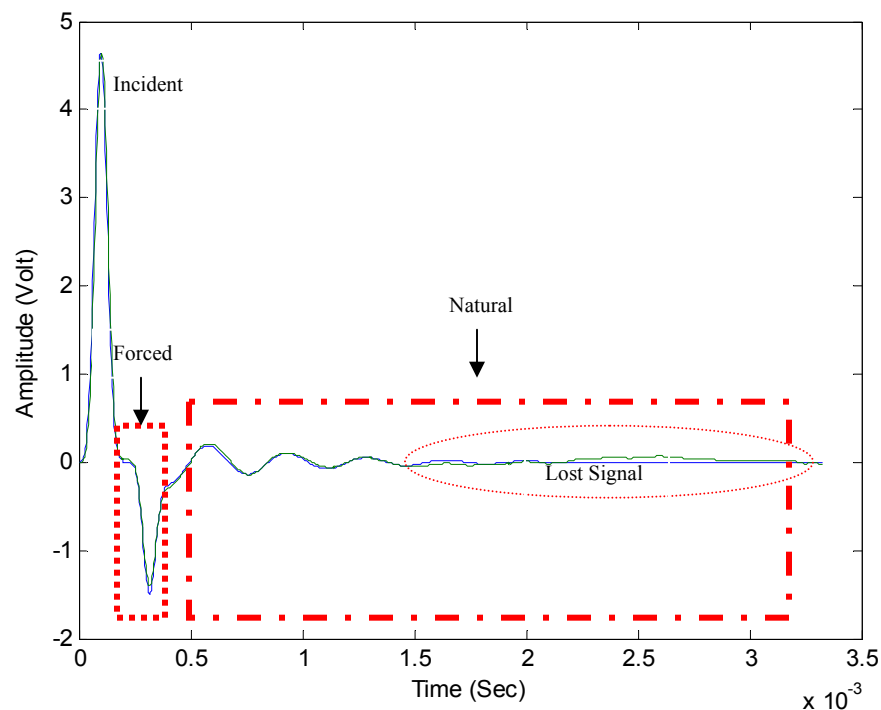


Fig. 4.35 Signal obtained in TLM simulation (blue) and measured acoustically (green). Dash line represents the forced response and dot-dash the natural response. The ellipse outlines the missed information.

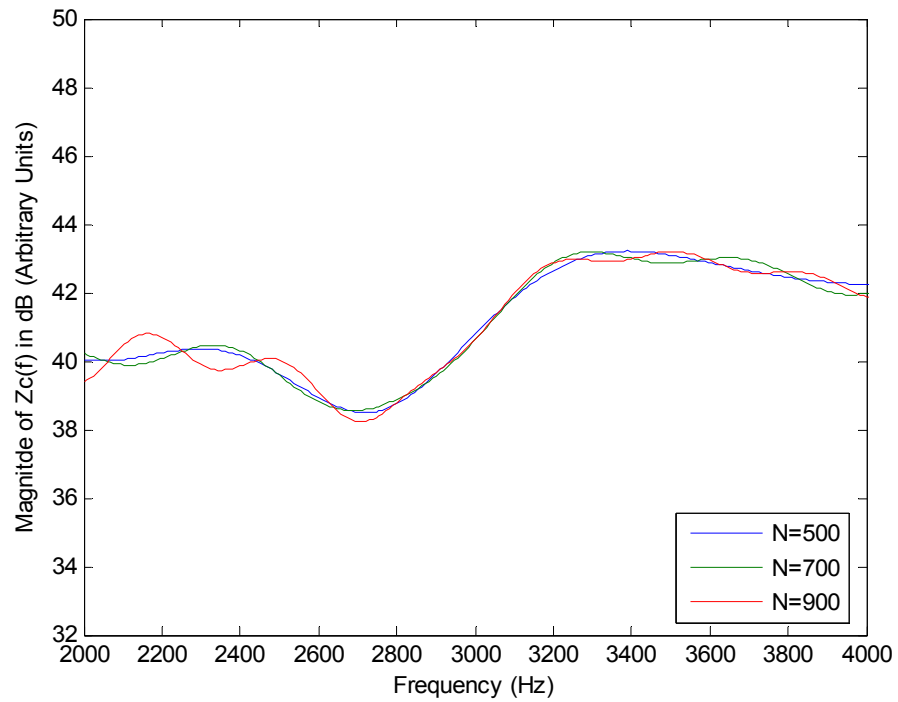


Fig. 4.36 Characteristic acoustic impedance of a tube with wall thickness of 0.119 cm when the length of the reflected signal was varied.

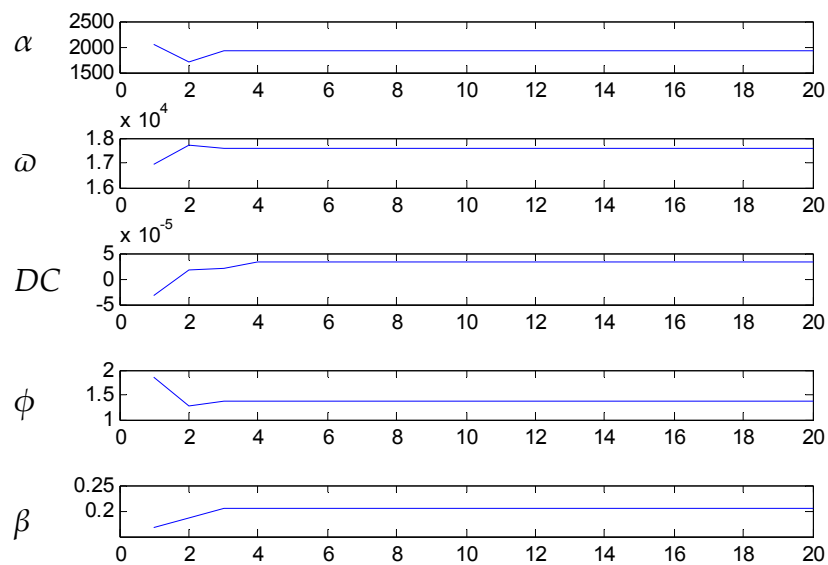


Fig. 4.37 Parameters behavior in iteration twenty of Gauss-Newton Algorithm.

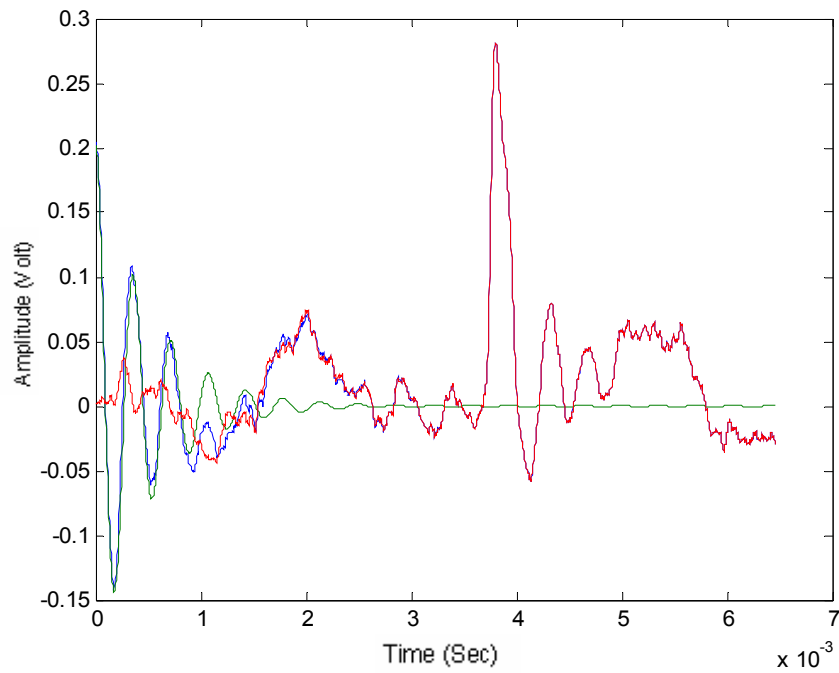


Fig. 4.38 Comparison among the estimated signal (green) and the natural response of the system (blue). The error between them is plotted in red.

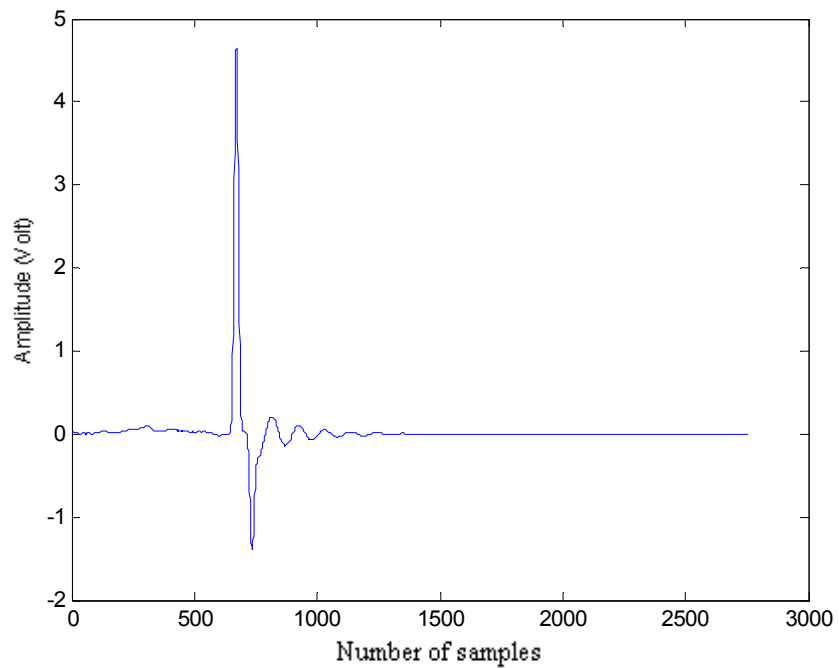
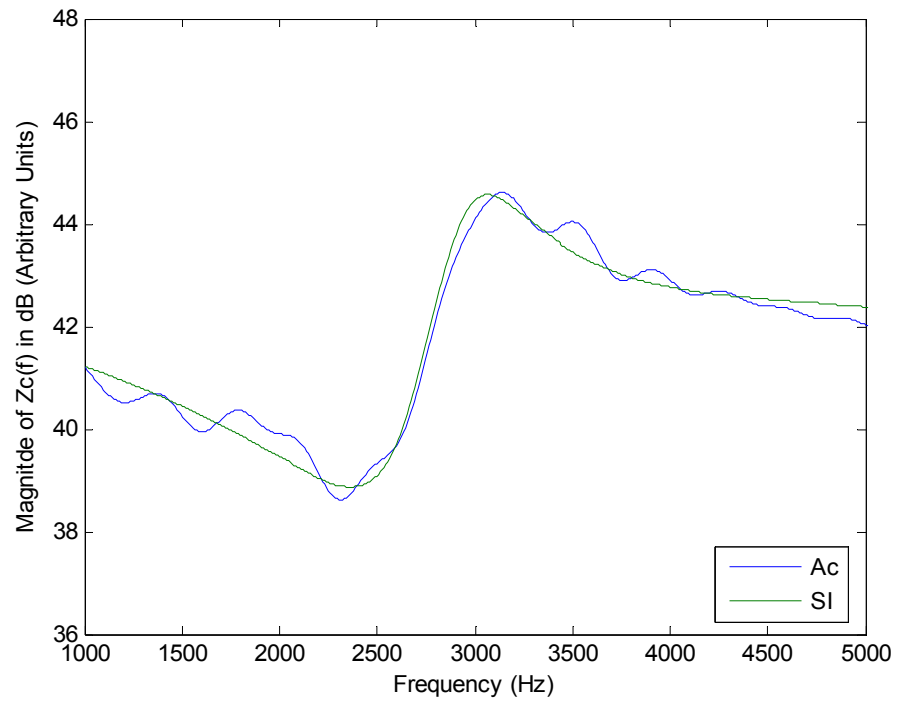
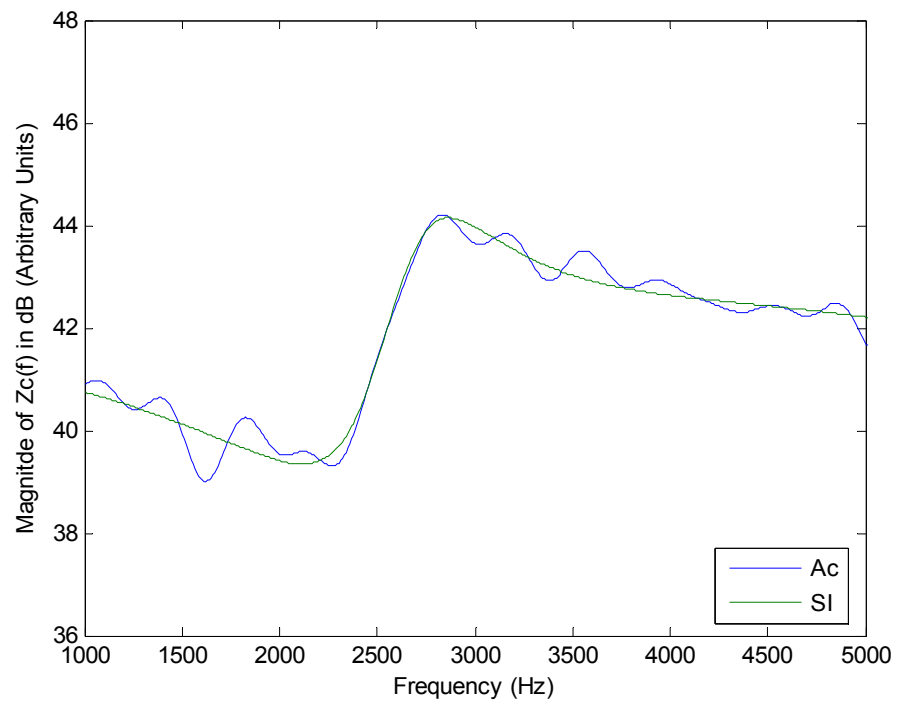


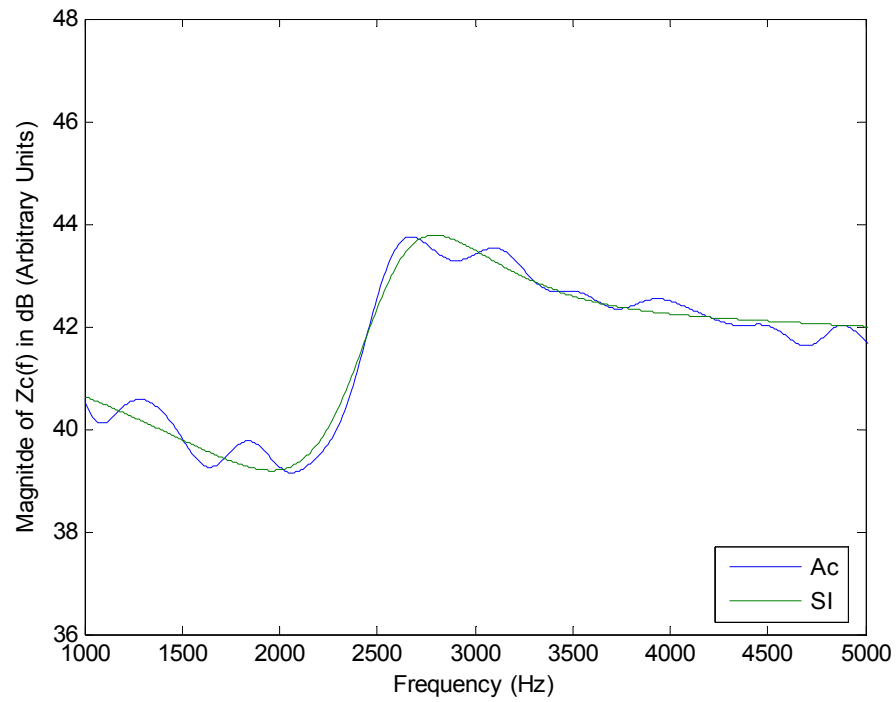
Fig. 4.39 Acoustic signal obtained after applying Gauss-Newton algorithm.



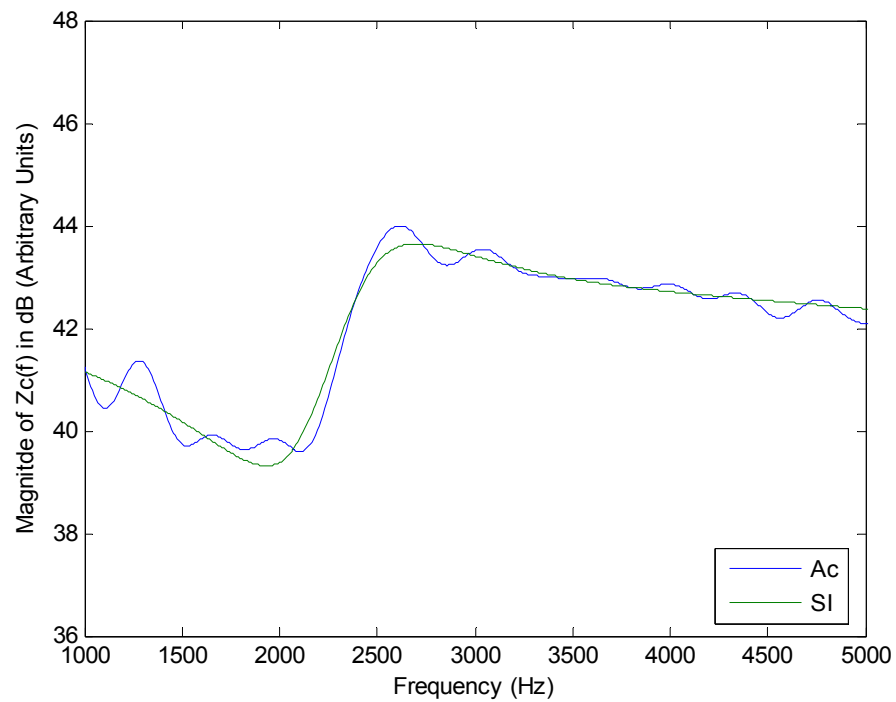
a)



b)



c)



d)

Fig. 4.40 Comparison of characteristic acoustic impedances obtained by system identification (green) with the acoustically measured (blue) for latex tubes with wall thickness: a) $h = 0.159$ cm, b) $h = 0.159$ cm, c) $h = 0.198$ cm, d) $h = 0.238$ cm, e) $h = 0.317$ cm.

4.7 Tubes wall compliance results.

The local wall compliance estimated by pulse-echo acoustic reflectometry (PEAR), and the mechanical and mathematical wall compliance are presented in this section. Initially, the wall compliance (Eq) was computed for the different rubber tubes, substituting the corresponding values of the Table XXXI in the following equation.

$$C_w = \frac{2\pi^3}{Eh} \frac{cm^4}{dyne} \quad (4.7-1)$$

TABLE XXXI TRANSMISSION LINE MODEL PARAMETERS USED IN SIMULATION

PROPERTY	SYMBOL/UNITS	RUBBER
Young's Modulus of Elasticity (<i>Test 1-5</i>)	$E(dyne/cm^2)$	1.8E7, 1.9E7, 2.1E7, 2.3E7, 2.6E7
Wall Thickness (<i>Test 1-5</i>)	$h(cm)$	0.317,0.238,0.198,0.159,0.119
Wall Radius	$r(cm)$	0.65

Table XXXII lists the obtained results for the computed (Eq) wall compliance. Additionally, the mechanic wall compliance (Mc) was measured for the different tubes and the obtained results are presented in Table XXXII. Mechanical measurements were taken in order to observe the mechanic wall compliance behavior of the rubber tubes when the wall thickness changes. These results obtained served to validate and compare the wall compliance computed from equation, measured by experimental PEAR (Ac) and system identification (SI).

TABLE XXXII WALL COMPLIANCE

Wall Thickness (cm)	Equation ($cm^4/dyne$)	Mechanic ($cm^4/dyne$)
0.119	$0.688 \cdot 10^{-7}$	$1.79 \cdot 10^{-7}$
0.159	$0.582 \cdot 10^{-7}$	$1.71 \cdot 10^{-7}$
0.198	$0.512 \cdot 10^{-7}$	$1.55 \cdot 10^{-7}$
0.238	$0.470 \cdot 10^{-7}$	$1.36 \cdot 10^{-7}$
0.317	$0.373 \cdot 10^{-7}$	$1.31 \cdot 10^{-7}$

From Table XXXII, it can be seen that the wall compliance decreases when the wall thickness increases. Additionally, notice that the mechanical values are higher than the computed one. These differences occur because the liquid in the tube is incompressible, and the total measured compliance is due only to the wall tubes distension.

Different compliant tubes were interrogated acoustically with an acoustic Hanning pulse and then system identification was applied to the recorded signals. With the resulting signals, pulse-echo acoustic reflectometry was applied to compute the reflection coefficients and characteristic acoustic impedances using 1000 samples of the reflected signal. The wall compliance was computed in two ways. First, it was computed from the transversal frequencies observed from the characteristic impedances. In the second method, the wall compliance was computed from the natural frequency and the wall resonant frequency that were obtained from the Fourier transform of the natural response and from the characteristic acoustic impedance.

4.7.1 Wall compliance estimation by acoustic input impedance

The wall compliance results from acoustic experimentation (AC) and noise removal algorithm (SI) at 1000 samples, mechanic (Mc) and equation (Eq) are shown in Fig. 4.41. From these figures it can be observed that the wall compliance decreases when the wall thickness increases. Additionally, it can be seen that the system identification predicts the wall compliance obtained acoustically. Note that the wall compliance values estimated acoustically are between the mechanic and transmission line model equation values. These differences occur because of the error in the transversal frequencies acquisition.

The transversal frequencies resulted from acoustic experimentation and system identification at 1000 samples, and equations are shown in Fig. 4.42, where figure (a) depicts the resonance frequency obtained by PEAR ($fres$), mathematical ($fresc$) and system identification ($fresSI$) and figure (b) depicts the extended frequency obtained by PEAR ($f2$), mathematical ($f2c$) and system identification ($f2SI$). Table XXXIII lists the error of the wall compliance estimated mechanically Mc , acoustically Ac , simulation Eq and using noise removal SI with respect to mechanic.

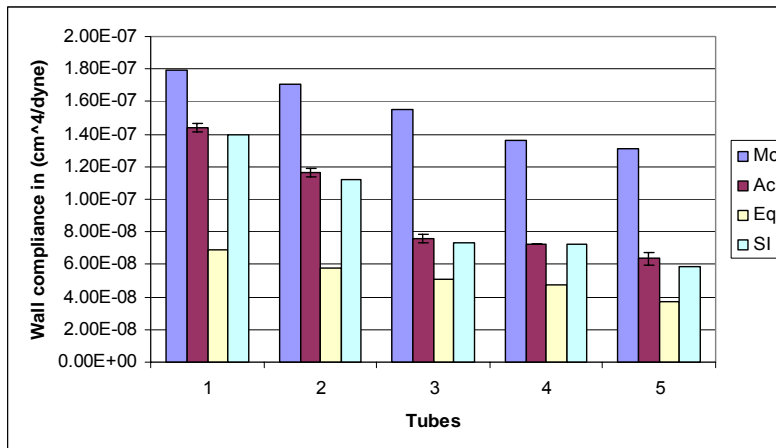
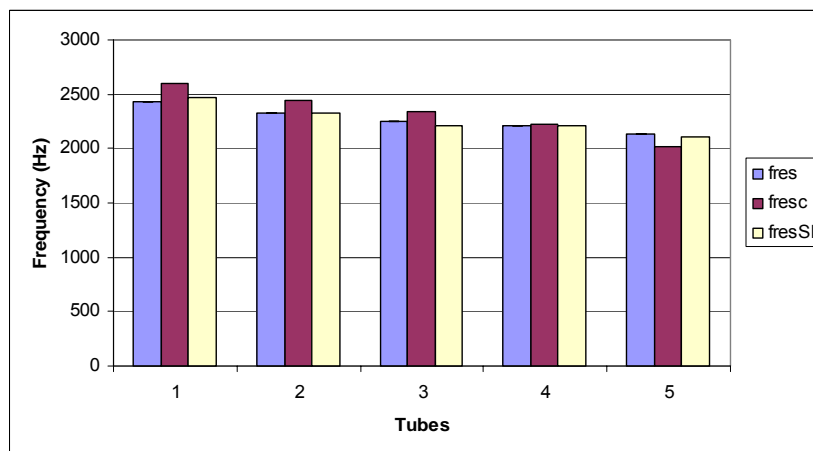
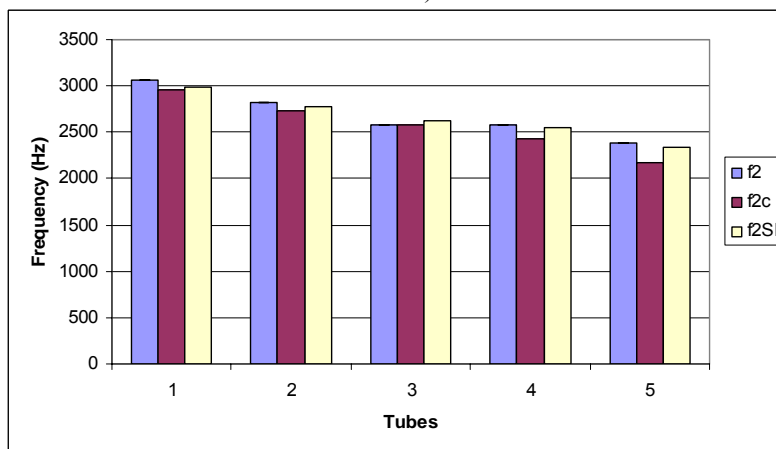


Fig. 4.41 Wall compliance obtained mechanically (Mc), acoustical (Ac), mathematically (Eq) and by system identification (SI) at 1000 samples. Tube 1: $E = 2.6E7$ dyne/cm², $h = 0.119$ cm; Tube 2: $E = 2.3E7$ dyne/cm², $h = 0.159$ cm; Tube 3: $E = 2.1E7$ dyne/cm², $h = 0.198$ cm; Tube 4: $E = 1.9E7$ dyne/cm², $h = 0.238$ cm; Tube 5: $E = 1.8E7$ dyne/cm², $h = 0.317$ cm.



a)



b)

Fig. 4.42 Transversal frequencies: a) acoustical ($fres$), mathematical ($fresc$) and system identification ($fresSI$), b) acoustical ($f2$), mathematical ($f2c$) and system identification ($f2SI$). Tube 1: $h = 0.119$ cm, Tube 2: $h = 0.159$ cm, Tube 3: $h = 0.198$ cm, Tube 4: $h = 0.238$ cm, Tube 5: $h = 0.317$ cm.

TABLE XXXIII PERCENT WALL COMPLIANCE WITH RESPECT TO MECHANICAL VALUES

Wall Thickness (cm)	Mc	Ac	Eq	SI	Units
0.119	100.00	81.10	38.41	62.01	($cm^4/dyne$)
0.159	95.53	64.92	32.50	56.42	($cm^4/dyne$)
0.198	86.59	43.79	28.58	54.08	($cm^4/dyne$)
0.238	75.98	40.41	26.28	44.02	($cm^4/dyne$)
0.317	73.18	35.57	20.83	31.79	($cm^4/dyne$)

4.7.2 Wall compliance estimation by reflection coefficient and natural response

The wall compliance results from the acoustic experimentation (AC) and noise removal algorithm (SI) at 1000 samples, mechanic (Mc) and equation (Eq) are shown in Fig. 4.43. From this figure it can be observed that the wall compliance decreases when the wall thickness increases. Notice that the wall compliance behavior expected because of wall thickness changes can be predicted with the method. Additionally, with the data obtained by system identification it can be observed that the wall compliance values estimated are close to the acoustically obtained (Ac).

The transversal frequencies results from acoustic experimentation and system identification at 1000 samples are shown in Fig. 4.42, where figure (a) depicts the natural frequency obtained by PEAR (fr), mathematical (frc) and system identification ($frSI$) and figure (b) depicts the resonant frequency obtained by PEAR ($fres$), mathematical ($fresc$) and system identification ($fresSI$). Notice that the natural frequency could be acquired with a lower error than the resonant frequency, because the first one does not depend on the wall viscosity. Table XXXIV lists the error of the wall compliance estimated mechanically Mc , acoustically Ac , simulation Eq and using noise removal SI with respect to mechanic.

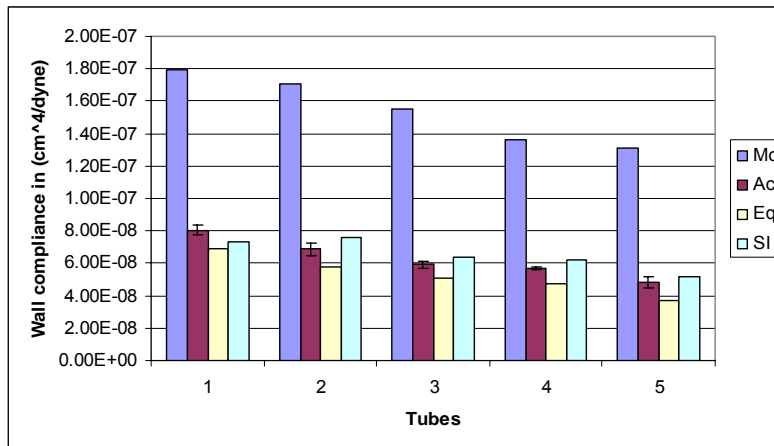
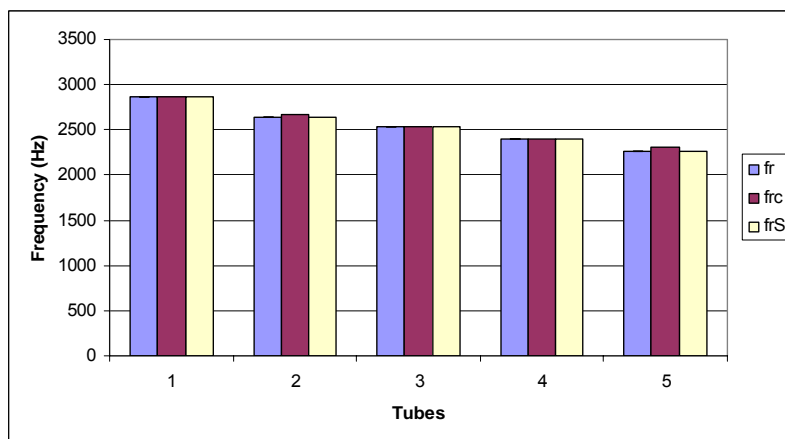
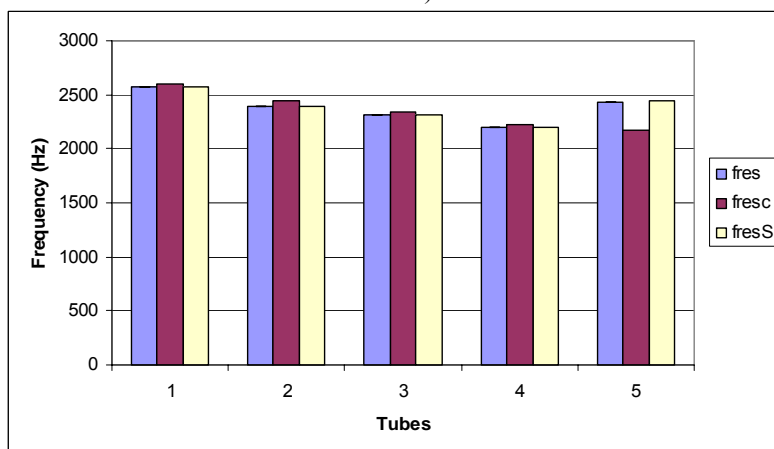


Fig. 4.43 Wall compliance obtained mechanically (Mc), acoustical (Ac), mathematically (Eq) and by system identification (SI) at 600 samples. Tube 1: $E = 2.6E7$ dyne/cm², $h = 0.119$ cm; Tube 2: $E = 2.3E7$ dyne/cm², $h = 0.159$ cm; Tube 3: $E = 2.1E7$ dyne/cm², $h = 0.198$ cm; Tube 4: $E = 1.9E7$ dyne/cm², $h = 0.238$ cm; Tube 5: $E = 1.8E7$ dyne/cm², $h = 0.317$ cm.



a)



b)

Fig. 4.44 Transversal frequencies: a) acoustical ($fres$), mathematical ($fresc$) and system identification ($fresSI$); b) acoustical ($f2$), mathematical ($f2c$) and system identification ($f2SI$). Tube 1: $h = 0.119$ cm, Tube 2: $h = 0.159$ cm, Tube 3: $h = 0.198$ cm, Tube 4: $h = 0.238$ cm, Tube 5: $h = 0.317$ cm.

TABLE XXXIV PERCENT WALL COMPLIANCE WITH RESPECT TO MECHANICAL VALUES

Wall Thickness (cm)	Mc	Ac	Eq	SI	Units
0.119	100.00	38.41	45.01	40.84	$(cm^4/dyne)$
0.159	95.53	32.50	38.32	42.29	$(cm^4/dyne)$
0.198	86.59	28.58	33.09	35.59	$(cm^4/dyne)$
0.238	75.98	26.28	31.93	34.64	$(cm^4/dyne)$
0.317	73.18	20.83	27.09	29.11	$(cm^4/dyne)$

5 Conclusion and Recommendations

In this research, the use of pulse echo acoustic reflectometry technique to estimate the local wall compliance was investigated through the use of computer simulation models, mechanical measurements, and *in vitro* acoustical measurements. This technique provides an innovative tool to measure the local wall compliance, without the necessity of touching the tube wall, inflating the tubes, or being near or underneath the affected area to estimate the tube wall properties. Additionally, the transient pulse can be designed with a specific bandwidth to interrogate the system between the resonant frequencies, without having to make a frequency sweep as with sinusoid interrogation.

The acoustic responses of several tubes were modeled using transmission line. A sensitivity analysis helped understand how the model parameters affect the acoustic response. From this analysis it was concluded that the system acoustic characteristic impedance is influenced by all parameters: wall density, wall viscosity, Young's modulus and wall thickness. The Young's modulus is the parameter which affects the system transverse frequencies the most. Particularly, the inner diameter, Young's modulus and wall viscosity are the parameters that affect the damping ratio and consequently, the quality factor. The wall viscosity in the enhanced analysis considering rubber was the parameter that most affects the damping ratio. From the results obtained by simulation, it was observed that an increase in the wall viscosity causes an increase in the damping ratio and consequently a decreases quality factor. The system is considered underdamped and the rate at which the wall oscillates is fixed by a damped frequency since there are dissipative elements. This explains why this parameter generates the largest errors between the transverse frequencies f_{res} calculated from the equations, compared with the transverse frequencies obtained from the characteristic acoustic impedance.

Pulse echo-acoustic reflectometry was used to estimate the wall compliance of five cylindrical rubber conduits from measurements of characteristic acoustic impedance and natural frequency. An acoustic Hanning pulse was used to interrogate the system, but in order to compensate for the acoustic transfer function of the speaker, microphone and electronic interface, an inverse filter technique was implemented from which a pulse was

obtained with a frequency range of 0-14kHz. The experimentally determined characteristic impedances were compared with the results obtained from the transmission line model. The inner diameter, wall thickness and wall density used in the model were measured, while the Young's modulus and wall viscosity were obtained from the literature. Particularly, we could not measure the dynamic Young's modulus with the available laboratory equipment, however from the literature it was observed that it is frequency depends. Additionally, the fabrication standard of the tubes used was unknown. Given these facts, a different Young's module value was used for each tube, following the range and magnitude order observed in the literature review. Using these parameters, the transmission line model accurately predicted the experimental acoustic response. From the results obtained in simulation and *in vitro* acoustic, the wall compliance was estimated. It can be seen that the wall compliance decreases when the wall thickness increases. This behavior is proper since the wall compliance is inversely proportional to the wall thickness.

Two methods were used to compute the wall compliance. In the first method, the wall compliance is estimated from the transversal frequencies considering a wall factor of 0.1 in practice for latex [29]. In the second method, the wall compliance is estimated from the natural and resonant frequencies. From the results obtained from simulation and *in vitro* acoustical measurements, it can be concluded that the second method results in a lower estimation error than the first method; for example, in the first method, the wall compliance was estimated with an error of 90% while with the second method, the wall compliance was estimated with an error of 1.2%. These differences occur since the transversal frequencies in the first method were acquired with an error of 5%, while the natural and resonant frequencies in the second method were obtained with an error of 1.3% and 0.73% respectively. These low errors in the frequency acquisition in the second method occur since the natural frequency does not depend of the wall viscosity, and we consider the neper frequency to obtain the resonant frequency. Similarly, the first method does not consider the wall loss factor in latex material to compute the wall compliance. From the obtained data, it can be concluded that both methods were able to detect the characteristic acoustic impedance changes due to variations in the wall

properties as composition and thickness, although the second method has better results for these particular cases.

The mechanic measurements obtained have the same behavior that the acoustic and simulated, but different values. The experimentally obtained results behaved as expected from the theoretical analysis and it was observed that as the wall thickness increases, the wall compliance decreases. The differences in values could be generated as a result of error introduced by the mechanical instrument and human appreciation. Additionally, it is important to consider that the compliance computed by simulation only consider the axial movement, while, the mechanical test measures the compliance due to axial and longitudinal distention of the tube wall.

5.1 Recommendations

The methods described in this research can be used to estimate the wall compliance using pulse-echo acoustic technique in new applications such as biomedical, physics, materials engineering, etc. In this thesis, the effect of the wall thickness in the wall compliance was demonstrated. As future work additional experiments could be performed. For example, experiments with liquid-filled compliant tubes can be made in order to prove if the theory is applicable to that particular case, and different tubes can be connected in series to prove if the wall compliance of the second tube can be estimated. One of the questions that should be solved in future research is what model should be used when the compliant pipe is submerged in a different medium than the one in its interior. Additionally, a better reflectometer can be designed to increase the range in frequency and extend the study making experiments where different parameters can be changed such as diameter, wall composition, etc. Subsequently, experiments with biological or organic tissue such as veins, arteries, airways, etc should be performed.

References

- [1] D. K. Arnett, "Arterial Stiffness and Hypertension," Division of Epidemiology, School of Public Health, University of Minnesota, USA.
- [2] S. E. Greenwald, "Pulse pressure and arterial elasticity," *Q. J. Med.*, pp. 107-112, 2002.
- [3] G. D. Zarins CK, Bharadvaj BK., "Carotid bifurcation atherosclerosis-quantitative correlation of plaque localization with flow velocity profile and wall shear stress.," *Circulation*, 1983.
- [4] M. L. S. Kitney RI, K., "3D visualization of arterial structures using ultrasound and voxel model.," *Cardiol Imaging*, vol. 4, pp. 135-43, 1989.
- [5] R. S. Lee RT, Loree HM, Grodzinsky AJ, Gharib SA., Schoen, F.J., et al., "Prediction of mechanical properties of human atherosclerotic tissue by high frequency intravascular ultrasound imaging: an invivo study.," *Intravascular Atherosclerosis and Trombosis*, pp. 1-5, 1992.
- [6] "www.lungusa.org."
- [7] "www.americanheart.org."
- [8] "<http://www.lung.ca/>."
- [9] I. C. D. Statistics, "American Heart Association - <http://www.americanheart.org/downloadable/heart/1059109452900FS06INT3REV7-03.pdf>."
- [10] "American Heart Association <http://www.americanheart.org>."
- [11] "<http://health.howstuffworks.com/heart-attack1.htm>."
- [12] R. M. Goldwyn, and T. B.Watt, "Arterial pressure pulse contour analysis via a mathematical model for the clinical quantification of human vascular properties," *IEEE Trans. Biomed Eng* 14, pp. 11-17, 1967.
- [13] M. F. O'Rourke, and M. G. Taylor, "Input impedance of the systemic circulation," *Circ. Res.* 20, pp. 365-380, 1967.
- [14] T. Pasierski, A. C. Pearson, and A. J. Labovitz, "Pathophysiology of isolated systolic hypertension in elderly patients: Doppler echocardiographic insights," *Am. Heart J.* 122, pp. 528-534, 1991.
- [15] R. Shankar, and M. G. Bond, "Correlation of noninvasive arterial compliance with anatomic pathology of atherosclerotic nonhuman primates," *Atherosclerosis* 85, pp. 37-46, 1990.

- [16] A. P. Hoeks, P. J. Brands, F. A. Smeets, and R. S. "Reneman. Assessment of the distensibility of superficial arteries," *Ultrasound Med. Biol* 16, pp. 121-128, 1990.
- [17] J. O. Arndt, H. F. Stegall, and H. J. Wicke, "Mechanics of the aorta in vivo-a radiographic approach," pp. *Circ. Res.* 28: 693-705, 1971.
- [18] A. M. Dart, F. Lacombe, J. K. Yeoh, J. D. Cameron, G. L. Jennings, E. "Laufer, and D. S. Esmore. Aortic distensibility in patients with isolated hypercholesterolaemia, coronary artery disease, or cardiac transplant," *Lancet* 338, pp. 270-273, 1991.
- [19] C. Stefanadis, C. Stratos, C. Vlachopoulos, S. Marakas, H. Boudoulas, I. Kallikazaros, E. Tsiamis, K. Toutouzas, L. Sioros, and P. Toutouzas, "Pressure-diameter relation of the human aorta. A new method of determination by the application of a special ultrasonic dimension catheter," *Circulation* 92, pp. 2210-2219, 1995.
- [20] R. H. Mohiaddin, S. R. Underwood, H. G. Bogren, D. N. Firmin, R. H. Klipstein, R. S. O. Rees, and D. B. Longmore, "Regional aortic compliance studied by magnetic resonance imaging: the effects of age, training, and coronary artery disease," *Br. Heart J.* 62, pp. 90-96, 1989.
- [21] J. G. Barra, L. Levenson, R. L. Armentano, E. I. Cabrera Fischer, R. H. Pichel, and A. Simon, "In vivo angiotensin II receptor blockade and converting enzyme inhibition on canine aortic viscoelasticity," *Am. J. Physiol.* 272 (*Heart Circ. Physiol.* 41):, pp. H859-H868, 1997.
- [22] E. Cabrera, J. Levenson, R. L. Armentano, J. Barra, R. Pichel, and A. Simon, "Constricting and stiffening action of atropine on aortic response to angiotensin in dogs," *Hypertension* 11, *Suppl 1*, pp. I-103-I-107, 1988.
- [23] D. Hayoz, Y. Tardy, F. D. Perret, B. Waeber, J. J. Meister, and H. R. Brunner, "Non-invasive determination of arterial diameter and distensibility by echo-tracking techniques in hypertension," *J. Hypertens* 10, pp. S95-S100, 1992.
- [24] D. J. Patel, F. M. de Freitas, J. C. Greenfield, and D. L. Fry, "Relationship of radius to pressure along the aorta in living dogs," *J. Appl. Physiol.* 18, 1963.
- [25] H. P. Pieper, and L. T. Paul, "Responses of aortic smooth muscle studied in intact dogs," *Am. J. Physiol.* 217, pp. 154-160, 1969.
- [26] M. Yano, T. Kumada, M. Matsuzaki, M. Kohno, T. Hiro, S. Kohtoku, T. Miura, K. Katayama, M. Ozaki, and R. Kusukawa, "Effect of diltiazem on aortic pressure-diameter relationship in dogs," *Am. J. Physiol.* 256 (*Heart Circ. Physiol.* 25), pp. H1580-H1587, 1989.
- [27] P. S. N. Stergiopoulos, and N. Westerhof, "Use of pulse pressure method for estimating total arterial compliance in vivo," *Am. Phy. Soc.*, 1999.

- [28] "<http://www2.eur.nl/fgg/thorax/elasto/technique.html>."
- [29] R. W. G. Wayne L. Capper, and Athony E. Bunn, "The estimation of tube wall compliance acoustic input impedance," *IEEE transaction on biomedical engineering* Vol. 38. NO. 6, 1991.
- [30] R. W. Guelke, "Transmission line theory applied to sound wave propagation in tubes with compliant walls," *Acoustica*, vol. 48, pp. 101-106, 1981.
- [31] D. B. Sharp, "Acoustic pulse reflectometry for the measurement of musical wind instrument," University of Edinburgs, 1996.
- [32] A. R. F. L. F. Kinsler, A. B. Coppens and J.V. Sanders, "Fundamentals of acoustics," in *Johns Wiley and sons, New York*, T. Edition, Ed., 1982.
- [33] B. M. Oliver, "Time domain reflectometry," *Hewlett-Packard Journal*, vol. 15, pp. 1-8, 1964.
- [34] H. Halverson, "Time domain reflectometry," *Cleveland Electronic Conference*, 1963.
- [35] J. L. Flanagan, in *Speech Analysis, Synthesis and perception*. New York: Springer-Verlag, 1983, pp. 25-35.
- [36] G. W. J.P. Mansfield, "Theory and application of acoustic reflectometry in the human body," Thesis submitted to the faculty of Purdue University, 1996.
- [37] H. F. Olson, *Music, Physics and Engineering*, 1967.
- [38] T. Pritz, "Frequency dependences of complex moduly and complex poisson's ratio of real solid materials," *J. of Sound and Vibration*, pp. 83-104, 1998.
- [39] A. W. Nolle, "Acoustic Determination of the Physic Constants of Rubber-Like Materials," *The J. of the Ac. Soc. of Am.*, vol. 19, pp. 194-201, 1947.
- [40] P.-E. Austrell, "Non-Linear Dynamic Properties of Rubber Components," November 8-9 2001.
- [41] W. M. M. a. G. F. Lee, "Automated dynamic Young's modulus and loss factor measurements," *J. Acoust. Soc. Am.*, pp. 345-349, 1979.
- [42] "<http://www.keytosteel.com/fr/Articles/images/Articles/Fig39-1.gif>"
- [43] "http://en.wikipedia.org/wiki/Elastic_modulus."